Fall 12-16-2022

REVELATIONS IN THE BLOOD: DETERMINATION OF BIOMARKERS AND ANALYTES

Jeremiah Jamrom

REVELATIONS IN THE BLOOD: DETERMINATION OF BIOMARKERS AND ANALYTES

A Dissertation

Submitted to Bayer School of Natural and Environmental Sciences

Duquesne University

In partial fulfillment of the requirements for

the degree of Doctor of Philosophy

By

Jeremiah Jamrom

December 2022

REVELATIONS IN THE BLOOD: DETERMINATION OF BIOMARKERS AND ANALYTES

By

Jeremiah Jamrom

Approved October 28, 2022

Dr. H. M. “Skip” Kingston Professor of Chemistry and Biochemistry (Committee Chair)	Dr. Mihaela Rita Mihailescu Professor of Chemistry and Biochemistry (Committee Member)
Dr. Stephanie Wetzel Assistant Professor of Chemistry and Biochemistry (Committee Member)	Dr. Scott Faber Developmental Integrative Pediatrics (Committee Member)
Dr. Ellen Gawalt Dean, Bayer School of Natural and Environmental Sciences Professor of Chemistry and Biochemistry	Dr. Mihaela Rita Mihailescu Interim Chair, Chemistry Department Professor of Chemistry and Biochemistry

ABSTRACT

REVELATIONS IN THE BLOOD: DETERMINATION OF BIOMARKERS AND ANALYTES

By

Jeremiah Jamrom

December 2022

Dissertation supervised by Dr. H. M. “Skip” Kingston

Changes in body chemistry have long been utilized as a tool for medical diagnosis. Whether blood panel, toxin level, antigen testing or any of the myriad other tests performed annually, searching for molecules which confer health status is a long-established practice. These tests give physicians more information and allow them to make a more accurate diagnosis, from which appropriate treatment can stem. Awareness of, and the subsequent search for, biomarkers for disease states have grown substantially in the past years as analytical, biochemical, and instrumental techniques have become more precises and powerful. In an era of increasingly personalized medicine, novel techniques are necessary to ensure the accuracy and sensitivity of clinical methodology. Adding to these fields, methods were developed and optimized for the extraction, separation, and quantification of analytes. This work contains several disparate projects with this goal, ranging from the

accurate quantification of a biomarker for autism spectrum disorder, methylmalonic acid, on dried blood spots from levels both above and below the limit of detection, detection of a suite of curcuminoids to determine the potential extraction efficiency curcumin from turmeric under an internal review board approved study utilizing patient blood and cerebrospinal fluid samples, and finally detection of lead isotopes in blood samples to determine potential radon exposure. Two novel proofs of concepts were developed utilizing the stable, organic molecule methylmalonic acid: quantitative dried blood spots utilizing isotope dilution mass spectrometry and a novel analytical technique for accurate quantitation below the limits of detection known as Thor's Hammer Isotope Dilution Mass Spectrometry. These methods are instrumental for the eventual creation of at home test kits to determine the toxification of the patent and their potential response to treatment. Two other projects were the answers to problems brought to the Kingston Research Group by physicians looking for our expertise to answer: the quantitation of curcumin and detection or radon exposure. The radon exposure experiment resulted in a collaboration between the Kingston Laboratory and UPMC hospital system for method development and experimentation. The methods developed in this work have significantly improved analytically upon existing methods and have resulted in unique and unexpected collaborations.

DEDICATION

This text and all the work herein, is dedicated to my wife, Caitlin Turk, as well as caffeine. Through the two of which all things are possible.

ACKNOWLEDGEMENT

First, this work is would not have been possible without the continuing love and support of my wife, Caitlin Turk, who supported me emotionally, physically, and financially. Without her, truly, none of this would have been possible. I must thank my sister, Moriah Jamrom, and her husband, Daniel Critics, for listening patiently to me as I tried to explain my work, they did their best to humor me. I would also like to thank my father and stepmother, Joshua and Melinda Jamrom, for being patient with me and giving me the time to explore what I wanted to do with my life.

The work found in this document would not have been possible with the advice, input, and mentorship of many people. In terms of sheer contribution to its completion, my advisor, H. M. Skip Kingston, is to thank for his help with this dissertation. He gave me the space I needed to experiment and time to understand rather than rushing for explanations and publications. He kept funders away when the data was not what they had hoped for. But, most importantly, Skip demonstrated the traits necessary to be a successful scientist and I will take them with me the rest of my life.

I need to thank, or perhaps blame, Fredrick Ebert and Jamie McKee for helping me eventually choose this field of study. I am especially grateful to Mark Stauffer and Matthew Luderer for encouraging me to pursue a more advanced degree. Thank you to all my colleagues over the years for their support and assistance: specifically: Logan Miller, Weier Hao, James Henderson, Ashley Trouten, Lauren Stubbert, and Matt Pamukcu. Finally, I would like to thank Sean Fisher, without whom I would not have attended Duquesne University.

TABLE OF CONTENTS

Page

LIST OF TABLES

Page

LIST OF FIGURES

Page

LIST OF ABBREVIATIONS

Autism Spectrum Disorder (ASD)

MicroRNAs (miRNAs)

Autism Diagnostic Observation Schedule, Second Edition (ADOS-II)

Dried Blood Spots (DBS)

Thor's Hammer Isotope Dilution Mass Spectrometry (TH-IDMS)

Isotope Dilution Mass Spectrometry (IDMS)

Lower Limit of Quantification (LLOQ)

Mass Bias Factor (MB)

Inductively Coupled Plasma Mass Spectrometer (ICP)

Quantitative Dried Blood Spots (QDBS)

Persistent Organic Pollutants (POPs)

Cobalamin (B-12)

Methylmalonic Acid (MMA)

Succinic Acid (SUC)

Mass to Charge Ratio (m/z)

Acetonitrile (ACN)

Curcumin (CUR)

Tetrahydrocucumin (THC)

Demethoxycurcumin (DMC)

Bisdemethoxycurcumin (BDMC)

S-turmerone (TUR)

Curcumin-beta-D-Glucuronide (GLU-CUR)

Deuterated Curcumin (D-CUR)

Ultraviolet (UV)

High Pressure Liquid Chromatography (HPLC)

United States Food and Drug Administration (FDA)

Lower Limit of Detection (LLOD)

Limit of the Blank (LOB)

International Commission on Radiological Protection (ICRP)

National Institute of Standards and Technology (NIST)

International Union of Pure and Applied Chemistry (IUPAC)

Chapter 1: Introduction

1.1 Autism Spectrum Disorder Research

1.1.1 History of Autism Spectrum Disorder

Autism spectrum disorder (ASD) is a term used to describe a group of early-appearing social communication deficits and repetitive sensory–motor behaviors.[1] The hypotheses of causes of ASD have evolved as the understanding of the condition has increased, historically emphasizing a single cause. An early predominant theory, which persisted for several decades, argued that emotionally unresponsive parenting led children to withdraw into their own worlds and seek comfort in repetitive behaviors.[2] Perhaps predictably, blame was laid on the mother with the use of the term "refrigerator mom" which was believed cold, uncaring style of parenting traumatized her child such that they retreated into ASD.[3] Belief began to change as prominent autism researchers published opposing views that drew attention to biologic factors and predicted genetic underpinning of the condition with twin and family recurrence studies seeming to bolster the evidence of this theory.[4-6] Eventually, technology had improved and neuroanatomic observations,[7, 8] neuroimaging data and cytogenetics and links with genetic syndromes had demonstrated aberrant brain development,[9-11] establishing a pathobiological basis for ASD, replacing the psychogenic explanation.[12, 13]What followed was a focus on single gene mutations operating alone or in combination dominated ASD etiologic research.[14-17] Currently, some evidence supports a role for numerous small, rare genetic variants and a small amount of common variants which comprise the bulk of ASD heritability and, more broadly, epigenetic influences.[18, 19]

1.1.2 Epigenetic Cause of Autism Spectrum Disorder

DNA methylation, which has been implicated in the pathophysiology of neurological disorders, is one of the most well-known examples of epigenetic regulation that generally correlates with close chromatin conformation and thus transcriptional silencing.[20, 21] While some studies have been inconclusive, a recent study showed that the mRNAs encoding the epigenetic proteins ten-eleven translocation methylcytosine dioxygenases-1, -2, and -3 were increased, DNA methyltransferase 1 was decreased, while methyl CpG binding protein-2 was unchanged in the frontal cortex in the brains of ASD subjects.[22] MicroRNAs (miRNAs), as important regulators of gene expression as part of the epigenetic machinery, are small non-coding regulatory RNAs which mediate mRNA destabilization and/or translational repression have also been implicated in ASD.[23-25] The biogenesis pathway of miRNAs can be seen in **Figure 1.1**.[26] A shared pattern of miRNA dysregulation was observed in brains from ASD patients, specifically, hsa-miR-21-3p, a miRNA of unknown central nervous system function which is upregulated in ASD that targets neuronal genes downregulated in ASD.[27] Another miRNA identified was has_can_1002-m, a primate-specific miRNA that is downregulated in ASD which regulates the epidermal growth factor receptor and fibroblast growth factor receptor signaling pathways involved in neural development and immune function.[27]

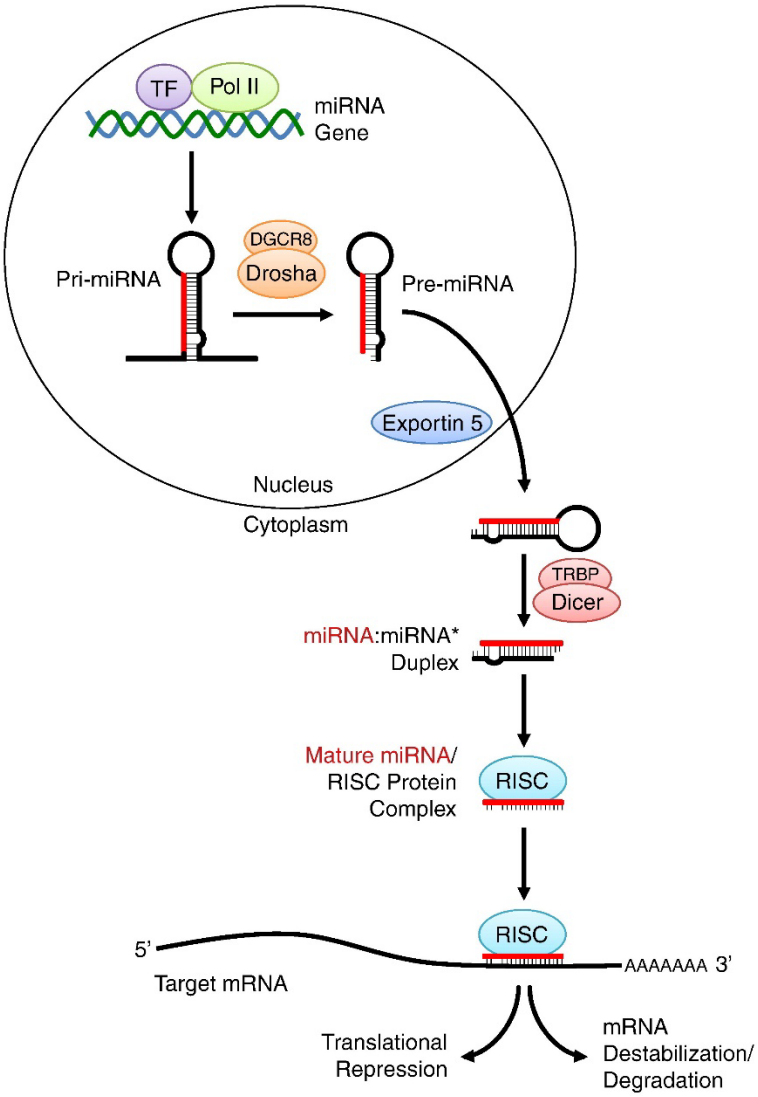

Figure 1.1. The miRNA biogenesis pathway. MiRNA genes are transcribed by RNA polymerase II, in combination with specific transcription factors, as long primary transcripts (pre-miRNA). These transcripts are then processed in the nucleus by the RNase III enzyme Drosha, in complex with DGCR8, into pre-miRNAs, which are exported into the cytoplasm by Exportin 5. Pre-miRNAs are processed by the RNase III enzyme Dicer, in complex with TRBP, into a duplex consisting of a guide strand (miRNA) and passenger star strand (miRNA*). The mature miRNA is loaded into the RNA-induced silencing complex (RISC) and acts as a guide strand that recognizes target mRNAs based on sequence complementarity. The RISC subsequently represses targets by inhibiting translation or promoting destabilization of target mRNAs. Taken from Gurtan and Sharp.[26]

While miRNA formation and regulation tells one part of the story, ASD is a complex condition which is believed to have more than one singular cause, and seems to, at least partially,

stem from toxification of the body or the depravation of essential nutrients.[28-30] Toxins, such as persistent organic pollutants and metals, as well as improper nutrition, may result in an increase of methylmalonic acid or a decrease in the reduced / oxidized glutathione ratio.[30-32] Toxins have been observed to alter the epigenome of the body, resulting in mistranslated miRNA which can increase gastrointestinal inflammation and decrease absorption of nutrients.[33-36] Should this gastrointestinal inflammation include the distal ileum, a known finding in children with regressive autism spectrum disorder,[37] cobalamin (B-12) absorption would be affected, which may result in an increased concentration of methylmalonic acid.[38] An emerging loss theory about treatment of children with autism spectrum disorder includes therapy for toxicant-induced loss of immune tolerance, a two-stage disease mechanism which results in an intolerance-like reaction which increases inflammation.[39, 40] This condition is often treated by a change of diet which includes the removal of the food causing intolerance, such as gluten, and the introduction of nutrients such as curcumin to reduce inflammation.[41, 42]

1.1.3 Autism Diagnostic Observation Schedule, Second Edition

The Autism Diagnostic Observation Schedule, Second Edition (ADOS-II) is a newly updated, semi-structured, standardized measure of communication, social interaction, play and imagination, and restricted and/or repetitive behaviors which was published by Western Psychological Services. [43, 44] The ADOS-II is used in clinical and research settings and is known as the "gold standard" for determination and diagnosis of ASD.[45] It can be administered and interpreted by professionals from medicine, psychology, or a related discipline in approximately 40 to 60 min, depending on the module selected and the specific behavior demonstrated by the examinee.[44] The ADOS-II kit is a large container consisting of most of the required toy items and

materials (some materials must be supplied and replenished by the examiner), and 10 protocols for each of the 5 modules.[44] The manual is expansive, beginning with an overview of the measure, guidelines for module selection, administration and coding procedures, instructions for each module, and case examples to assist with interpretation.[44] The precursor to the ADOS-II, the ADOS-I, was used by a psychologist trained to the level of experimental expertise, to confirm the diagnosis of autism prior to biomarker testing in this study.

1.1.4 Prevalence of autism spectrum disorder

The reported rates of ASD have been increasing since it was accepted as a medical diagnosis. How people think about and diagnose autism has changed substantially since the diagnosis was first introduced nearly 80 years ago, in 1943 by Leo Kanner.[46] In 1966, researchers estimated that about 1 in 2,500 children had autism, however this was focused on estimates of children at the severe end of the spectrum.[46] In 1980, ASD was first introduced into the Diagnostic and Statistical Manual of Mental Disorders.[46] In 1987, ASD was estimated to be in 1 in 1,400 children as it expanded the criteria by allowing a diagnosis even if symptoms became apparent after 30 months of age.[46] In 1991, the U.S. Department of Education ruled that a diagnosis of autism qualifies a child for special education services, which may have encouraged families to get a diagnosis of autism for their child.[46] Currently, 1 in 30 (3.49%) children in the United States, and 1 in 100 children (1%) throughout the world are diagnosed with ASD.[47] This increase may be partially explained by expanded diagnosis, including children formerly diagnosed with Asperger's syndrome, greater awareness for testing, allowing ASD to be diagnosed in tandem with attention deficit hyperactive disorder, screening in African American and Hispanic communities, and the recent trend of having children at an older age.[48]

1.2 Dried Blood Spots

As early as 1924, many of the major advantages of using dried blood spots (DBS) had been identified by Orren Chapman including: a reduction of volume of blood collected and lack of invasive sampling, which is important for pediatric medicine, a minimal risk of bacterial infection or hemolysis, and the ease of preservation of DBS samples.[49] One additional advantage of using DBS samples is the difficulty and expense of shipping viable blood samples internationally due to the risk of disease introduction.[50] DBS have been utilized as a diagnostic tool since 1963 when Robert Guthrie introduced the technique to determine phenylalanine in newborns.[51-53] Since that time, Guthrie's application has been replaced, but the use of DBS has expanded.[54-56] Under the proper storage conditions, low humidity without an air tight seal to prevent moisture build up and at -20 °C DBS cards can be stored and retrieved for over a year, and potentially longer, with some being stored from as far back as 1987[57-60] Once storage and testing of DBS are validated these spots could potentially be utilized throughout the life of a patient to test for changing health or environmental impacts.[59] An additional scarcity involves pediatric patients, who have a limit of available blood to draw based on weight.[61] Whether the sample is limited by time, or collection volume it is important to do more testing with less sample.

Despite their potential benefits, DBS testing tends to be qualitative rather than quantitative. This has many potential factors including method run time, low sample volume, and difficulty in creating calibration curves. Thus, the use of Isotope Dilution Mass Spectrometry (IDMS) can prove to be an invaluable tool. A traditional quantitation using calibration curves requires a bookended ten-point calibration curve with at least three quality control samples and blanks in addition to the samples themselves. The use of IDMS removes the need of calibration curves which greatly decreases the time requirement for testing as every sample is its own calibration curve.

Additionally, the use of DBS as a sampling tool can be difficult due to the loss of analyte when utilizing a fully automated system. This can be overcome by utilizing a novel analytical technique developed herein, known as Thor's Hammer Isotope Dilution Mass Spectrometry (TH-IDMS), for which a patent is being reviewed with no contention on nine out of ten claims (WO US2021055242).[62] TH-IDMS will be described in Chapter 4, but can provide accurate quantitation two orders of magnitude below previously established limits of detection on all mass spectrometers.

1.3 Development of Home Test Kits

For children with ASD, clinical blood draws can be difficult and traumatic due to the pain, discomfort of being in a new space, and fear of the patient.[63] This can often facilitate the necessity of abundant practice and application of coping mechanisms on the part of the parent and a expertly trained, and ideally specialized, medical individual on the part of the phlebotomist.[63] In addition to the logistical difficulties of drawing blood of children with ASD, there is a limit to the volume, and thus frequency of testing, of blood that can be drawn from children.[64] This can cause large lapses in metrology of intervention and, in absence of data, this can lead to negative outcomes as the physician is forced to rely only on qualitative testing, experience, and instinct. The lack of clear information makes dosing protocols and accuracy difficult for even the most practiced expert and leads to a trial-and-error medication schedule which can be traumatic for both the patient and their family and may lead to underdosing, which will slow time for proper symptom relief and overdosing may lead to toxicity. Both are associated with negative outcomes and would ideally be tested for routinely rather than the current annual or biannual testing from unreliable calibration curves. Thus, it would be of benefit to the patient and, potentially, their parent to be able to perform

these finger stick blood draws in a less painful, less intrusive, and more minimally invasive manner which would allow a more frequent schedule of testing. A finger stick is less traumatic for the patient, as compared to phlebotomy blood draws and can be performed at home by a parent with minimal training and utilizes a small amount of blood typically 10 – 30 μL of blood per blood spot.

One of the long-term goals of this project is to develop a home test kit for biomarkers and analytes in human blood which would allow for rapid, frequent, and minimally invasive testing for patients the globe over. While shipping viable blood samples across borders is difficult and fraught with regulation due to increased risk of transmissible disease and pandemic, the shipping of dried blood, a non-viable sample, is a relatively simpler affair.[65] Nonviable samples can be shipped through regular mail in a Teflon drying bag with desiccant agent to aid in drying. These kits are currently being developed and tested such that small, non-invasive finger sticks can be utilized for testing as frequently as necessary giving the physician more information to work with when administering medication and will, hopefully, lead to better and more rapid patient outcomes with fewer side effects as well as decreasing patient stress and allowing for a greater quality of life.

1.4 Radon Detection

1.4.1 Radon Origin

Radon is a colorless, odorless, and flavorless inert gas with a half-life of 3.8 days that occurs naturally from the decay of unstable isotopes of uranium or thorium.[66, 67] As radon is heavier than air, it tends to concentrate in enclosed spaces such as underground mines or basements, and is a major contributor to the ionizing radiation to which the general population is exposed.[68] While thorium is several times the concentration of uranium in the Earth's crust, the distribution is not

equivalent in all areas. Uranium and thorium are both unstable elements with long half-lives based on isotopic abundance. They are localized inside the contiguous United States at various approximate concentrations. In Western Pennsylvania, radon originating from uranium decay is deposited significantly in the Marcellus Shale region.[69, 70] Roughly 390 million years ago, what is now Western Pennsylvania was part of a large inland sea.[69] As the ocean retreated, uranium naturally found in sea water was left behind and salted the land. [71]Ocean water from the northern Atlantic contains two to four times more uranium than thorium.[72, 73]

1.4.2 Radon Prevalence

Despite remediation efforts developed through the Indoor Radon Abatement Act of 1988, there are still 21,000 small cell lung cancer deaths linked to radon exposure annually. Of these approximately 2,900 of have never smoked.[68, 71, 74] Worldwide total radon related deaths are estimated to be approximately 84,000 yearly, prominently noted in India and Korea. The US accounts for a quarter of these deaths.[68, 71] Currently, Allegheny County has an average indoor radon concentration of 6.5 pCi/L, significantly above the 4.0 pCi/L level deemed safe by the EPA.[75] Elevated radon levels are estimated to affect 43% of households in Allegheny County and may expose as many as 520,000 individuals.[75] This is a significant issue in this region and, as such, hospital networks in Allegheny County have been searching for diagnostic tests to determine if radon exposure has occurred. Presently, such a test is not available.

1.5 Equations

1.5.1 Isotope Dilution Mass Spectrometry

Quantification by isotope dilution mass spectrometry (IDMS) is based on the application and equilibration of an isotopically enhanced analog of each analyte of interest in the sample prior to extraction.[76, 77] The use of the IDMS equation, Equation 1.1, is predicated on the foreknowledge of certain information. This includes the isotopic abundance of both endogenous and isotopically labeled analyte, the amount of spike added to the known amount of sample, concentration of the spike added, and the altered isotopic ratio in the purchased isotopically labeled analyte. Where, C_X is an unknown, the concentration of the natural analog in the sample, C_S is the concentration of the isotopically labeled analog of the target molecule, W_S and W_X are the masses of the isotopic analog which has been spiked into the sample and the natural sample respectively, $^{13}A_S$ and $^{13}A_X$ are the abundance of the heavy isotope in the isotopic analog which has been spiked into the sample and the natural sample respectively(in this case carbon-13), $^{12}A_S$ and $^{12}A_X$ are the abundance of the light isotope in the isotopic analog which has been spiked into the sample and the natural sample respectively (in this case carbon-12), and $R_{13/12}$ is the measured ratio of heavy over light isotopes, which is measured in a mass spectrometer (in this case carbon-13/12).

$$C_x = \left(\frac{C_S W_S}{W_x}\right)\left(\frac{{}^{13}A_S - \left(R_{13/12}\,{}^{12}A_s\right)}{\left(R_{13/12}\,{}^{13}A_X\right) - {}^{12}A_x}\right) \quad \text{(Equation 1.1)}$$

Using this equation, the concentration of the endogenous molecule in the sample can be directly calculated through a mathematical comparison and not the use of traditional external calibration cuves.[78]

Being chemically identical an in equilibrium in solution, the endogenous and spiked isotopes are extracted with equivalent efficiency and recovery. These chemically indistinguishable

isotopically distinct analytes create an advantage in IDMS as compared to traditional calibration curves, even those utilizing internal standards and response factor quantification. Once equilibrium is achieved between endogenous and isotopically labeled compounds, IDMS can mathematically correct for 23 of the 26 errors associated with mass spectrometry, leaving only mass bias, dead time, and isobaric and polyatomic interferences.[78] Thus, IDMS reduces the contributions of random and analyst errors to overall quantitative quality, resulting in greater reliability and uniformity of accuracy and precision.

1.5.2 Error Propagation Factor

Reduction of the potential error associated with isotopic spiking in IDMS measurements require an optimum mixture of the spike and sample which can be calculated prior to experimentation.[79] Some pitfalls of the application of the isotopic spike can occur, namely the spiked sample ratio approaching the spike ratio, known as overspiking, or approaching the natural isotopic ratio, known as underspiking.[79] The effect of the error propagation factor is dependent on the mass spectrometric precision, and the relative enrichment of the spike isotope and natural isotope.[79] From an error propagation standpoint alone, the optimal mole ratio occurs when the determined ratio equals the square root of the product of the ratios of the spike and the natural isotope (Equation 1.2).[79] Error propagation factor equations can be plotted as curves with the optimal addition concentration being seen in the vertex.[79] Traditionally, the best mass spectrometric precision is achieved for ratios near one, however, due to the nature of the error propagation factor curve, there is usually several orders of magnitude in which adjustment of the isotopic mixture will not drastically affect the total error in negative catastrophic ways.[79] Later in this document these curves will be utilized to produce an amplification of signal and reduction of

error of analytes below the traditional limit of detection. With few exceptions, the atomic abundances of natural isotopes are constant and have been published.[80] Isotopic abundances of the spike are similarly known prior to experimentation as they are either tested for or supplied by the company from which the spike was purchased. With this information, it is a relatively simple task to determine the correct spiking ratio to add to an endogenous sample for optimal quantification.

$$EPF = \sqrt{\left(\frac{MI_{Spike}}{UI_{Spike}}\right) * \left(\frac{UI_{Sample}}{MI_{Sample}}\right)} \quad \text{(Equation 1.2)}$$

Where MI_{Spike} is the percentage of the main isotope in the spike, UI_{Spike} is the percentage of minor isotope in the spike, UI_{Sample} is the minor isotope in the sample, and MI_{Sample} is the percentage of major isotope in the sample.

1.5.3 Thor's Hammer Isotope Dilution Mass Spectrometry

Quantitation by TH-IDMS is based on the IDMS equation with the key difference of the addition of the MetaSpike™. After addition and equilibration, the MetaSpike™ elevates the signal of the analyte and reduces the signal-to-noise ratio allowing quantification below previously demonstrated lower limit of quantification (LLOQ). The MetaSpike™ is an artificially enhanced isotope mixture, usually with adjusted enrichments of between 20 and 80 percent natural analyte and the remainder a heavy (or light depending on the abundance of the natural isotope) isotopically enhanced version of the analyte which is used as internal standard, calibrant, and one point calibration curve which enables quantification from IDMS. While abundances must be taken and incorporated into the IDMS equation each time a MetaSpike™ is created, and possibly more

frequently if the isotope or analyte is unstable, there is little difference between the math of IDMS and the novel TH-IDMS. Application of the MetaSpike™ to endogenous sample of carbon can be seen in **Figure 1.2**. Proper application of the MetaSpike™ can raise the signal from an analyte below the limit of quantification and allow accurate quantitation far below the point at which calibration curves have ceased to be able to determine discrete data points.

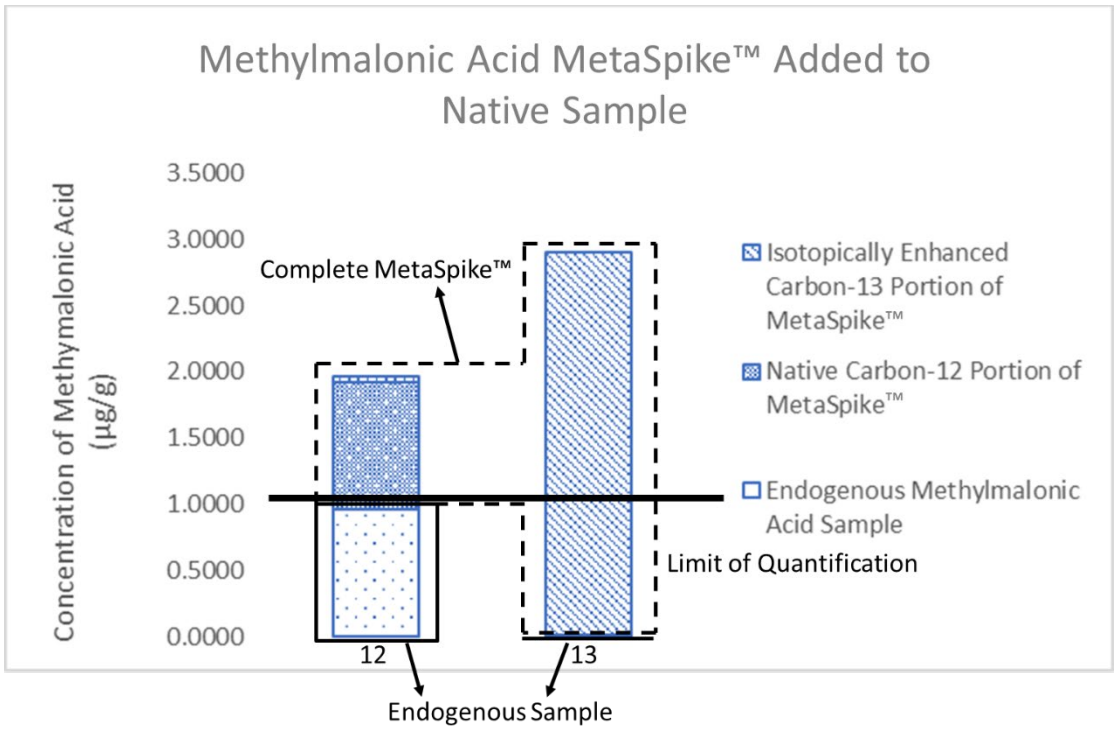

Figure 1.2. Addition of the MetaSpike™ to endogenous sample of carbon boosts the signal of the natural analyte above the previously determined limit of detection while simultaneously enabling the use of isotope dilution mass spectrometry and transforming it into a quantitative process known as Thor's Hammer isotope dilution mass spectrometry. As abundances of the MetaSpike™ are tested prior to analyte quantitation, the IDMS equation can be updated to reflect the new reality of the added spike.

1.5.4 Mass Bias Factor

A mass difference factor must be determined experimentally to mathematically correct for the differences in ionization between the natural and isotopic forms of an analyte in samples at identical concentrations.[81] This mass bias factor (MB), is applied as a correction factor to the isotope signals in the traditional IDMS equation, Equation 1.3.

$$C_x\left(\frac{\mu mol}{g}\right) = MB\left(\frac{C_s W_s}{W_x}\right)\left(\frac{{}^{13}A_s - \left(R_{13/12}\,{}^{12}A_s\right)}{\left(R_{13/12}\,{}^{12}A_x\right) - {}^{13}A_x}\right)$$

$$MB = \frac{A_N C_I}{A_I C_N}$$

(Equation 1.3)

Where A_N and A_I are the signal obtained from a QTOF-MS for the natural analyte and the isotopic analog, respectively.[81] C_N and C_I are the concentrations of the natural analyte and isotopic analog, respectively.[81] MB factors were computed for each compound that was reasonably obtainable and used as an internal correction factor in the quantitative method.

1.5.5 Mass Difference

The theory of special relativity shows a direct relationship between energy and mass, with a loss of mass directly correlating to a loss of energy. An example of this is what is known as mass bias, or the loss of energy (and thereby mass) from the formation of the atom ion and molecule.[82] Relativity is not confined to the nucleus. Bond energy and bond-dissociation energy are the measures of the binding energy between the atoms in a chemical bond, which appears as chemical energy. Typical chemical reactions involve a small net energy per mole which causes an even smaller change in mass per kg of substance. These defects are usually too small to be easily measured.[83] Due to the small loss of mass through the formation of a molecule, it is important to

use enough significant figures in the calculation to show the energy change. Rounding should not take place prior to the calculation, as this will result in a no mass difference. When calculating mass difference, the traditional calculation can be seen below in Equation 1.4.

$$MD = M - \left[\left(Z * \left(m_e + m_p\right)\right) + (N * m_n)\right] \text{ (Equation 1.4)}$$

Where M is the atomic mass of the atom, m_p is the mass of a proton (1.67262×10^{-27}), m_e is the mass of an electron (9.10938×10^{-31}), $m_n$is the mass of a neutron (1.67492×10^{-27}), Z is the number of protons, and N is number of neutrons.

When calculating the mass defect there is a slight change to the normally accepted formula. In this amended equation, when running in positive mode, there is one fewer electron due to its loss in the ionization process, while in negative mode, there is an extra electron present. This is signified by changing the atomic number times the mass of an electron to the atomic number minus one, or plus one multiplied by the mass of an electron which can be seen in Equation 1.5. Prior to calculations using data from the lab, these theoretical calculations can be done to compare the data taken from the mass spectrometer and determine a percent error associated with the mass spectrometer. As the ionization source was run in positive mode, the equation was amended to reflect the loss of an electron.

$$MD_I = M - \left[\left(\left(Z * m_p\right) + \left((Z-1) * m_e\right)\right) + (N * m_n)\right] \text{ (Equation 1.5)}$$

Using this amended mass difference equation, mass differences were calculated for lead isotopes obtained from National Institute of Standards and Technology and Oak Ridge National Laboratory traceable standards.

1.5.6 Mass Bias Magnitude Correction

There is a well-documented phenomena of isotopic bias when utilizing an inductively coupled plasma mass spectrometer (ICP). The measurement of isotopic ratios using an ICP will deviate from true values because of the preferential transport of the heavier isotopes into the mass analyzer.[84] Several different processes are considered to contribute to this deviation, including space charge effects in the region of the skimmer cone.[85] It is usual to assume that bias is a constant amount per unit mass and can be predicted and corrected by the following formula (Equation 1.6).[86]

$$R_{True} = R_{Measured}\,(1 + C)^{\delta m} \quad \text{(Equation 1.6)}$$

Where R_{True} is the true value, $R_{Measured}$ is the measured ratio, C is the mass bias, and δM is the mass difference. The mass bias magnitude correction was used in all measurements requiring the use of an ICP.

1.6 Relevance to Research

It was the objective of this research to develop a novel analytical technique which allows for the precise and accurate quantitation of ultra-trace analytes, with a proof of concept using the stable, organic molecule methylmalonic acid. This was done by taking principals of the chemistry

of standard addition and IDMS and combining them into a novel technique which is known as TH-IDMS which allows for accurate quantitation at two orders of magnitude below the determined LOQ. This technique was and will be used to quantitate ultra-trace analytes in a fully automated extraction of DBS matrixes for future development as a home test kit.

1.7 References

1. Lord, C.; Elsabbagh, M.; Baird, G.; Veenstra-Vanderweele, J., Autism spectrum disorder. *The Lancet* **2018,** *392* (10146), 508-520.

2. Bettelheim, B., *Infantile autism and the birth of the self*. Free Press: 1967.

3. Rimland, B., Infantile autism. **1964**.

4. Folstein, S.; Rutter, M., Genetic influences and infantile autism. *Nature* **1977,** *265* (5596), 726-728.

5. Pickles, A.; Bolton, P.; Macdonald, H.; Bailey, A.; Le Couteur, A.; Sim, C. H.; Rutter, M., Latent-class analysis of recurrence risks for complex phenotypes with selection and measurement error: a twin and family history study of autism. *American journal of human genetics* **1995,** *57* (3), 717.

6. Folstein, S. E.; Rutter, M. L., Autism: familial aggregation and genetic implications. *Journal of autism and developmental disorders* **1988,** *18* (1), 3-30.

7. Courchesne, E.; Yeung-Courchesne, R.; Hesselink, J.; Jernigan, T., Hypoplasia of cerebellar vermal lobules VI and VII in autism. *New England Journal of Medicine* **1988,** *318* (21), 1349-1354.

8. Piven, J.; Berthier, M. L.; Starkstein, S. E.; Nehme, E.; Pearlson, G.; Folstein, S., Magnetic resonance imaging evidence for a defect of cerebral cortical development in autism. *The American journal of psychiatry* **1990**.

9. Cohen, I. L.; Sudhalter, V.; Pfadt, A.; Jenkins, E. C.; Brown, W. T.; Vietze, P., Why are autism and the fragile-X syndrome associated? Conceptual and methodological issues. *American Journal of Human Genetics* **1991,** *48* (2), 195.

10. Folstein, S. E.; Piven, J., Etiology of autism: genetic influences. *Pediatrics* **1991,** *87* (5), 767-773.

11. Smalley, S. L.; Tanguay, P. E.; Smith, M.; Gutierrez, G., Autism and tuberous sclerosis. *Journal of autism and developmental disorders* **1992,** *22* (3), 339-355.

12. Wassink, T. H.; Piven, J., The molecular genetics of autism. *Current psychiatry reports* **2000,** *2* (2), 170-175.

13. Wassink, T. H.; Piven, J.; Patil, S. R., Chromosomal abnormalities in a clinic sample of individuals with autistic disorder. *Psychiatric genetics* **2001,** *11* (2), 57-63.

14. Abrahams, B. S.; Geschwind, D. H., Advances in autism genetics: on the threshold of a new neurobiology. *Nature reviews genetics* **2008,** *9* (5), 341-355.

15. Bartlett, C. W.; Gharani, N.; Millonig, J. H.; Brzustowicz, L. M., Three autism candidate genes: a synthesis of human genetic analysis with other disciplines. *International Journal of developmental neuroscience* **2005,** *23* (2-3), 221-234.

16. Bespalova, I. N.; Buxbaum, J. D., Disease susceptibility genes for autism. *Annals of medicine* **2003,** *35* (4), 274-281.

17. Wassink, T. H.; Brzustowicz, L. M.; Bartlett, C. W.; Szatmari, P., The search for autism disease genes. *Mental retardation and developmental disabilities research reviews* **2004,** *10* (4), 272-283.

18. Gaugler, T.; Klei, L.; Sanders, S. J.; Bodea, C. A.; Goldberg, A. P.; Lee, A. B.; Mahajan, M.; Manaa, D.; Pawitan, Y.; Reichert, J., Most genetic risk for autism resides with common variation. *Nature genetics* **2014,** *46* (8), 881-885.

19. Eshraghi, A. A.; Liu, G.; Kay, S. S.; Eshraghi, R. S.; Mittal, J.; Moshiree, B.; Mittal, R., Epigenetics and Autism Spectrum Disorder: Is There a Correlation? *Front Cell Neurosci* **2018,** *12*, 78.

20. Ellis, S. E.; Gupta, S.; Moes, A.; West, A. B.; Arking, D. E., Exaggerated CpH methylation in the autism-affected brain. *Molecular Autism* **2017,** *8* (1), 1-8.

21. Ladd-Acosta, C.; Hansen, K. D.; Briem, E.; Fallin, M. D.; Kaufmann, W. E.; Feinberg, A. P., Common DNA methylation alterations in multiple brain regions in autism. *Molecular psychiatry* **2014,** *19* (8), 862-871.

22. Zhubi, A.; Chen, Y.; Guidotti, A.; Grayson, D. R., Epigenetic regulation of RELN and GAD1 in the frontal cortex (FC) of autism spectrum disorder (ASD) subjects. *International Journal of Developmental Neuroscience* **2017,** *62*, 63-72.

23. Hammond, S. M., An overview of microRNAs. *Advanced drug delivery reviews* **2015,** *87*, 3-14.

24. Mohr, A. M.; Mott, J. L. In *Overview of microRNA biology*, Seminars in liver disease, Thieme Medical Publishers: 2015; pp 003-011.

25. Soltanzadeh-Yamchi, M.; Shahbazi, M.; Aslani, S.; Mohammadnia-Afrouzi, M., MicroRNA signature of regulatory T cells in health and autoimmunity. *Biomedicine & Pharmacotherapy* **2018,** *100*, 316-323.

26. Gurtan, A. M.; Sharp, P. A., The role of miRNAs in regulating gene expression networks. *J Mol Biol* **2013,** *425* (19), 3582-600.

27. Wu, Y. E.; Parikshak, N. N.; Belgard, T. G.; Geschwind, D. H., Genome-wide, integrative analysis implicates microRNA dysregulation in autism spectrum disorder. *Nature neuroscience* **2016,** *19* (11), 1463-1476.

28. Jick, H.; Kaye, J. A., Epidemiology and possible causes of autism. *Pharmacotherapy: The Journal of Human Pharmacology and Drug Therapy* **2003,** *23* (12), 1524-1530.

29. Main, P. A.; Angley, M. T.; O'Doherty, C. E.; Thomas, P.; Fenech, M., The potential role of the antioxidant and detoxification properties of glutathione in autism spectrum disorders: a systematic review and meta-analysis. *Nutrition & metabolism* **2012,** *9* (1), 1-37.

30. Faber, S.; Fahrenholz, T.; Wolle, M. M.; Kern, J. C., 2nd; Pamuku, M.; Miller, L.; Jamrom, J.; Skip Kingston, H. M., Chronic exposure to xenobiotic pollution leads to significantly higher total glutathione and lower reduced to oxidized glutathione ratio in red blood cells of children with autism. *Free Radic Biol Med* **2019,** *134*, 666-677.

31. Boggess, A.; Faber, S.; Kern, J.; Kingston, H. M. S., Mean serum-level of common organic pollutants is predictive of behavioral severity in children with autism spectrum disorders. *Sci Rep* **2016,** *6*, 26185.

32. Faber, S.; Zinn, G. M.; Kern Ii, J. C.; Skip Kingston, H. M., The plasma zinc/serum copper ratio as a biomarker in children with autism spectrum disorders. *Biomarkers* **2009,** *14* (3), 171-180.

33. Tiffon, C., The impact of nutrition and environmental epigenetics on human health and disease. *International journal of molecular sciences* **2018,** *19* (11), 3425.

34. Dai, R.; Ahmed, S. A., MicroRNA, a new paradigm for understanding immunoregulation, inflammation, and autoimmune diseases. *Transl Res* **2011,** *157* (4), 163-79.

35. O'Connell, R. M.; Rao, D. S.; Baltimore, D., microRNA Regulation of Inflammatory Responses. *Annual Review of Immunology* **2012,** *30* (1), 295-312.

36. Kushak, R. I.; Buie, T. M.; Murray, K. F.; Newburg, D. S.; Chen, C.; Nestoridi, E.; Winter, H. S., Evaluation of Intestinal Function in Children With Autism and Gastrointestinal Symptoms. *J Pediatr Gastroenterol Nutr* **2016,** *62* (5), 687-91.

37. Ashwood, P.; Anthony, A.; Pellicer, A. A.; Torrente, F.; Walker-Smith, J. A.; Wakefield, A. J., Intestinal lymphocyte populations in children with regressive autism: evidence for extensive mucosal immunopathology. *J Clin Immunol* **2003,** *23* (6), 504-17.

38. Stabler, S. P., Clinical practice. Vitamin B12 deficiency. *N Engl J Med* **2013,** *368* (2), 149-60.

39. Masri, S.; Miller, C. S.; Palmer, R. F.; Ashford, N., Toxicant-induced loss of tolerance for chemicals, foods, and drugs: assessing patterns of exposure behind a global phenomenon. *Environmental Sciences Europe* **2021,** *33* (1).

40. Genuis, S. J.; Lobo, R. A., Gluten sensitivity presenting as a neuropsychiatric disorder. *Gastroenterology research and practice* **2014,** *2014*.

41. Heilbrun, L. P.; Palmer, R. F.; Jaen, C. R.; Svoboda, M. D.; Perkins, J.; Miller, C. S., Maternal chemical and drug intolerances: potential risk factors for autism and attention deficit hyperactivity disorder (ADHD). *The Journal of the American Board of Family Medicine* **2015,** *28* (4), 461-470.

42. Irving, G. R.; Karmokar, A.; Berry, D. P.; Brown, K.; Steward, W. P., Curcumin: the potential for efficacy in gastrointestinal diseases. *Best practice & research Clinical gastroenterology* **2011,** *25* (4-5), 519-534.

43. McCrimmon, A.; Rostad, K., Test Review: Autism Diagnostic Observation Schedule, Second Edition (ADOS-2) Manual (Part II): Toddler Module. *Journal of Psychoeducational Assessment* **2013,** *32* (1), 88-92.

44. Luyster, R., Autism Diagnostic Observation Schedule, (ADOS-2) Manual (Part II): Toddler Module. **2012**.

45. Kanne, S. M.; Randolph, J. K.; Farmer, J. E., Diagnostic and assessment findings: a bridge to academic planning for children with autism spectrum disorders. *Neuropsychol Rev* **2008,** *18* (4), 367-84.

46. Zeidan, J.; Fombonne, E.; Scorah, J.; Ibrahim, A.; Durkin, M. S.; Saxena, S.; Yusuf, A.; Shih, A.; Elsabbagh, M., Global prevalence of autism: A systematic review update. *Autism Res* **2022,** *15* (5), 778-790.

47. Li, Q.; Li, Y.; Liu, B.; Chen, Q.; Xing, X.; Xu, G.; Yang, W., Prevalence of Autism Spectrum Disorder Among Children and Adolescents in the United States from 2019 to 2020. *JAMA Pediatr* **2022**.

48. Hultman, C. M.; Sandin, S.; Levine, S. Z.; Lichtenstein, P.; Reichenberg, A., Advancing paternal age and risk of autism: new evidence from a population-based study and a meta-analysis of epidemiological studies. *Mol Psychiatry* **2011,** *16* (12), 1203-12.

49. Chapman, O. D., The Complement-Fixation Test for Syphilis. *Archives of Dermatology and Syphilology* **1924,** *9* (5).

50. WHO, Guidance on Regulations for the Transport of Infectious Substances 2021-2022. Geniva, 2021.

51. Guthrie, R.; Susi, A., A Simple Phenylalanine Method for Detecting Phenylketonuria in Large Populations of Newborn Infants. *Pediatrics* **1963,** *32* (3), 338-343.

52. Kand'ar, R.; Zakova, P., Determination of phenylalanine and tyrosine in plasma and dried blood samples using HPLC with fluorescence detection. *J Chromatogr B Analyt Technol Biomed Life Sci* **2009,** *877* (30), 3926-9.

53. Hofman, L. F.; Roe, C. R.; Kahler, S. G.; Terada, N.; Millington, D. S.; Chace, D. H., Rapid diagnosis of phenylketonuria by quantitative analysis for phenylalanine and tyrosine in neonatal blood spots by tandem mass spectrometry. *Clinical Chemistry* **1993,** *39* (1), 66-71.

54. Lehmann, S.; Delaby, C.; Vialaret, J.; Ducos, J.; Hirtz, C., Current and future use of "dried blood spot" analyses in clinical chemistry. *Clin Chem Lab Med* **2013,** *51* (10), 1897-909.

55. Crossle, J.; Elliot, R. B.; Smith, P., Dried-Blood Spot Screening for Cystic Fibrosis in the Newborn. *The Lancet* **1979,** *313* (8114), 472-474.

56. McDade, T. W.; Williams, S.; Snodgrass, J. J., What a drop can do: dried blood spots as a minimally invasive method for integrating biomarkers into population-based research. *Demography* **2007,** *44* (4), 899-925.

57. Mei, J., Dried Blood Spot Sample Collection, Storage, and Transportation. In *Dried Blood Spots*, 2014; pp 21-31.

58. Gruner, N.; Stambouli, O.; Ross, R. S., Dried blood spots--preparing and processing for use in immunoassays and in molecular techniques. *J Vis Exp* **2015,** (97).

59. Sok, P.; Lupo, P. J.; Richard, M. A.; Rabin, K. R.; Ehli, E. A.; Kallsen, N. A.; Davies, G. E.; Scheurer, M. E.; Brown, A. L., Utilization of archived neonatal dried blood spots for genome-wide genotyping. *PLoS One* **2020,** *15* (2), e0229352.

60. Batterman, S.; Chernyak, S., Performance and storage integrity of dried blood spots for PCB, BFR and pesticide measurements. *Sci Total Environ* **2014,** *494-495*, 252-60.

61. Becan-McBride, D. G. a. K., *Phlebotomy Handbook : Blood Collection Essentials*. Prentice Hall, Inc: 2018; Vol. 10th, p 672.

62. Kingston, H. M. Quantification of previously undetectable quantities cross-referene to related applcation. 2022.

63. Speaks, A., Parent's Guide to Blood Draws for Children with Autism. Network, A. S. A. T., Ed. 2011.

64. Howie, S. R., Blood sample volumes in child health research: review of safe limits. *Bull World Health Organ* **2011,** *89* (1), 46-53.

65. USDOT, Transporting infectious substances safely. Transportation, D. o., Ed. Pipeline and Hazardous Materials Safety Administration Outreach, Engagement, and Grants Division: Washington DC, 2011.

66. Samet, J. M., Radon and lung cancer. *J Natl Cancer Inst* **1989,** *81* (10), 745-57.

67. Al-Zoughool, M.; Krewski, D., Health effects of radon: a review of the literature. *Int J Radiat Biol* **2009,** *85* (1), 57-69.

68. WHO, WHO Handbook on Indoor Radon: A Public Health Perspective. World Health Organization: France, 2009.

69. Rose, A. W., Schmiermund, Ronald L., and Mahar, Dennis L. , Geochemical dispersion of uranium near prospects in Pennsylvania. Administration, U. S. E. R. a. D., Ed. Pennsylvania State University, 1977.

70. Klemic, H., Uranium Occurances in Sedementary Rocks of Pennsylvania. Survey, U. G., Ed. Washington DC, 1962; pp 243-287.

71. USEPA Health Risk of Radon https://www.epa.gov/radon/health-risk-radon (accessed May 12, 2022).

72. EXXON NUCLEAR COMPANY, I., Extraction of Uranium from Seawater: Evaluation of Uranium Resources and Plant Siting Volume 1. Energy, U. D. o., Ed. Oregon State University, 1979; Vol. XN-RT-14, p 168.

73. Smith, K. J.; Leon Vintro, L.; Mitchell, P. I.; Bally de Bois, P.; Boust, D., Uranium-thorium disequilibrium in north-east Atlantic waters. *J Environ Radioact* **2004,** *74* (1-3), 199-210.

74. Yoon, J. Y.; Lee, J. D.; Joo, S. W.; Kang, D. R., Indoor radon exposure and lung cancer: a review of ecological studies. *Ann Occup Environ Med* **2016,** *28*, 15.

75. PADEPA, Pennsylvania Citizen's Guide to Radon. 5/2021 ed.; Protection, P. D. o. E., Ed. Harrisburgh, 2021; p 24.

76. Agency, U. E. P., Method 6800: Elemental and speciated isotope dilution mass spectrometry. Agency, U. S. E. P., Ed. Washington DC, 2007.

77. De Hevesy, G., Some applications of isotopic indicators. *Nobel Lecture* **1944,** *12*.

78. Aggarwal, S.; Ichikawa, H.; Takada, Y.; Sandur, S. K.; Shishodia, S.; Aggarwal, B. B., Curcumin (diferuloylmethane) down-regulates expression of cell proliferation and antiapoptotic

and metastatic gene products through suppression of IkappaBalpha kinase and Akt activation. *Mol Pharmacol* **2006,** *69* (1), 195-206.

79. Rodríguez-González, P.; Garcia Alonso, J., Isotope Dilution Mass Spectrometry. 2018.

80. Patterson, K. Y.; Veillon, C.; O'Haver, T. C., Error Propagation in Isotope Dilution Analysis As Determined by Monte Carlo Simulation. *Analytical Chemistry* **2002,** *66* (18), 2829-2834.

81. Wagner, R.; Wetzel, S. J.; Kern, J.; Kingston, H. M., Improved sample preparation of glyphosate and methylphosphonic acid by EPA method 6800A and time-of-flight mass spectrometry using novel solid-phase extraction. *J Mass Spectrom* **2012,** *47* (2), 147-54.

82. Frisch, A. M., Thorndike, David H., *Elementary Particles*. 1 ed.; D. Van Nostrand Company: 1964.

83. DOE, DOE Fundamentals Handbook: Nuclear Physics and Reactor Theory. Energy, D. o., Ed. U.S. Department of Energy: Washington, D.C. 20585, 1993; Vol. 1 of 2, p 142.

84. Walder, A. J.; Freedman, P. A., Communication. Isotopic ratio measurement using a double focusing magnetic sector mass analyser with an inductively coupled plasma as an ion source. *Journal of Analytical Atomic Spectrometry* **1992,** *7* (3).

85. Gillson, G. R.; Douglas, D. J.; Fulford, J. E.; Halligan, K. W.; Tanner, S. D., Nonspectroscopic interelement interferences in inductively coupled plasma mass spectrometry. *Analytical Chemistry* **1988,** *60* (14), 1472-1474.

86. Russ III, G. P.; Bazan, J., Isotopic ratio measurements with an inductively coupled plasma source mass spectrometer. *Spectrochimica Acta Part B: Atomic Spectroscopy* **1987,** *42* (1-2), 49-62.

Chapter 2. Detection and quantification of stable organic molecule methylmalonic acid on quantitative dried blood spot cards as a proof of concept for stable dried blood spot testing.

2.1 Introduction

As early as 1924, many of the major advantages of using dried blood spots (DBS) had been identified by Orren Chapman including: a reduction of volume of blood collected and lack of invasive sampling, which is important for pediatric medicine; a minimal risk of bacterial infection or hemolysis; and the ease of preservation of DBS samples.[1] One additional advantage of using DBS samples is the difficulty and expense of shipping viable blood samples internationally due to the risk of disease introduction. [2] DBS have been utilized as a diagnostic tool since 1963 when Robert Guthrie introduced the technique to determine phenylalanine in newborns.[3-5] Since that time, Guthrie's application has been replaced, but the use of DBS has expanded.[6-8] Under the proper storage conditions, low humidity without an air tight seal to prevent moister build up and at -20 °C DBS cards can be stored and retrieved for over a year, and potentially longer, with some being stored from as far back as 1987[9-12] Once storage and testing of DBS are validated these spots could potentially be utilized throughout the life of a patient to test for changing health or environmental impacts.[11] An additional scarcity involves pediatric patients, who have a limit of available blood to draw based on weight.[13] Whether the sample is limited by time, or collection volume it is important to do more testing with less sample.

Several challenges have, thus far, hindered the wider adoption of DBS as analytical matrix including correlations between venous and capillary blood concentrations, contamination risk, lack of sensitivity, chromatographic effect and influence of the site of punching, influence of spotted blood volume, and most difficult to overcome, the hematocrit effect.[14] With the exception of

hematocrit, these hinderances can be overcome by the use of a fully automated desorption system, such as the Gerstel DBSA system which allows for rapid and repeatable extraction from the cellulose matrix of a DBS card. Hematocrit is defined as the volume fraction of the blood that is taken in by red blood cells (**Figure 2.1**). Reference ranges are available at the population level (approximately 0.41–0.50 for men and 0.36–0.44 for women),[15] however important inter- as well as intra-individual differences exist.[16] Among the factors determining the hematocrit are age, sex, health, and nutritional status with higher values observed in newborns, people living at high altitudes, and persons suffering from lung diseases such as polycythemia or chronic obstructive pulmonary disease.[16] Hematocrit varies between patients and even individual hematocrit values have been known to change throughout the day due to hydration.[17] Thus, constructing accurate calibration curves proves to be elusive.[14] Due to these complications, it is difficult to use DBS as a quantifiable matrix through the application of calibration curves which would require individualized standard addition calibration curves per patient made with excess blood taken at the time of draw.[14] Several strategies to overcome what is known as the hematocrit effect have been employed such as the development of commercially available special filtration substrates for cards which separate and lessen the hematocrit effects.[18] A second strategy to overcome hematocrit effects is to measure and correct for these effects by measuring the concentration of potassium or lithium in the dried blood spot have been attempted.[18] These strategies, while potentially promising, have not been validated and are yet to be widely adopted by those who attempt quantification on DBS cards. A potentially more efficient way of quantification than using traditional calibration curves which would overcome inherent biases, isotope dilution mass spectrometry (IDMS) should be considered and applied.

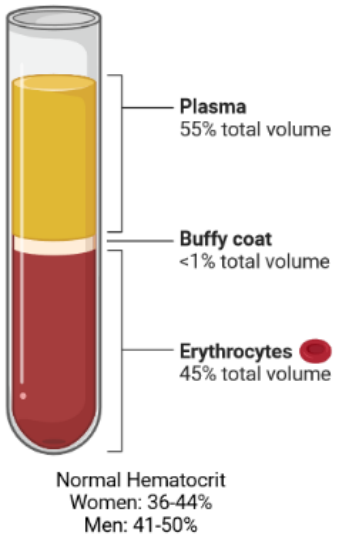

Figure 2.1. Relative makeup of hematocrit (percentage of erythrocytes) in whole blood along.

One use of an IDMS method utilized is the refinement and improvement of methylmalonic acid testing previously performed by Quest Diagnostics during the initial ASD study by other methods, such as UV-VIS spectroscopy or an enzyme-linked immunosorbent assay.[19] Utilization of mass spectrometry on this matter can be difficult, however, due to interferences of the confirmational isomer, succinic acid.[20-22] These measurements being further developed focus on quantification using IDMS due to the unparalleled accuracy, removing 23 of the 26 possible interference or noise issues that occur while using mass spectrometry.[23, 24]

IDMS is a quantification technique developed by George de Hevesy which won a Nobel Prize in 1943.[25] IDMS allows for accurate quantitation without the use of a calibration curve by means of isotopic measurement, or perhaps it is better explained as the use of a one-point internal calibration curve. A heavy isotopic labeled version of the analyte in question, which does not exist in high quantity in the natural world, is purchased or synthesized and added to a sample and equilibrated. Once equilibrated, the foreknowledge of the weight and concentration of this isotopically labeled molecule allows for accurate quantitation without the use of a calibration curve

using the IDMS equation (Equation 1). This combined with the knowledge that the chemistry of the isotopes is identical, meaning the rate of ionization of the added spike and the natural chemical are similar in most cases, allow for quantitation to be based on ratio without time constraints of using calibration curves. Compared to traditional calibration curves, both accuracy and precision are increased even at low levels. The application of IDMS to a DBS matrix allows for the DBS to be quantitative (QDBS).

However, care must be taken when choosing or synthesizing isotopically labeled analyte. Attention must be given to the overall isotopic mass shift. The mass shift should not overlap with the masses of any other potential analyte or interference, which requires some research on the part of the analyst prior to the start of the project.[26] Attention should also be paid to the species of labeled isotope and the potential placement on the molecule.[26] The placement of the isotopic species must be on a position on the molecule which will not react during sample preparation and will not exchange with any other species or fall off in a reaction. The placement must also survive and remain attached to the major molecule fragment post reaction in a collision cell.[26] These isotopically enhanced species need not exclusively be heavier than the natural analyte, it must only be a unique isotopic weight and an exact molecular copy of the analyte of interest. In addition, some isotopic analytes are preferable to others. For example, an isotopically enhanced carbon-13 version of a molecule is preferable to a deuterated version of a molecule.[26] This is due to frequency of hydrogen exchange on organic molecules,[27] and the retention time shift on HPLC systems due to Van der Waals interactions.[28]

The prevalence of Autism Spectrum Disorder (ASD) has been increasing throughout the world with estimates from the Centers for Disease Control and Prevention stating that in the United States, at least one in thirty children are on the spectrum.[29] This phenomenon is not limited to the

western world and reported global rates of ASD have been increasing throughout the developed world.[30] Despite the increased prevalence of the reporting of disease in all age groups, and attempts to use techniques such as machine learning, questionnaires, and gene expression tests, no predictive test yet exists for use in the medical community.[31-33] Physicians are currently limited to diagnostic tools, such as the Autism Diagnostic Observation Schedule 2 (ADOS-II) and the Autism Diagnostic Interview.[34-36] Continued research has linked environmental factors, such as persistent organic pollutants (POPs),[37, 38] to the degradation of body systems which can help detoxify the body, such as glutathione levels which helps mitigate toxins and oxidative stress.[23, 39] Measurements of 409 parameters in a recent $1.4 million dollar study have identified 21 statistically significant biomarkers.[19, 40] One of these biomarkers was an increase in the levels of methylmalonic acid (MMA) in the blood.

MMA buildup in the body is most associated with a deficiency in cobalamin (B-12), though a small minority of patients have a genetic predisposition to not producing the enzyme methylmalonyl-CoA mutase. B-12 plays an essential role in several important processes of brain growth and development such as: DNA synthesis, methylation of biomolecules, and odd-chain fatty acid metabolism.[41] B-12 deficiency has been implicated in disorders including anemia, megaloblastosis, neuropathy, neuropsychiatric disorders, and ASD.[42] The most serious manifestations are neurologic: demyelination followed by axonal degeneration.[43] One common form of B-12 deficiency is known as “pernicious anemia” where in the patient fails to absorb vitamin B-12 due to intrinsic factor deficiency.[43] B-12 levels are difficult to measure directly, however, due to biologically low levels of the vitamin and the fact that B-12 is highly protein bound.[44] The simplest method for determining the extent of B-12 deficiency is to measure it indirectly by quantifying MMA.[44] MMA is directly related to levels of B-12, but found in 1000-

fold higher concentrations in the blood than B-12.[44] MMA is an intermediate in the conversion of propionic acid to succinic acid (SA) which requires B-12 as a cofactor and has a normal range in the human body of 70 nmol/L to 270 nmol/L.[45-47] Elevated MMA levels, known as methylmalonic aciduria, are caused by one of at least eight inherited diseases which stem from a deficiency in the mitochondrial enzyme methylmalonyl-CoA mutase or in the synthesis of its cofactor, 5'-deoxyadenosylcobalamin.[48-50]

In healthy odd-chain fatty-acid metabolism propionyl-CoA is converted to succinyl-CoA, in a process that involves three enzymes, which is then inserted into the citric acid cycle.[51] First, Propionyl-CoA is carboxylated to form (D)-methylmalonyl-CoA by a biotin containing molecule, propionyl-CoA carboxylase, and the hydrolysis of an adenosine triphosphate (ATP) molecule.[51] Second, (D)-methylmalonyl-CoA is converted to (L)-methylmalonyl-CoA by methylmalonyl-CoA epimerase.[51] Finally, (L)-methylmalonyl-CoA is then repositioned to form succinyl-CoA by a coenzyme of methylmalonyl-CoA mutase and B-12.[51] MMA forms when methylmalonyl-CoA mutase fails to function properly either through genetic deficiency or (more commonly) through B-12 deficiency.[51] A visual representation of this metabolic pathway can be seen in **Figure 2.2**.

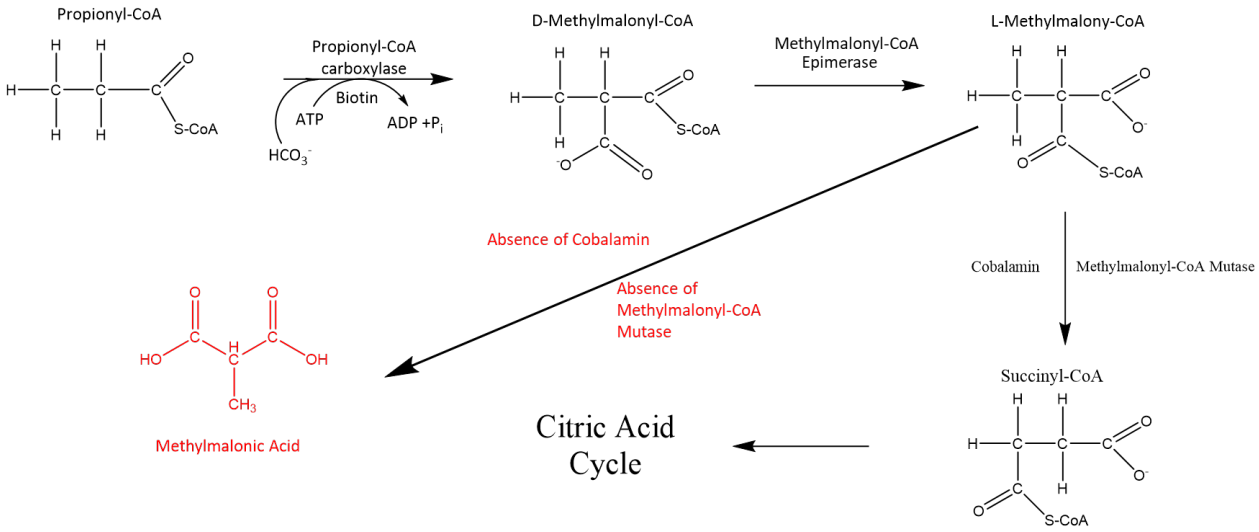

Figure 2.2. The metabolic pathway from propionyl coenzyme A, the final product of Lipolysis of odd-chain fatty acids. If there is a deficiency in cobalamin or methylmalonl coenzyme A mutase, a toxic and potentially fatal buildup of methlmaonic acid will occur.

MMA is widely tested in neonates through heal sticks or urine as a qualitative test, but is often not tested for beyond infancy as the diagnosis of B-12 deficiency can be problematic.[52] MMA has been determined to be a marker for disease states, specifically those affecting the brain, in all ages of human development, but especially in those of early childhood.[53] Experimentation in rats has produced several neurological structural changes such as delayed myelination of neurons and hypodensity of the globi pallidi, resulting in permanent neurological damage and changes in the basal ganglia.[54] These effects are the result of hypoglycemia in the maturing brain.[54] The immature mammalian brain generally utilizes both glucose and ketone bodies for metabolism and energy production.[54] MMA inhibits an important enzyme inhibits the transportation of malate into the mitochondrial matrix, which results in significantly lower than average levels of ATP.[54] MMA is also known to be a competitive inhibitor of succinate dehydrogenase, which would further decrease cell ATP by limiting gluconeogenesis through blocked pathways in the citric acid cycle.[54]

For the past twenty years, the most effective instrument for separating MMA from similarly weighted non-polar molecules such as SA (**Figure 2.3**) has been utilizing a high-pressure liquid chromatography (HPLC) system. One of the most common obstacles for MMA analysis in biological fluids is the presence of other low-molecular weight organic acids such as SA, a product of MMA degradation and a constitutional isomer, which is present in concentrations even higher than the desired analyte (2-20 μM SA vs. 0-0.4 μM SA).[44] SA interference is difficult to overcome due to almost identical chromatographic characteristics and mass spectrometer fracturing as MMA.[44] Columns for this technique have become more specialized and there is a great range that can be selected for greater sensitivity to provide wider, more dynamic peaks in the mass spectrometer. The field of mass spectrometry has also been shown to be quite effective testing for MMA, both from whole blood and urine.[48, 55]

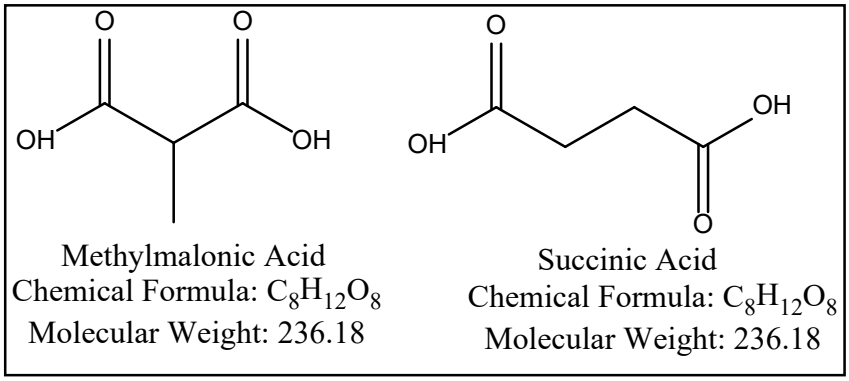

Figure 2.3. Molecular structure and mass of methylmalonic and succinc acid. These are conformational isormers which require separation on a liquid chromatography system for accurate quantification.

One of the most efficient ways to allow these tests to be administered around the world is through the development of a quantitative blood card, which will allow for fast and accurate testing. Utilizing methods that have already been developed and reproduced to practice, the first

fully automated blood card method will use an automated dried blood card isotopic quantitative method. These methods use isotope quantification of DBS systems. New research applications of these methods will be applied for individuals and children which will be assessed in a clinical study with Dr. Scott Faber.

2.2 Materials and Methods

2.2.1 Chemicals and Sample Preparation

MMA purchased from Sigma Aldrich (Lot STBB4671) and SUC purchased from Alfa Aesar (Lot Y12A042) were made into standards of approximately 1 µg/g being dissolved in 15-mL Fisher Scientific (Lot 035329) in Fisherbrand metal free disposable centrifuge tubes (Lot 26920041) utilizing 18.2 MΩ deionized water was which was made in lab using a 7146 Barnstead NANOpure system (Model 251115-102), which was then passed through a D7035 Easypure II water filtration system (Model 1305080906425). These solutions were allowed to mix on a Vortex Genie 2 Digital Serial (Model A3-1896) for 30 seconds at 5000 RPM. The samples were then filtered via a 10-mL Norm-Ject luer lock solo syringe (Lot 20F01C8) and passed through a 0.22 µm pore size polypropylene Agilent technologies filter (Lot FG4627). Solutions of MMA, SUC, and a combination of the two were made and used for liquid chromatography separation and mass spectrometry optimization. Once separation and optimization had been achieved an 4C13 isotopically enhanced standard of MMA was purchased from Cerillant (Lot FN06121302) which had been enhanced to 98.53%, which was diluted with 18.2 MΩ deionized water to create an 84.037 ng/g isotopically enhanced standard, which would be utilized as an internal standard for calibration curve measurements as well as heavy isotopic standards for IDMS quantification. It was determined using error propagation factors that samples should be spiked 0.08 µmol of 4C-13

in an optimal ratio of 0.85 natural to isotopically enhanced MMA per 200 µL of sample for optimal quantification.

Blood and serum samples were made first from bovine whole blood and serum with Ethylenediaminetetraacetic acid purchased from Lampire on 11/29/2016 which had been stored in a -80 °C freezer until needed and was then thawed overnight on ice which had been spiked with MMA and SUC Blood card testing was application of 20 µL of spiked bovine blood samples to cellulose Whatman C-Pak cards (Lot ET7059416). These blood and serum samples were created with a concentration of 0.0349 µg/g MMA and 0.0367 µg/g isotopically enhanced MMA and allowed to dry on the Whatman C-Pack blood cards for 24 hours. Manual extraction was performed by removal of the dried blood spot from the Whatman C-Pack blood card utilizing a Harris Uni-Core 8-mm diameter manual blood spot hole punch (), cutting the blood spot into quarters, then placing the pieces into an Avantor 1.5 mL microcentrifuge tube (Lot 211009653-D) with a 50:50 (w/w) solution of 500 µL of acetonitrile and 18.2 MΩ deionized water which was placed in a Branson sonicator (Model 5510) for one-hour at 60 °C. Samples were mixed on a Model SI-A236 Vortex Genie 2 Digital for 1 minute at 3000 rpm, and centrifuged in a Model AG 5453 Eppendorf Mini Spin Plus centrifuge for 10 minutes at 30000 rpm. Supernatant was collected in an additional 1.5 mL microcentrifuge tube and the process was repeated two additional times to extract the maximum concentration of analyte. Microcentrifuge tubes were then dried and concentrated in a Model SPD1010-115 ThermoFisher Savant SpeedVac Concentrator which was programed to run a vacuum pressure of 5.1 torr for two hours while heating to 50 °C for the first hour. Samples were then reconstituted in 18.2 MΩ deionized water with 0.1% formic acid solution and centrifuged an additional time to remove any solids. Finally, 125 µL of sample was placed in small volume

polypropylene Agilent Technology vials and injected through the chromatography and mass spectrometry systems.

Calibration curves were prepared in bovine blood and dried on Whatman C-Pack blood cards which then were passed through the method developed on the Gerstel SPExos system as well as the liquid chromatography separation achieved on the Agilent 1200 liquid chromatography system and the optimization parameters which were determined on the Agilent 6460 triple quadrupole mass spectrometer after they had dried for 24 hours. Calibration curves were designed to be ten points such that at least six points could be preserved to improve linearity and contained three quality control standards. While it would be best practice to bookend the analytical samples to measure instrument drift, due to time and sample availability restraints, only one calibration curve and replicate of quality control standers were run. Stability testing for the molecule was performed in the same way, but with samples left to dry for longer time increments.

2.2.2 Instrumentation

Detection was achieved using an Agilent 6460 triple quadruple mass spectrometer (Model US92170174) in negative mode selecting for an ion of mass/charge ratio (m/z) of 117 in the first quadrupole and 73 in the third through multiple reaction monitoring.[56-58] While many of the literature values for determining MMA in the MS have derivatized the molecule to aid in detection and analysis, one of the goals of the experiment was to automate the process as much as possible.[53, 59, 60] As such, it was determined that no additional derivatization should be performed on the MMA and all detection and quantification would occur for the natural state of the organic acid. This may potentially decrease the sensitivity of detection, however the increase of detection through instrumental optimization should overcome this discrepancy.

An Agilent 1200 Liquid Chromatography System comprised of a G13798B degasser, a G1312B binary pump, a G1367D high performance autosampler, a G1330B thermostat, and a G1316B column compartment, was utilized for separation which was then ionized via electrospray using a G1958-65138 Agilent Jet-Stream Electrospray Ionization source. Samples were separated on a Phenomenex Synergi 4 µm Hydro-RP 80 Å 150 x 4.6 mm column (Lot 00F-475-F0) was used for successful peak separation. A flow rate of 1.000 mL/min was utilized with a mobile phase consisting of 18.2 Ω deionized water from a Barnstead NANOpure system manufactured by Thermo Scientific (Model 7146) which was then passed through an Easypure II water filtration system manufactured by Thermo Scientific (Model D7035) and HPLC grade acetonitrile purchased from Fisher Scientific (Lot 190931) to both of which 0.1% optima grade formic acid from Fisher Chemical (Lot 173815) had been applied to aid in the ionization process.[61] The complete method can be seen below (**Table 2.1**).

Table 2.1. Final LC-MS method for separation of methylmalonic acid and succinic acid on an Agilent 1200 liquid chromatography system through a Phenomenex Synergi 4 µm Hydro-RP 80 Å 150 x 4.6 mm column for detection on an Agilent 6460 triple quadrupole mass spectrometer. This method resulted in complete baseline separation with Gaussian peaks.

Time (Min)	H_2O %	Acetonitrile %
0.00	99.0	1.0
4.00	90.0	10.0
4.50	35.0	65.0
4.75	5.0	95.0
5.75	5.0	95.0
5.80	99.0	1.0

After complete separation was achieved, the Agilent 6460 triple quadrupole mass spectrometer was optimized for the detection of MMA over SUC by utilizing the source optimization program in Agilent's software. The optimal factors are shown below in **Table 2.2**.

Table 2.2. Optimization parameters for the detection of methylmalonic acid on an Agilent 6460 triple quadrupole mass spectrometer which was run in negative mode.

Parameter	Optimization
Gas Temperature	230 ˚C
Gas Flow	4 L/min
Nebulizer	45 PSI
Sheath Gas Temp	300 ˚C
Sheath Gas Flow	9 L/min
Capillary Voltage	4000 V
Nozzle Voltage	500 V

The change in detection after optimization had a logarithmic increase in signal as can be observed in **Figure 2.4**. With a greater signal response for MMA compared to SA, which had not been observed in the literature. [62, 63]

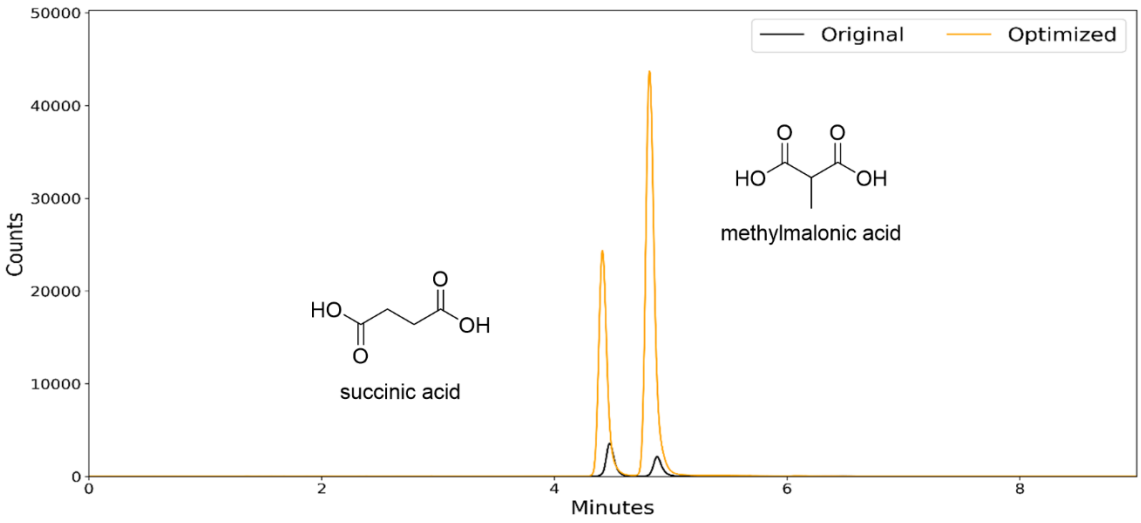

Figure 2.4. Separation and optimization of succinic acid (4.5 minutes) and methylmalonic acid (5.1 minutes) on by an Agilent 1200 liquid chromatography system through a Phenomenex Synergi 4 µm Hydro-RP 80 Å 150 x 4.6 mm column as seen on an Agilent 6460 triple quadrupole mass spectrometer.

With the MMA and SA peaks separated and the detection of the MMA optimized, the next step was to see if the organic acid could be detected and quantified from blood cards using an automated system. A Gerstel Inc. DBSA SPExos Automated Blood Card system comprised of a model 730 high pressure dispenser, a model 725 automated cartridge extraction system, a model 410 dried blood spot desorption unit, and a model 014-02A multipurpose sampler arm was used. This was controlled by Maestro software (Version 1.4.25.1) was utilized for this purpose and samples were applied to Whatman FTA DMPK-C Card with a nitrocellulose membrane and a 0.1-12.0 μm pore size and analytes were collected on Spark Holland SPExos strong hydrophobic resin (Lot 86.329) single use cartridges before being injected into the liquid chromatography system and further detection on the mass spectrometer. First, the pure MMA sample was tested, then the mixed MMA and SA sample, next the spiked blood sample, and finally the isotopically spiked blood sample. Twenty μL of sample was added to each of the four spots on the card and allowed to dry overnight. Once dried, the blood card was inserted into the Gerstel SPExos and a method was developed for detection and quantification. It began by conditioning a Gerstel SPExos cartridge with a strong hydrophobic resin (styrene-divinylbenzene) inside. The desorption hot cap was set to 80 ˚C (which aids in the removal of analyte from DBS) and the flow rate was set to 4000 μL/min with a 1000 μL/min dispense, which was then optimized to 250 μL/min. After detection of the analyte, it was necessary to determine if the analyte had been lost in the washing step of the MMA elution for a possible increase in response from MMA. The complete method for desorption can be seen below (**Table 2.3**).

Table 2.3. Method for desorption of methylmalonic acid from a quantitative dried blood spot using a Gerstel SPExos system onto strong hydrophobic resin (styrene-divinylbenzene) cartridges. All solvents contained 0.1% formic acid except the clean mix (acetonitrile, methanol, isopropanol, and 18.2 Ω deionized water in a 3:3:2:2 Ratio) which had 0.05% formic acid.

	Cartridge Conditioning		Wash			Desorption
Solvent	Methanol	H_2O	0.1% NH_4OH	Clean Mix	H_2O	H_2O
Dispense Rate	1000 µL/min	1000 µL/min	1000 µL/min	1000 µL/min	1000 µL/min	250 µL/min
Dispense Volume	1000 µL	2000 µL	2000 µL	1000 µL	1000 µL	250 µL

Using this desorption method from a fully automated Gerstel dried blood spot SPExos system provides quantifiable levels of MMA which are baseline separated from SUC (**Figure 2.5**). These discrete peaks maintain a consistent elution time with manual desorption and automatic injection methods and have direct overlap of the 4C13 isotopically enhanced MMA and natural MMA peaks.

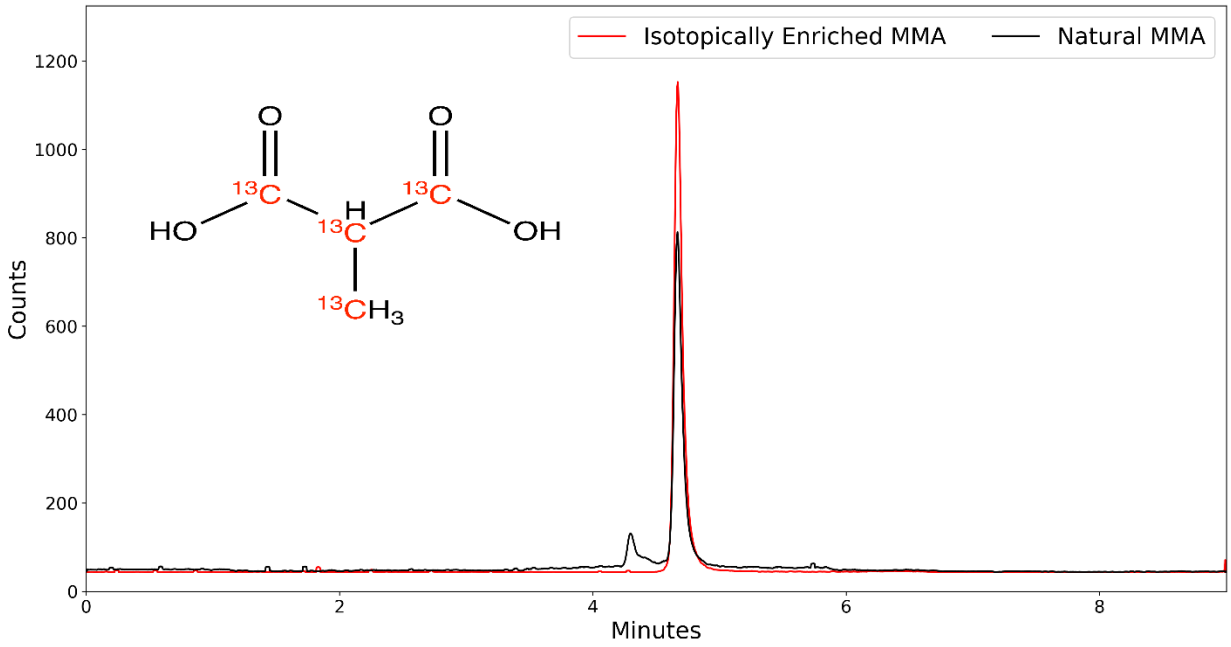

Figure 2.5. Separation of succinic acid (4.5 minutes), methylmalonic acid (5.1 minutes), and isotopically enhanced 4C13 methylmalonic acid (5.1 minutes) which had been desorbed from a Whatman C-Pack dried blood spot card using a Gerstel SP*Exos* system and was retained on a on Spark Holland SP*Exos* strong hydrophobic resin single use cartridge by an Agilent 1200 liquid chromatography system through a Phenomenex Synergi 4 µm Hydro-RP 80 Å 150 x 4.6 mm column as seen on an Agilent 6460 triple quadrupole mass spectrometer.

Prepared dried blood spots were subject to these desorption methods for detection and quantification.

2.3 Discussion

Elevated MMA is seen at levels of one in 48,000 patients in North America, and at a level of one in 26,000 patients in China.[64] Some physicians estimate a higher prevalence in the general, and especially aging, population,[43] but this relative infrequency is explained by infrequent testing, a need for a more sensitive test for MMA, and reservoir of B-12 in the liver which can exist at levels up to 10 µg per gram of protein.[65] MMA is widely tested for as a qualitative test for neonates, but rarely used in quantitative testing for older individuals, despite negative patient outcomes

associated with slightly elevated levels.[43, 64] These negative outcomes are often seen to be neurological in nature, with delayed myelination or atrophy being seen pediatric patients and altered mental status, depression, mania, irritability, paranoia, or delusions in geriatric patients.[66]

2.3.1. Statistical Determination of Methylmalonic Acid as a Biomarker for Autism Spectrum Disorder.

MMA as a biomarker was determined through a recent $1.4 million dollar study have identified 21 statistically significant biomarkers.[19, 40] This study compared children who had been diagnosed with ASD through the ADOS-I scale to age, gender, race, and socioeconomically matched controls. Quantitation of MMA in the patient's blood was performed outside of the Kingston lab by a local commercial testing laboratory. Statistical comparisons between the two groups were performed using an ANOVA test for equality of the mean acid concentration across two groups was significant at the 5% level (**Figure 2.6**).

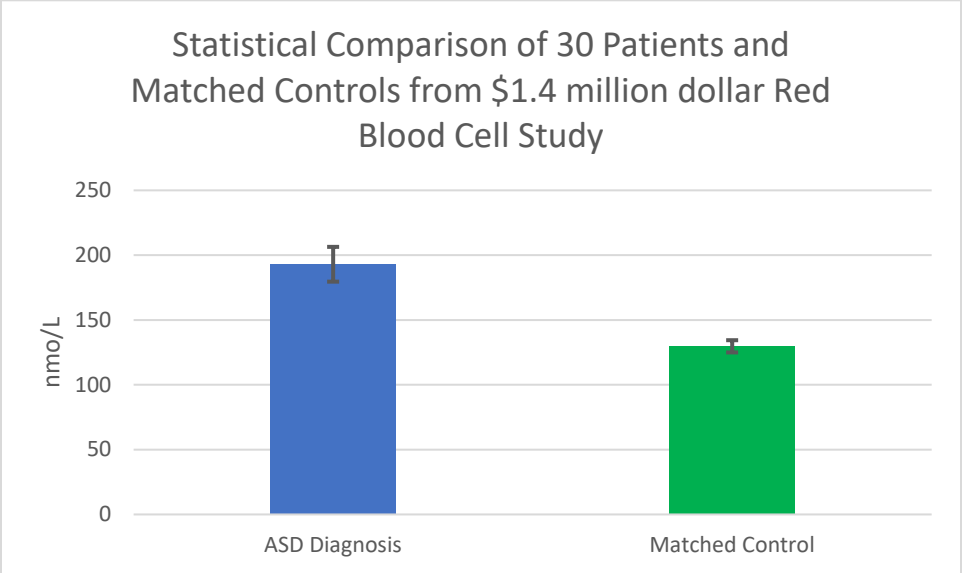

Figure 2.6. Comparison of the methylmalonic acid children which had been diagnosed with autism spectrum disorder through the Autism Diagnostic Observation Schedule as compared to age, gender, race, and socioeconomic status matched controls ($p = 0.00361$).

Multiple comparisons revealed a significant difference between the mean MMA of the children diagnosed with ASD and their matched controls with children diagnosed with ASD having the higher mean ratio ($p = 0.00361$). Overall, 14 out of 29 patients (48.3%) had MMA concentrations below 170 nmol/L (the midpoint of normal and 25 out of 30 control samples (83.3%). Four of 29 patient samples (13.8%) were outside the range of normal MMA concentration (70-270 nmol/L), while none of the control samples exceeded 220 nmol/L (**Figure 2.7**).

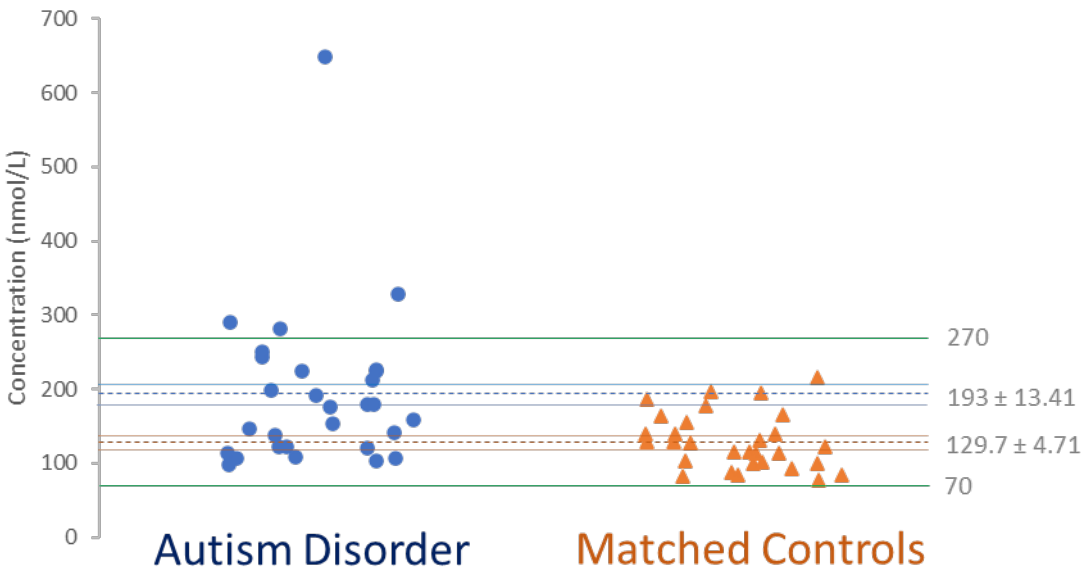

Figure 2.7. The methylmalonic acid serum concentration for each individual patient diagnosed with autism spectrum disorder and their matched control set separated by data set. The normal methylmalonic acid concentrations are represented by solid, green bands (70-270 nmol/L). The color matched dashed lines represent the average concentration of methylmalonic acid in each sample (193 nmol/L for children with autism disorder and 129.7 nmol/L for matched controls). The color matched dotted lines (206.41 and 179.59 nmol/L for children with autism disorder and 134.4 to 124.5 for the matched controls) represent the 95% confidence limits of each sample set.

2.3.2. Comparison of Desorption Techniques for Methylmalonic Acid from Dried Blood Spots

After separation and optimization of MMA detection, quantitation was performed on dried blood which had been desorbed manually utilizing various solvent systems as well as those desorbed automatically using a Gerstel SPExos dried blood spot system which is a fully online system requiring limited analyst input. These tests were performed to determine the efficiency of the Gerstel system extraction as well as determine the optimal method for manual desorption to allow comparison between methods. Bovine blood mixtures, which were previously tested to determine their ambient MMA levels, were prepared through the addition of concentrated MMA solution for a final concentration of concentration of 3.67×10^{-02} µmol/g. These solutions were then applied to Whatman C-Pak dried blood spot cards and allowed to dry for 24 hours in a clean room at ambient temperature. Blood spots were either manually punched using an 8-mm punch with samples run in quadruplicate, or a complete card of four blood spots were utilized when testing the Gerstel SPExos system desorption method. These results were averaged and compared to the known value via IDMS. The results (**Table 2.4**) showed that the application of IDMS was consistent across all desorption methodologies with confidence intervals overlapping for every method.

Table 2.4. Comparison of desorption methodologies for methylmalonic acid utilizing a combination of 18.2 MΩ deionized water (H_2O) and optima grade acetonitrile (ACN) from Whatman C-Pak cellulose blood cards as separated on an Agilent 1200 liquid chromatography system through a Phenomenex Synergi 4 µm Hydro-RP 80 Å 150 x 4.6 mm column as seen on an Agilent 6460 triple quadrupole mass spectrometer. Gerstel analytes were tested using a Gerstel SPExos system and was retained on a on Spark Holland SPExos strong hydrophobic resin single use cartridge.

Desorption Method	Average Concentration (µmol/g)	95% Confidence	Associated Error (%)
Gerstel	0.03675	0.0023	0.005
Sonicated, Speed Vac H_2O	0.03783	0.0063	0.113
Vortexed H_2O	0.03739	0.0074	0.069
Sonicated, Speed Vac 50/50 H_2O/ACN	0.03620	0.0032	0.05
Vortexed, Speed Vac 50/50 H_2O/ACN	0.03479	0.0053	0.191
Sonicated, Speed Vac 60/40 H_2O/ACN	0.03783	0.0036	0.113

Despite the range of methodological desorption techniques applied, all samples were within acceptable error and overlapping confidence intervals (**Figure 2.8)**. Thus, IDMS quantification was able to overcome any sample desorption efficiencies which may resulted from the application of these methodologies. The Gerstel desorption system had the lowest overall associated error followed by a 50/50 mixture of 18.2 MΩ deionized water and optima grade acetonitrile. For future comparisons, these two methodologies were to be employed.

While all measurements were statistically the same, one of the major differences for quantification was time. Automatic, online desorption utilizing a Gerstel SPExos system had a run time of 22-minutes, while manual extraction was a prolonged affair. Between the required three hours for desorption from the blood card to extract in triplicate, then an additional two hours to dry, and twenty minutes of centrifugation, manual extraction requires over five hours of sample preparation just using instrumentation. This time window does not account for any time the analyst

might take to label, combine, transfer, filter, or separate any samples. Thus, the inherent value of time associated with utilization of a fully automated, online Gerstel system is obvious.

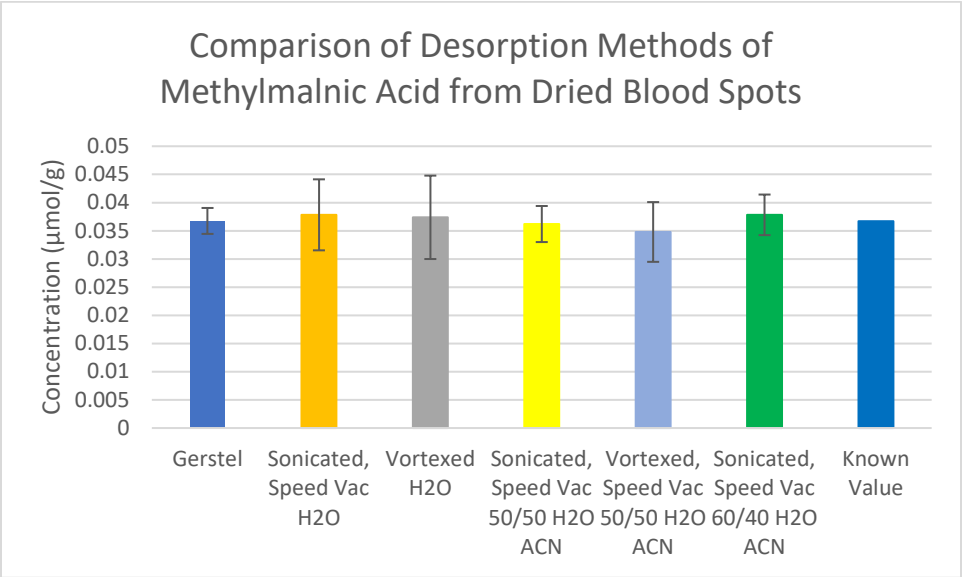

Figure 2.8. Quantified concentration of methylmalonic acid in both automated, online desorption (6 mm punch size) and manual elution (8 mm punch size) for methylmalonic acid utilizing a combination of 18.2 MΩ deionized water (H_2O) and optima grade acetonitrile (ACN) from Whatman C-Pak cellulose blood cards as separated on an Agilent 1200 liquid chromatography system through a Phenomenex Synergi 4 µm Hydro-RP 80 Å 150 x 4.6 mm column as seen on an Agilent 6460 triple quadrupole mass spectrometer. Gerstel analytes were tested using a Gerstel SPExos system and was retained on a on Spark Holland SPExos strong hydrophobic resin single use cartridge.

Once the efficiency of desorption from dried blood spots utilizing a Gerstel SPExos online automated desorption system had been demonstrated, a direct comparison between calibration curve quantitation to IDMS quantitation was performed. Among the potential benefits of utilization of IDMS over calibration curves is a savings of time and cost. Calibration curves require at least six points of linearity on a line of best fit, three quality control samples, and statistical blanks, all of which are ideally bookended to the unknowns to account for instrument drift. Despite optimization of extraction methodology and a decrease of time to 22-minutes a sample utilizing the Gerstel SPExos system, time utilization for calibration curves can still prohibit the use of dried

blood spots as a quantitative matrix. As there are four spots on a dried blood card, which would all be used for optimal statistical variation, the total run time for a single unknown sample utilizing calibration curves would be greater than a 24-hour period and the materials cost would be greater than ten times a sample utilizing IDMS. Thus, for optimization of time, as well as materials, dried blood spots are best analyzed utilizing IDMS quantification.

2.3.3. Comparison of Quantitation of Methylmalonic Acid Utilizing Calibration Curves Compared to Isotope Dilution Mass Spectrometry

Methodological comparisons between calibration curves an IDMS were performed utilizing the fully online automatic Gerstel SPExos system. Time comparison was considered as well as accuracy and associated error. Due to time constraints, and difficulty in maintaining solvent levels, a 16-hour series of measurements was utilized with only one calibration curve and set of quality control samples was utilized rather than a complete 32-hour book ended sample set. Samples were prepared and spiked with ^{13}C isotopically enriched MMA, which was utilized for both internal standard for calibration curves and for enabling IDMS quantitation, and the desorption methodology was applied (**Table 2.5**).

Table 2.5. Concentrations of methylmalonic acid standards for calibration curve, as well as quality control standards, unknown, and a blank as well as detected counts of natural methylmalonic acid and ^{13}C isotopically enriched methylmalonic acid from Whatman C-Pak cellulose blood cards as separated on an Agilent 1200 liquid chromatography system through a Phenomenex Synergi 4 µm Hydro-RP 80 Å 150 x 4.6 mm column as seen on an Agilent 6460 triple quadrupole mass spectrometer with analytes retained on a on Spark Holland SPExos strong hydrophobic resin single use cartridge.

Calibration Curve Level	Concentration (µg/g)	MMA Counts		^{13}C MMA Counts	
		Average	Std Dev	Average	Std Dev
1	21.640	15747.39	236.01	398.70	67.54
2	11.047	9489.84	124.57	499.93	68.77
3	4.878	4758.42	36.92	553.78	32.11
4	2.399	2257.28	87.50	470.76	68.55
5	1.117	1252.27	41.51	581.77	77.60
6	0.522	859.79	41.51	581.77	49.85
QC 1	3.198	5492.208	101.43	575.87	110.27
QC 2	1.899	2370.563	103.44	427.09	112.98
QC 3	0.826	1428.553	6.98	561.53	100.76
Unknown	1.152	1524.84	72.83	503.10	97.03
Card Blank	0.000	24.92	21.70	35.94	17.96

These determinations were utilized to construct a six-point calibration curve which was normalized and blank subtracted to ensure the most accurate linear response possible all of which were above the lower limit of detection. When confidence intervals were applied to the data points, all levels overlapped the linear regression (**Figure 2.9**).

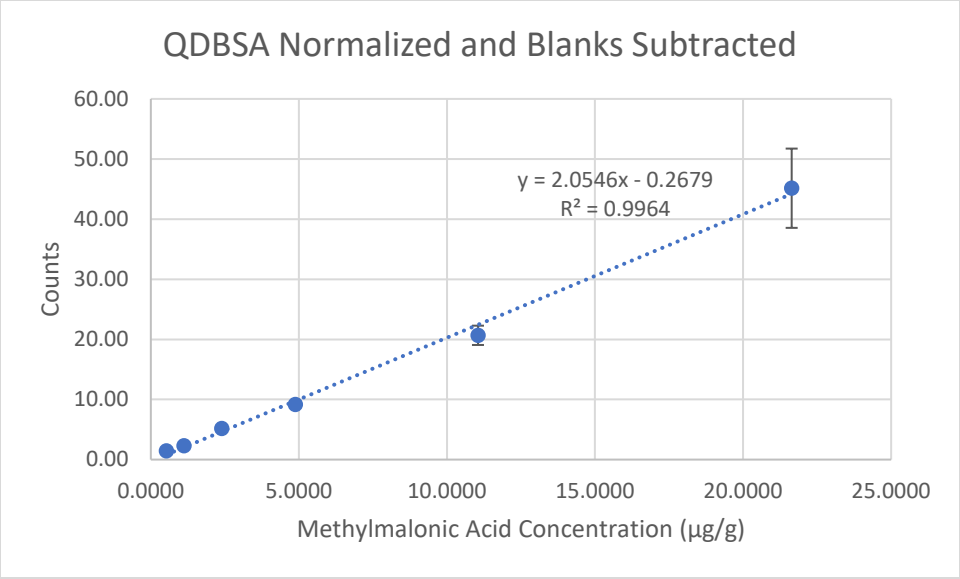

Figure 2.9. Normalized, and blank subtracted calibration curve as well as line of best fit and correlation coefficient with 95% confidence intervals applied for the quantitation of methylmalonic acid from Whatman C-Pak cellulose blood cards as separated on an Agilent 1200 liquid chromatography system through a Phenomenex Synergi 4 µm Hydro-RP 80 Å 150 x 4.6 mm column as seen on an Agilent 6460 triple quadrupole mass spectrometer utilizing a Gerstel SPExos system and was retained on a on Spark Holland SPExos strong hydrophobic resin single use cartridge.

With calibration curves completed, quantitation of the unknown as well as the quality control samples were performed using both calibration curves and IDMS (**Table 2.6**). Each sample was quantified in quadruplicate with its methodology and these quantitative methods were used to compare intra-sample. While both were able to accurately quantify the concentration of the unknown sample, IDMS did so with lower associated error and with better confidence limits.

Table 2.6. Comparative methodology between calibration curves an isotope dilution mass spectrometry quantitation for methylmalonic acid automatically desorbed from Whatman C-Pak cellulose blood cards as separated on an Agilent 1200 liquid chromatography system through a Phenomenex Synergi 4 µm Hydro-RP 80 Å 150 x 4.6 mm column as seen on an Agilent 6460 triple quadrupole mass spectrometer utilizing a Gerstel SPExos system and was retained on a on Spark Holland SPExos strong hydrophobic resin single use cartridge.

Level	Concentration (µg/g)	Calibration Curve Quantitation (µg/g)	Error (%)	IDMS Quantitation (µg/g)	Error (%)
QC 1	3.198	5.061 ± 1.869	58.2	3.468 ± 0.325	7.8
QC 2	1.899	3.006 ± 1.157	58.3	2.046 ± 0.203	6.9
QC 3	0.826	1.211 ± 0.353	46.7	0.867 ± 0.062	4.7
Unknown	1.615	1.487 ± 0.458	7.9	1.574 ± 0.141	2.6

When compared (**Figure 2.10**), these systems of quantitation showed a difference in favor of IDMS. While both methods were able to have statistically overlapping confidence limits with at last 67% of quality control standards in accordance with the bioanalytical method validation guidelines provided by the National Institutes of Health (with IDMS being able to accurately quantify 100% of quality control samples) only IDMS had an error rate (less than 15%) which is low enough to be accepted. The error associated with the unknown value was reduced using IDMS from 7.9% to 2.6%. Errors associated with quality control standards were reduced by an order of magnitude. Errors associated with calibration curves could have, perhaps, been overcome by utilizing a book ended 32-hour calibration curve and quality control standard methodology. Quantification utilizing IDMS was superior to traditional calibration curves for all three quality control samples as well as the unknown sample. When comparing time required for these two methods, IDMS would require only slightly over two hours of sample introduction for the sample and blanks which result in a superior quantitation while traditional calibration curves would require up to 32-hours for a double book ended calibration curves.

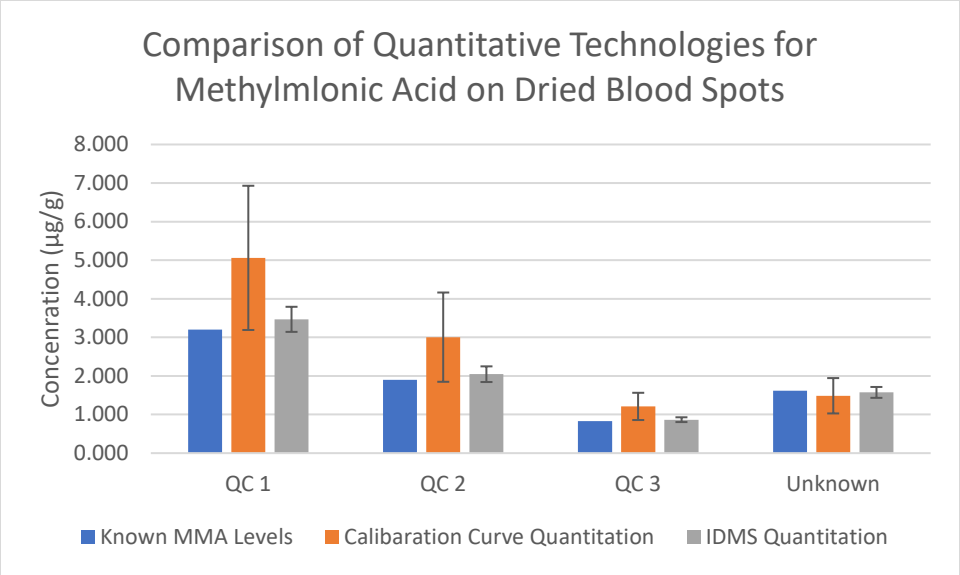

Figure 2.10. Comparison of calibration curve and isotope dilution mass spectrometry quantitation for methylmalonic acid automatically desorbed from Whatman C-Pak cellulose blood cards as separated on an Agilent 1200 liquid chromatography system through a Phenomenex Synergi 4 µm Hydro-RP 80 Å 150 x 4.6 mm column as seen on an Agilent 6460 triple quadrupole mass spectrometer utilizing a Gerstel SPExos system and was retained on a on Spark Holland SPExos strong hydrophobic resin single use cartridge.

2.3.4. Stability Test for Methylmalonic Acid on Dried Blood Spots

Once IDMS had been proven to be superior to calibration curve quantitation for MMA for dried blood spot quantification, a longevity study was performed. Blood cards were prepared at the same time and at a concentration of 2.14 µg/g. They were allowed to sit in ambient clean room air to test any degradation that may occur in ambient storage conditions. These cards were then tested utilizing automated online desorption of the Gerstel SPExos system at one day, one month, six months, and one year (**Table 2.7**). All four blood spots were tested on each card to give the maximum statistical significance for each sample. While samples did degrade slightly over time, IDMS was able to correct for these factors as all four measurements were within acceptable error and overlapped the true value at the 95% confidence interval.

Table 2.7. Calculated concentration utilizing isotope dilution mass spectrometry and associated error in a stability study for methylmalonic acid on dried blood spots which had been stored in ambient air in a clean room and were automatically desorbed from Whatman C-Pak cellulose blood cards as separated on an Agilent 1200 liquid chromatography system through a Phenomenex Synergi 4 µm Hydro-RP 80 Å 150 x 4.6 mm column as seen on an Agilent 6460 triple quadrupole mass spectrometer utilizing a Gerstel SPExos system and was retained on a on Spark Holland SPExos strong hydrophobic resin single use cartridge.

Time of Measurement	Concentration (µg/g)	Error (%)
1 Day	2.174± 0.033	0.25
1 Month	2.163 ± 0.021	2.33
6 Months	2.200 ± 0.060	5.87
12 Months	2.174 ± 0.033	3.39
True Value	2.14	

Degradation of MMA was minimal and accurate quantitation was still possible after one year on dried blood spot cards. All error was in acceptable limits (less than 15%) and all confidence intervals overlapped the true value (**Figure 2.11**). This leads to the possibility of analyte storage and future testing which can be compared or tested for novel analytes as deemed necessary.

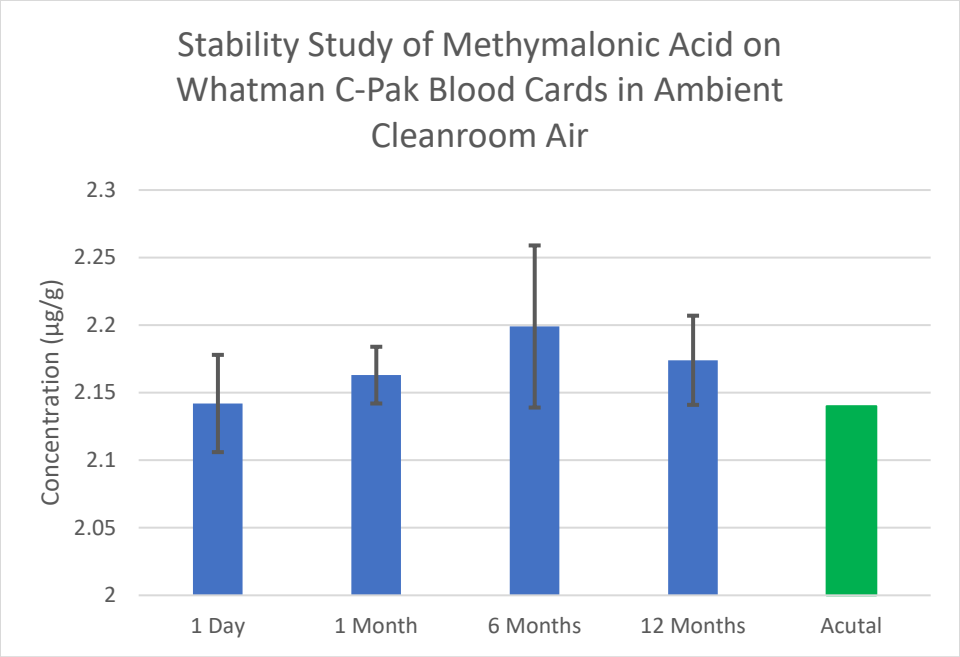

Figure 2.11. Plotted concentrations, which were calculated utilizing isotope dilution mass spectrometry, and associated error in a stability study for methylmalonic acid on dried blood spots which had been stored in ambient air in a clean room which were automatically desorbed from Whatman C-Pak cellulose blood cards as separated on an Agilent 1200 liquid chromatography system through a Phenomenex Synergi 4 µm Hydro-RP 80 Å 150 x 4.6 mm column as seen on an Agilent 6460 triple quadrupole mass spectrometer utilizing a Gerstel SPExos system and was retained on a on Spark Holland SPExos strong hydrophobic resin single use cartridge.

Utilizing a dried blood spot matrix, MMA was able to be quantified accurately on an automated, online Gerstel SPExos DBSA system faster and more accurately than would be possible using manual desorption. Utilization of IDMS proved to be a more robust analytical technique than calibration curves and allowed for accurate quantitation for up to a year on the stable organic acid.

2.4. Conclusion

MMA is a stable, organic acid which results in the human body from a defect in odd-chain fatty acid catabolism.[41] MMA, which had been theorized due to its neurological effects including its role in demyelination,[42] was determined to be a biomarker for ASD. While, currently, MMA is

primarily utilized as a qualitative measurement for B-12 deficiency and test for dangerous methylmalonic acidemia in neonates, there is a growing body of evidence which suggests MMA is a biomarker for ASD and should be tested for more frequently B-12 deficiency may become more prominent with age suggesting the need for broader testing in the general population.[42] Accurate quantitation of MMA levels was able to be performed through automatic online desorption from DBS cards utilizing a Gerstel SPExos system which was detected on an Agilent 6460 triple quadrupole mass spectrometer using IDMS. Quantitation utilizing IDMS was determined to be more accurate and more efficient than quantitation utilizing calibration curves though accurate quantitation of all three quality control standards as well as a reduction in error for the unknown sample from 7.9% to 2.6%. Stability studies of MMA determined that the organic acid was stable and quantifiable utilizing IDMS on cellulose blood cards for up to a year in ambient, open-air conditions in a clean room with all measurements being statistically indistinguishable from the starting, known concentration of MMA of 2.14 µg/g.

2.5 References

1. Chapman, O. D., The Complement-Fixation Test for Syphilis. *Archives of Dermatology and Syphilology* **1924,** *9* (5).

2. WHO, Guidance on Regulations for the Transport of Infectious Substances 2021-2022. Geniva, 2021.

3. Guthrie, R.; Susi, A., A Simple Phenylalanine Method for Detecting Phenylketonuria in Large Populations of Newborn Infants. *Pediatrics* **1963,** *32* (3), 338-343.

4. Kand'ar, R.; Zakova, P., Determination of phenylalanine and tyrosine in plasma and dried blood samples using HPLC with fluorescence detection. *J Chromatogr B Analyt Technol Biomed Life Sci* **2009,** *877* (30), 3926-9.

5. Hofman, L. F.; Roe, C. R.; Kahler, S. G.; Terada, N.; Millington, D. S.; Chace, D. H., Rapid diagnosis of phenylketonuria by quantitative analysis for phenylalanine and tyrosine in neonatal blood spots by tandem mass spectrometry. *Clinical Chemistry* **1993,** *39* (1), 66-71.

6. Lehmann, S.; Delaby, C.; Vialaret, J.; Ducos, J.; Hirtz, C., Current and future use of "dried blood spot" analyses in clinical chemistry. *Clin Chem Lab Med* **2013,** *51* (10), 1897-909.

7. Crossle, J.; Elliot, R. B.; Smith, P., Dried-Blood Spot Screening for Cystic Fibrosis in the Newborn. *The Lancet* **1979,** *313* (8114), 472-474.

8. McDade, T. W.; Williams, S.; Snodgrass, J. J., What a drop can do: dried blood spots as a minimally invasive method for integrating biomarkers into population-based research. *Demography* **2007,** *44* (4), 899-925.

9. Mei, J., Dried Blood Spot Sample Collection, Storage, and Transportation. In *Dried Blood Spots*, 2014; pp 21-31.

10. Gruner, N.; Stambouli, O.; Ross, R. S., Dried blood spots--preparing and processing for use in immunoassays and in molecular techniques. *J Vis Exp* **2015,** (97).

11. Sok, P.; Lupo, P. J.; Richard, M. A.; Rabin, K. R.; Ehli, E. A.; Kallsen, N. A.; Davies, G. E.; Scheurer, M. E.; Brown, A. L., Utilization of archived neonatal dried blood spots for genome-wide genotyping. *PLoS One* **2020,** *15* (2), e0229352.

12. Batterman, S.; Chernyak, S., Performance and storage integrity of dried blood spots for PCB, BFR and pesticide measurements. *Sci Total Environ* **2014,** *494-495*, 252-60.

13. Becan-McBride, D. G. a. K., *Phlebotomy Handbook : Blood Collection Essentials*. Prentice Hall, Inc: 2018; Vol. 10th, p 672.

14. De Kesel, P. M.; Sadones, N.; Capiau, S.; Lambert, W. E.; Stove, C. P., Hemato-critical issues in quantitative analysis of dried blood spots: challenges and solutions. *Bioanalysis* **2013,** *5* (16), 2023-41.

15. Berger, C. C. a. B., Hematocrit (Hct) – blood. In *Laboratory Tests and Diagnostic Procedures*, 6 ed.; Berger, C. C. a. B., Ed. Elsevier Saunders: St. Louis, MO, 2012; pp 620-621.

16. Denniff, P.; Spooner, N., The effect of hematocrit on assay bias when using DBS samples for the quantitative bioanalysis of drugs. *Bioanalysis* **2010,** *2* (8), 1385-95.

17. Talan, M. I.; Engel, B. T., Morning increase in whole blood viscosity: a consequence of a homeostatic nocturnal haemodynamic pattern. *Acta Physiol Scand* **1993,** *147* (2), 179-83.

18. De Kesel, P. M.; Capiau, S.; Lambert, W. E.; Stove, C. P., Current strategies for coping with the hematocrit problem in dried blood spot analysis. *Bioanalysis* **2014,** *6* (14), 1871-4.

19. Boggess, A.; Faber, S.; Kern, J.; Kingston, H. M. S., Mean serum-level of common organic pollutants is predictive of behavioral severity in children with autism spectrum disorders. *Scientific Reports* **2016,** *6*, 26185.

20. Fowler, B.; Leonard, J. V.; Baumgartner, M. R., Causes of and diagnostic approach to methylmalonic acidurias. *J Inherit Metab Dis* **2008,** *31* (3), 350-60.

21. Ma, X.; Zou, Y.; Tang, Y.; Wang, D.; Zhou, W.; Yu, S.; Qiu, L., High-throughput analysis of total homocysteine and methylmalonic acid with the efficiency to separate succinic acid in serum and urine via liquid chromatography tandem mass spectrometry. *J Chromatogr B Analyt Technol Biomed Life Sci* **2022,** *1193*, 123135.

22. Brozovic, M.; Hoffbrand, A. V.; Dimitriadou, A.; Mollin, D. L., The excretion of methylmalonic acid and succinic acid in vitamin B 12 and folate deficiency. *Br J Haematol* **1967,** *13* (6), 1021-32.

23. Fahrenholz, T.; Wolle, M. M.; Kingston, H. M.; Faber, S.; Kern, J. C., 2nd; Pamuku, M.; Miller, L.; Chatragadda, H.; Kogelnik, A., Molecular speciated isotope dilution mass spectrometric methods for accurate, reproducible and direct quantification of reduced, oxidized and total glutathione in biological samples. *Anal Chem* **2015,** *87* (2), 1232-40.

24. Agency, U. S. E. P., Elemental and molecular speciated isotope dilution mass spectrometery. Update V ed.; U.S. Government Printing Office: Washington D.C., 2013; Vol. Method 6800.

25. De Hevesy, G., Some applications of isotopic indicators. *Nobel Lecture* **1944,** *12*.

26. Matucha, M.; Jockisch, W.; Verner, P.; Anders, G., Isotope effect in gas—liquid chromatography of labelled compounds. *Journal of Chromatography A* **1991,** *588* (1-2), 251-258.

27. Engen, J. R.; Wales, T. E., Analytical Aspects of Hydrogen Exchange Mass Spectrometry. *Annu Rev Anal Chem (Palo Alto Calif)* **2015,** *8*, 127-48.

28. Turowski, M.; Yamakawa, N.; Meller, J.; Kimata, K.; Ikegami, T.; Hosoya, K.; Tanaka, N.; Thornton, E. R., Deuterium isotope effects on hydrophobic interactions: the importance of dispersion interactions in the hydrophobic phase. *J Am Chem Soc* **2003,** *125* (45), 13836-49.

29. Li, Q.; Li, Y.; Liu, B.; Chen, Q.; Xing, X.; Xu, G.; Yang, W., Prevalence of Autism Spectrum Disorder Among Children and Adolescents in the United States from 2019 to 2020. *JAMA Pediatr* **2022**.

30. Elsabbagh, M.; Divan, G.; Koh, Y. J.; Kim, Y. S.; Kauchali, S.; Marcin, C.; Montiel-Nava, C.; Patel, V.; Paula, C. S.; Wang, C.; Yasamy, M. T.; Fombonne, E., Global prevalence of autism and other pervasive developmental disorders. *Autism Res* **2012,** *5* (3), 160-79.

31. Kupper, C.; Stroth, S.; Wolff, N.; Hauck, F.; Kliewer, N.; Schad-Hansjosten, T.; Kamp-Becker, I.; Poustka, L.; Roessner, V.; Schultebraucks, K.; Roepke, S., Identifying predictive features of autism spectrum disorders in a clinical sample of adolescents and adults using machine learning. *Sci Rep* **2020,** *10* (1), 4805.

32. Skafidas, E.; Testa, R.; Zantomio, D.; Chana, G.; Everall, I. P.; Pantelis, C., Predicting the diagnosis of autism spectrum disorder using gene pathway analysis. *Mol Psychiatry* **2014,** *19* (4), 504-10.

33. Sizoo, B. B.; Horwitz, E. H.; Teunisse, J. P.; Kan, C. C.; Vissers, C.; Forceville, E.; Van Voorst, A.; Geurts, H. M., Predictive validity of self-report questionnaires in the assessment of autism spectrum disorders in adults. *Autism* **2015,** *19* (7), 842-9.

34. Lord, C.; Risi, S.; Lambrecht, L.; Cook, J. E. H.; Leventhal, B. L.; DiLavore, P. C.; Pickles, A.; Rutter, M., *Journal of Autism and Developmental Disorders* **2000,** *30* (3), 205-223.

35. McCrimmon, A.; Rostad, K., Test Review: Autism Diagnostic Observation Schedule, Second Edition (ADOS-2) Manual (Part II): Toddler Module. *Journal of Psychoeducational Assessment* **2013,** *32* (1), 88-92.

36. Rutter, M.; Le Couteur, A.; Lord, C., Autism diagnostic interview-revised. *Los Angeles, CA: Western Psychological Services* **2003,** *29* (2003), 30.

37. Ye, B. S.; Leung, A. O. W.; Wong, M. H., The association of environmental toxicants and autism spectrum disorders in children. *Environmental pollution* **2017,** *227*, 234-242.

38. Bölte, S.; Girdler, S.; Marschik, P. B., The contribution of environmental exposure to the etiology of autism spectrum disorder. *Cellular and Molecular Life Sciences* **2019,** *76* (7), 1275-1297.

39. Alan S. Brown; Keely Cheslack-Postava; Panu Rantakokko; Hannu Kiviranta; Susanna Hinkka-Yli-Salomäki; Ian W. McKeague; Heljä-Marja Surcel; Andre Sourander, Association of Maternal Insecticide Levels With Autism in Offspring From a National Birth Cohort. *American Journal of Psychiatry 0* (0), appi.ajp.2018.17101129.

40. Faber, S.; Zinn, G. M.; Kern Ii, J. C.; Skip Kingston, H. M., The plasma zinc/serum copper ratio as a biomarker in children with autism spectrum disorders. *Biomarkers* **2009,** *14* (3), 171-180.

41. Schroder, T. H.; Mattman, A.; Sinclair, G.; Vallance, H. D.; Lamers, Y., Reference interval of methylmalonic acid concentrations in dried blood spots of healthy, term newborns to facilitate neonatal screening of vitamin B12 deficiency. *Clin Biochem* **2016,** *49* (13-14), 973-8.

42. Selhub, J.; Morris, M. S.; Jacques, P. F., In vitamin B12 deficiency, higher serum folate is associated with increased total homocysteine and methylmalonic acid concentrations. *Proc Natl Acad Sci U S A* **2007,** *104* (50), 19995-20000.

43. Elin, R. J.; Winter, W. E., Methylmalonic acid: a test whose time has come? *Arch Pathol Lab Med* **2001,** *125* (6), 824-7.

44. Kushnir, M. M.; Komaromy-Hiller, G.; Shushan, B.; Urry, F. M.; Roberts, W. L., Analysis of dicarboxylic acids by tandem mass spectrometry. High-throughput quantitative measurement of methylmalonic acid in serum, plasma, and urine. *Clin Chem* **2001,** *47* (11), 1993-2002.

45. Bjorke Monsen, A. L.; Ueland, P. M., Homocysteine and methylmalonic acid in diagnosis and risk assessment from infancy to adolescence. *Am J Clin Nutr* **2003,** *78* (1), 7-21.

46. Kolker, S.; Schwab, M.; Horster, F.; Sauer, S.; Hinz, A.; Wolf, N. I.; Mayatepek, E.; Hoffmann, G. F.; Smeitink, J. A.; Okun, J. G., Methylmalonic acid, a biochemical hallmark of methylmalonic acidurias but no inhibitor of mitochondrial respiratory chain. *J Biol Chem* **2003,** *278* (48), 47388-93.

47. Elghetany MT, S. K., Banki K., Erythrocytic disorders. In *Henry's Clinical Diagnosis and Management by Laboratory Methods*, 23rd ed.; Richard McPherson, M. P., Ed. Elsevier: St. Lous, MO, 2017.

48. Magera, M. J.; Helgeson, J. K.; Matern, D.; Rinaldo, P., Methylmalonic acid measured in plasma and urine by stable-isotope dilution and electrospray tandem mass spectrometry. *Clin Chem* **2000,** *46* (11), 1804-10.

49. Kolker, S.; Ahlemeyer, B.; Krieglstein, J.; Hoffmann, G. F., Cerebral organic acid disorders induce neuronal damage via excitotoxic organic acids in vitro. *Amino Acids* **2000,** *18* (1), 31-40.

50. Jafari, P.; Braissant, O.; Zavadakova, P.; Henry, H.; Bonafe, L.; Ballhausen, D., Brain damage in methylmalonic aciduria: 2-methylcitrate induces cerebral ammonium accumulation and apoptosis in 3D organotypic brain cell cultures. *Orphanet J Rare Dis* **2013,** *8*, 4.

51. Frenkel, E. P., Abnormal fatty acid metabolism in peripheral nerves of patients with pernicious anemia. *J Clin Invest* **1973,** *52* (5), 1237-45.

52. Hyman, D. B.; Saunders, A. M.; Tanaka, K., A rapid spot test for urinary methylmalonic acid collected on ion-exchange filter paper. *Clinica Chimica Acta* **1983,** *132* (3), 219-227.

53. Ueland, P. M.; Schneede, J., Automated assay of methylmalonic acid in serum and urine by derivatization with 1-pyrenyldiazomethane, liquid chromatography, and fluorescence detection. *Clinical Chemistry* **1993,** *39* (3), 392-399.

54. Wajner, M.; Coelho, J. C., Neurological dysfunction in methylmalonic acidaemia is probably related to the inhibitory effect of methylmalonate on brain energy production. *J Inherit Metab Dis* **1997,** *20* (6), 761-8.

55. Lakso, H. A.; Appelblad, P.; Schneede, J., Quantification of methylmalonic acid in human plasma with hydrophilic interaction liquid chromatography separation and mass spectrometric detection. *Clin Chem* **2008,** *54* (12), 2028-35.

56. Douglas A. Skoog, F. J. H., Stanley R. Crough, *Instrumental Analysis*. 2007; p 3.

57. Petrović, M.; Hernando, M. D.; Díaz-Cruz, M. S.; Barceló, D., Liquid chromatography–tandem mass spectrometry for the analysis of pharmaceutical residues in environmental samples: a review. *Journal of Chromatography A* **2005,** *1067* (1), 1-14.

58. Verkerk, P. K. a. U. H., Electrospray: From Ions in Solution to Ions in the Gas Phase, What We Know Now. *Mass Spectrometry Reviews* **2009,** *28*, 898-917.

59. Windelberg, A.; Arseth, O.; Kvalheim, G.; Ueland, P. M., Automated assay for the determination of methylmalonic acid, total homocysteine, and related amino acids in human serum or plasma by means of methylchloroformate derivatization and gas chromatography-mass spectrometry. *Clin Chem* **2005,** *51* (11), 2103-9.

60. Schmedes, A.; Brandslund, I., Analysis of methylmalonic acid in plasma by liquid chromatography-tandem mass spectrometry. *Clin Chem* **2006,** *52* (4), 754-7.

61. Wu, Z.; Gao, W.; Phelps, M. A.; Wu, D.; Miller, D. D.; Dalton, J. T., Favorable effects of weak acids on negative-ion electrospray ionization mass spectrometry. *Anal Chem* **2004,** *76* (3), 839-47.

62. de Baulny, H. O.; Benoist, J. F.; Rigal, O.; Touati, G.; Rabier, D.; Saudubray, J. M., Methylmalonic and propionic acidaemias: management and outcome. *J Inherit Metab Dis* **2005,** *28*.

63. Brandslund, A. S. a. I., Analysis of Methylmalonic Acid in Plasma by Liquid Chromatography–Tandem Mass Spectrometry. *American Association for Clinical Chemistry* **2006,** *52* (4), 4.

64. Irini Manoli, J. L. S., and Charles P Venditti, *Isolated Methylmalonic Acidemia*. GeneReviews® [Internet]: 2005 [Updated 2022].

65. Boachie, J.; Adaikalakoteswari, A.; Samavat, J.; Ilona, G.; Saravanan, P., B12 Receptors and transporters regulate the uptake and storage of vitamin B12 in hepatocytes. *Endocrine Abstracts* **2018**.

66. Stabler, S. P., Clinical practice. Vitamin B12 deficiency. *N Engl J Med* **2013,** *368* (2), 149-60.

Chapter 3: Extraction and attempted quantification of curcumin and its metabolites in human blood and cerebrospinal fluid for secondary dosing through an internal review board study.

3.1 Introduction

Curcumin (CUR) is the active ingredient of the spice turmeric which is thought to be a potential treatment for the progression of Alzheimer's disease, but it is not readily bioavailable due to poor absorption, fast metabolic conversion, and short half-life. A physician and researcher had contacted the Kingston Research Group as a collaborator as he believed he had invented a novel extraction method which would allow increased absorption of CUR as well decreased degradation and facilitate passing through the blood brain barrier. The first of the human trials under an internal review board had begun, dosing three patients, 01-03, with their extracted CUR mixture. These three patients would then have their blood drawn at certain intervals as well as cerebrospinal fluid taken at the end of the trial. A method for extraction, detection, and quantification needed to be developed in order to give dosing information to the physician for the second set of patients, four through six. Patient samples and numbers can be seen below (**Table 3.1**). The neurologist. a rather well-known medical researcher, had designed this study and obtained the Internal Review Board approval in such a way as the remaining doses of patients were dependent on results of blood and cerebrospinal fluid results of curcumin constituents measured in initial patient's blood and CSF. The laboratory originally engaged to produce the patient measurements was not able to achieve these required quantitative concentrations. Due to the metabolization and degradation and metabolization of CUR as it passes it was determined to monitor not only for the analyte of interest (CUR), but also a suite of curcuminoid, including:

Tetrahydrocucumin (THC), Demethoxycurcumin (DMC), Bisdemethoxycurcumin (BDMC), S-turmerone (TUR), Curcumin-beta-D-Glucuronide (GLU-CUR), and a deuterated CUR standard (D-CUR), **Table 3.2**. The molecular weight and structures of the curcuminoids which were selected for in patients 01-03 can be seen in **Figure 3.1** and **3.2**.

Table 3.1: Patient codes, vials, and blood and cerebrospinal fluid draw times for all paints from both portions of the trial.

Patient	Patient Code	Vial	Time	Code
1	700794990	1	Pre-Dose	1248887761
1	700794990	2	10 Minutes	124888141
1	700794990	3	20 Minutes	124888151
1	700794990	4	30 Minutes	124888161
1	700794990	5	60 Minutes	124888171
1	700794990	6	90 Minutes	124888121
1	700794990	7	120 Minutes	124888181
1	700794990	8	240 Minutes	124888191
1	700794990	9	360 Minutes	124888201
1	700794990	10	480 Minutes	124888211
1	700794990	11	Day 7	124888131
2	700794991	1	Pre-Dose	1248887791
2	700794991	2	10 Minutes	124888281
2	700794991	3	20 Minutes	124888291
2	700794991	4	30 Minutes	124888301
2	700794991	5	60 Minutes	124888311
2	700794991	6	90 Minutes	124888261
2	700794991	7	120 Minutes	124888321
2	700794991	8	240 Minutes	124888331
2	700794991	9	360 Minutes	124888341
2	700794991	10	480 Minutes	124888351
2	700794991	11	Day 7	124888371
3	700794993	1	Pre-Dose	1248887941
3	700794993	2	10 Minutes	124888421
3	700794993	3	20 Minutes	124888431
3	700794993	4	30 Minutes	124888441
3	700794993	5	60 Minutes	124888451
3	700794993	6	90 Minutes	124888401
3	700794993	7	120 Minutes	124888461
3	700794993	8	240 Minutes	124888471
3	700794993	9	360 Minutes	124888481
3	700794993	10	480 Minutes	124888491
3	700794993	11	Day 7	124888511
1	700798451	CSF	Day 7	0516235000004*
2	700798451	CSF	Day 7	516345000008
3	700798451	CSF	Day 7	516345000012

Patient	Patient Code	Vial	Time	Code
4	700798385	1	Pre-Dose	124888091
4	700798385	2	10 Minutes	125122691
4	700798385	3	20 Minutes	125122701
4	700798385	4	30 Minutes	125122711
4	700798385	5	60 Minutes	125122721
4	700798385	6	90 Minutes	125122671
4	700798385	7	120 Minutes	125122731
4	700798385	8	240 Minutes	125122741
4	700798385	9	360 Minutes	125122751
4	700798385	10	480 Minutes	125122761
4	700798385	11	Day 7	125122781
5	70098386	1	Pre-Dose	124887881
5	70098386	2	10 Minutes	125122831
5	70098386	3	20 Minutes	125122841
5	70098386	4	30 Minutes	125122851
5	70098386	5	60 Minutes	125122861
5	70098386	6	90 Minutes	125122811
5	70098386	7	120 Minutes	125122871
5	70098386	8	240 Minutes	125122881
5	70098386	9	360 Minutes	125122891
5	70098386	10	480 Minutes	125122901
5	70098386	11	Day 7	125122921
6	700798388	1	Pre-Dose	124887911
6	700798388	2	10 Minutes	125122971
6	700798388	3	20 Minutes	125122981
6	700798388	4	30 Minutes	125122991
6	700798388	5	60 Minutes	125123001
6	700798388	6	90 Minutes	125122951
6	700798388	7	120 Minutes	125123011
6	700798388	8	240 Minutes	125123021
6	700798388	9	360 Minutes	125123031
6	700798388	10	480 Minutes	125123041
6	700798388	11	Day 7	125123061
4	700798451	CSF	Day 7	5163450000015
5	700798451	CSF	Day 7	5163450000019
6	700798451	CSF	Day 7	5163450000023

*Cerebrospinal fluid of patient 1 was contaminated with blood.

Table 3.2: Compound, manufacturer, and batch number of curcumin and its metabolites to be investigated

Compound	Abbreviation	Manufacturer	Batch
Curcumin	CUR	Sigma Aldrich	WXBC5392V
Tetrahydrocurcumin	THC	Sigma Aldrich	SLBML199V
Demethoxycurcumin	DMC	Sigma Aldrich	BCB37351V
Bisdemethoxycurcumin	BDMC	Sigma Aldrich	BCB51226V
S-turmerone	TUR	Sigma Aldrich	BCBV3815
Deuterated Curcumin	D-CUR	Clear Synth	CS-CM-338
Curcumin-beta-D-Glucuronide	G-CUR	CellMosaic	290881

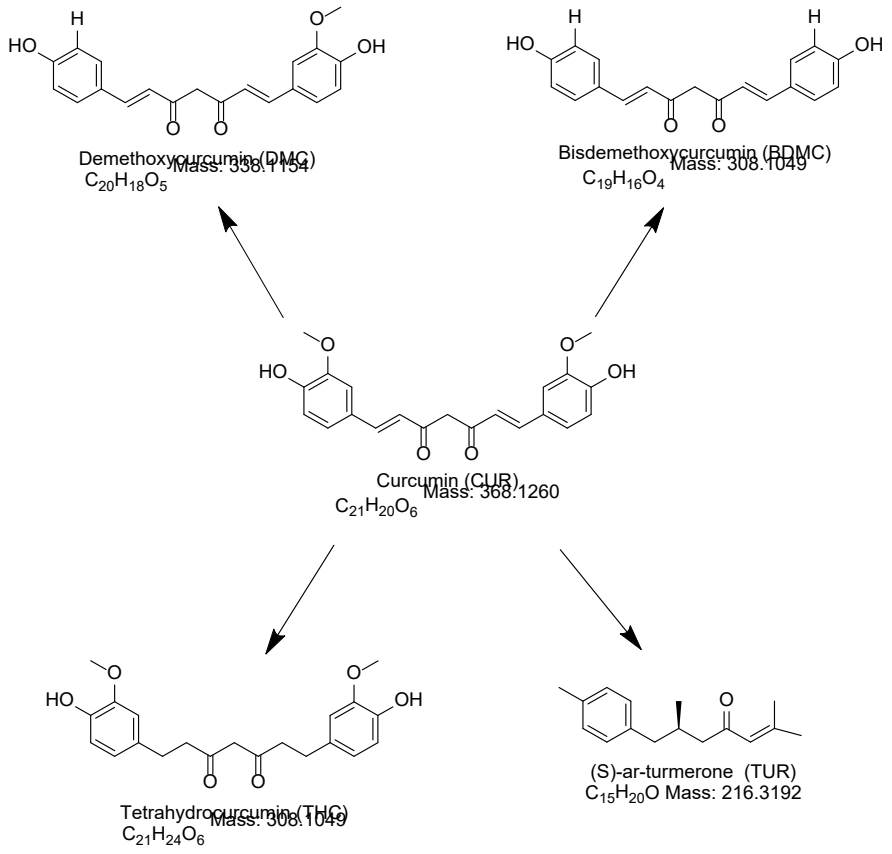

Figure 3.1: Chemical structures, exact masses, and molecular formulas of curcumin, and its analogues and metabolites, demothoxycurcumin, bisdemethoxycurcumin, tetrahydrocurcumin, and S-Turmerone.

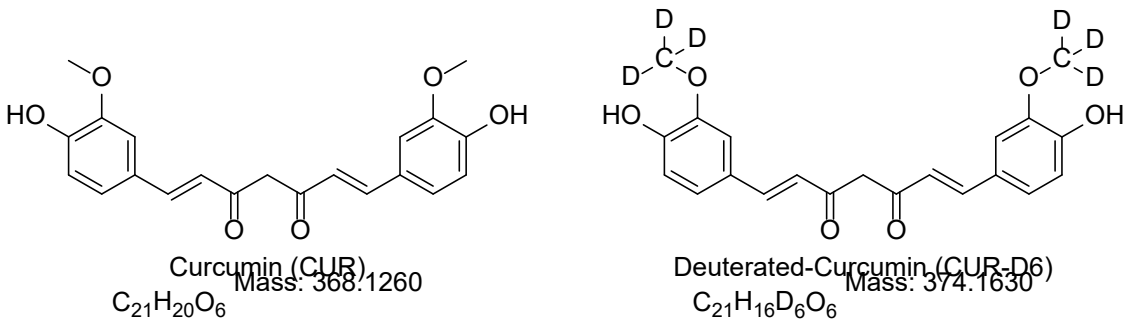

Figure 3.2: Difference in mass and structure of curcumin and its deuterated internal standard.

3.2 Background

CUR is the active ingredient in the traditional herbal remedy, coloring agent, and spice called tumeric.[1-3] Turmeric, which has a vibrant yellow color, is derived from the plant *Curcuma longa* and is commonly used in south Asian cooking and traditional medicine.[1] Turmeric's use as a medicine has spanned centuries and has an extensive list of anecdotal reported usages, including eye aliments, wound dressings, childbirth recovery, dental diseases, digestive disorders such as dyspepsia and acidity, indigestion, flatulence, ulcers, as well as alleviation of the hallucinatory effects of psychotropic drugs.[1] Due to the extensive list of anecdotal remedies and its tolerance level in humans researchers have begun to investigate potential therapeutic treatments of CUR.[1, 4, 5] A wide array of healing and anti-cancer benefits for the use of CUR have already been described including: anti-inflammatory and antioxidant activities;[6-8] chemopreventive, chemotherapeutic, and chemosensitizing activities;[9-11] radiosensitization in cancer cells and radioprotection in healthy cells;[12-14] inhibition of angiogenesis and metastasis in cancer cells;[15-17] a signaling molecule in key survival pathways regulated by NF-κB and Aκt,[18-20] as well as cytoprotective pathways dependent on Nrf2,[21] p53 tumor suppressor,[22] induction of phase II enzymes,[23] Signal-transducer-and-activator-of-transcription-3 activation,[24] modulation of growth factors,[25] and mitogen-activated protein kinases.[26]

In addition to anti-cancer properties, CUR has also been reported to slow or arrest the onset of symptoms of Alzheimer's disease.[27-30] This is theorized to take place due to one of several possibilities. CUR may help reduce the inefficiency in, or reduce defective phagocytosis of, macrophages and increase their ability to remove beta-amyloid plaques.[31] While the reduction of beta-amyloid plaques have been theorized as one potential mechanism of action for the reported arresting or reversing of symptoms of Alzheimer's disease, recent controversy over potentially doctored data in the original paper has led to some to question this pathway. Recent histological studies have revealed activated microglia and reactive astrocytes around amyloid beta plaques with chronic activation shown to secret cytokines which exacerbate pathology.[32] CUR has demonstrated anti-proliferative actions on microglia[32] as well as an overall reduction in "plaque burden" by destabilization of the amyloid beta polymer and increased phagocytosis.[33, 34] Inflammation is another possible cause of Alzheimer's disease, and CUR has been found to have anti-inflammatory effects through inhibition of early growth response gene-1 DNA-binding activity[35] as well as the inhibition of cyclooxygenase, phospholipases, transcription factor and enzymes involved in metabolizing the membrane phospholipids into prostaglandins.[36, 37] Curcuminoids are also strong anti-oxidants, removing reactive oxygen species, the free radicals of which have a proven correlation to deterioration of neurons,[36, 38, 39] and are an inducing agent of heme oxygenase-1, which increases the concentration of reduced glutathione.[40-42] Curcuminoids have also been observed to have a chelation effect for copper and heavy metals which have been shown to damage neurons.[43-45] Finally, CUR has been shown to reduce cholesterol which has been linked to increase in amyloid plaques by the intracellular accumulation of cholesteryl esters.[46, 47] A chart of these potential benefits to the brain can be seen below, **Figure 3.3**. While the reduction of amyloid plaques has been theorized as one potential mechanism of action for the reported arresting or

reversing of symptoms of Alzheimer's disease, recent controversy over potentially doctored data in the original paper has led some to question this pathway.[48, 49]

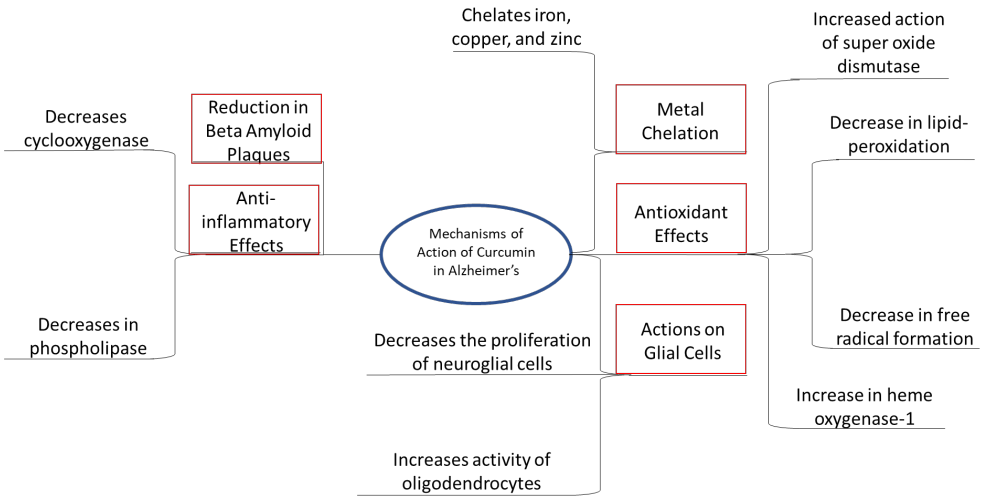

Figure 3.3: Possible effects on Alzheimer's disease by curcumin. Adapted from Chen et al.[29]

Despite the myriad of possible benefits of CUR to humans, its pharmacokinetic properties are not widely utilized due to its poor bioavailability due to low intrinsic activity, poor absorption from gastrointestinal tract, high rate of metabolism, inactivity of metabolic products and/or rapid elimination, and clearance from the body.[50-52] Serum concentration of CUR and its metabolites has been shown to have extremely poor absorption, requiring a high dose to see any appreciable concentration in blood.[53-55] The dose dependent bioavailability in the blood shows an even smaller concentration reach tissues due to processes such as sulphuration, hydration, glucuronidation, and rapid degradation at physiological pH meaning only trace amounts are available once CUR has reached the target organ system.[51, 55, 56] One final problem is the measured half-life of CUR in the body, which appears to be dose independent but has been observed to be as little as 1.45 hours.[50, 57, 58]

CUR has a difficult time surviving the rigors of the body, it is a fragile molecule that is being thermally, photo, pH, and water sensitive.[59-62] In temperatures above 25 °C, CUR rapidly degrades into 4-vinyl guaiacol, which has little information on therapeutic benefits.[59] CUR is likewise pH sensitive, with rapid degradation taking place after only three minutes at physiological pH and requiring an acidic pH for long term storage.[60] Due to its ring structure, CUR is also photosensitive degrading in less than 24 hours when exposed to ultraviolet (UV)-light of 254 nm wavelength, requiring a yellow wavelength of 405 nm for long term stability.[61, 63] Water also has a negative effect on CUR stability, decreasing the overall concentration of the molecule by 15.7% per day of storage with CUR being so sensitive concentrations in analysis are known to fluctuate due to humidity.[62, 64] Thus, samples need to be processed and tested in a cool, dry, light controlled environment.

3.3 Patient 01-03 Materials and Methods

3.3.1 Reagents and Materials

Materials purchased for the project included chemical analytes of interest, internal standard, extraction materials, mobile phase, and bovine serum for method optimization and calibration curve standards. These chemicals were stored as recommended in the packaging so as not to cause degradation. Materials were stored in a -80 °C freezer: CUR, THC, DMC, BDMC, and TUR after being diluted in methanol, as well as D-CUR which was used as an internal standard. For the quantification of curcumin and its metabolites in the first part of the experiment, patient samples 1 through 3, calibration curves were made from the analytes described in **Table 3.2**. Patient samples were shipped to Duquesne University the day of collection by Federal Express on dry ice and were immediately cataloged and placed in a -80 °C freezer until they were to be

utilized. They were thawed on ice and covered with a non-transparent lid to be protected from exposure to UV radiation.

For extraction, optima grade ethyl acetate, Fisher Chemical (Lot 112360), and ethanol, Pharmco (Lot LR5178) were utilized. 18.2 Ω deionized water was made using a 7146 Barnstead NANOpure system (Model 251115-102), which was then passed through a D7035 Easypure II water filtration system (Model 1305080906425). This water was used for all dilutions and rinses. High pressure liquid chromatography (HPLC) grade methanol (Lot 170293) and acetonitrile (Lot 216634) was purchased from Fisher Chemical. Bovine serum purchased from Lampire on 01/30/2017 which had been stored in -80 °C freezer was utilized. Calibration curve levels were made by taking stock solutions of natural analytes: CUR, THC, DMC, BDMC, and TUR with concentration of approximately 11,000 ng/g and performing serial dilutions in methanol as well as a constant level of deuterated internal standard: CUR-D6. All samples were prepared by spiking 100 µL of bovine serum, acquired from Lampire with 10 µL of internal standard and 10 µL of spike from the corresponding calibration level.

Artificial cerebrospinal fluid was synthesized using a method from Azlet Osmotic Pumps[65] in two one-liter solutions to decrease potential bacterial growth. Solution A was made by mixing 4.33 g of sodium chloride, Amresco (Lot 0732C116), 0.112 g potassium chloride, Mallinckrodt (Lot 6858 KAAL), 0.103 g of calcium chloride hydride, EM Science (Lot 3440425) and 0.0815 g of magnesium chloride hydride, Alfa Aesar (Lot C26W046). Solution B was comprised of 0.0071 g of sodium hydrogen phosphate, Fischer Scientific (Lot 744526) and 0.107 g sodium dihydrogen phosphide hydrate, Fischer Scientific (Lot 923489). These solutions were mixed in a 50:50 proportion for all cerebrospinal fluid method development and calibration curves. All masses were taken on an XS105 Dual Range Mettler Toledo balance (Model 1129191055). Samples were

mixed on a SI-A236 Vortex Genie 2 Digital (Model A3-1896), centrifuged in an AG 5453 Eppendorf Mini Spin Plus centrifuge (Model 5453ZL055696), and dried and concentrated in a SPD1010-115 ThermoFisher Savant SPD1010 SpeedVac Concentrator (Model O23W-433565-OW). VWR low volume micropipettes and Eppendorf micropipettes were used. Collection, centrifugation, and drying were completed in 1.5 mL VWR microcentrifuge tubes (Lot 211009653-D).

An Agilent 1200 Liquid Chromatography System comprised of a G13798B degasser, a G1312B binary pump, a G1367D high performance autosampler, a G1330B thermostat, and a G1316B column compartment, was utilized for separation which was then ionized via electrospray using a G1958-65138 Agilent Jet-Stream Electrospray Ionization source and passed into an Agilent 6460 Mass Spectrometer. Contents were separated on a Supelco Ascentis Express RP-Amide HPLC Column 10cm x 2.1mm, 5µm (Lot S14013). Quantification was performed using Agilent Technologies MassHunter software (Version B.06.00 SP1) that was loaded on a computer which Windows 10 Pro (Version 1909, OS Build 18363.1139) operating system had been installed.

All sample, calibration curve, blank, and quality control samples were prepared and extracted in a 20 °C walk in refrigerator under a 405 nm wavelength yellow light-emitting diode bulb which to prevent degradation. After extraction, samples were placed into amber glass Agilent 2 mL liquid chromatography vials and the sample chamber of the liquid chromatography system was chilled to 20 °C for the duration of the experiment. Due to some proteins not responding to ultracentrifugation and remaining suspended in solution, some samples were allowed to sit on ice for 10 minutes to allow settling and then were as much of the top layer of liquid was removed as possible into a separate amber liquid chromatography vial to prevent column damage. Due to time

constraints, samples were run in replicates of four, separated by blanks, and book-ended by calibration curves and quality control standards to measure and correct for instrument drift.

3.3.2 Liquid Chromatography Mass Spectrometry Separations and Detections and Sample Processing

Prior to development of liquid chromatography separation methods, detection of analytes must be achieved. This is done by direct injection and scanning for parent ion then, once achieved, utilizing a product ion scan to determine mass transitions after the collision of the ions with inert nitrogen gas. Once these identifying markers are discovered, an optimization program is run to give the largest possible response to the analytes and give quantification at the lowest possible levels. These potential parameters include: the fragmentor and collision energies and the gas temperature and flow rate which improved collision efficiency; the polarity of the instrument which selects for one of the two possible ionization states; the nebulizer pressure, sheath gas temperature and flow rate which determines the efficiency of the electrospray ionization chamber; and the capillary and nozzle voltage which determines the efficiency of ions entering the mass spectrometer. Due to the potential number of analytes in the sample, the largest response of each was taken and used to determine the best average response (**Tables 3.3** and **3.4**).

Table 3.3: Fragmentation weights, energies, and polarity for detection of curcuminoids: curcumin, tetrahydrocurcumin, demethoxycurcumin, bisdemethoxycurcumin, and S-turmerone for detection on an Agilent 6460 triple quadrupole mass spectrometer.

Analyte	Weight (DA)	Fragment Weight (DA)	Fragmentor Energy (V)	Collision Energy (V)	Polarity
BDMC	307.3	186.9	95	10	Negative
BDMC	307.3	142.9	95	10	Negative
BDMC	307.3	118.9	95	30	Negative
CUR	367.1	217.1	95	5	Negative
CUR	367.1	149.1	95	10	Negative
CUR	367.1	134	95	30	Negative
CUR-D6	373.4	219.9	95	5	Negative
CUR-D6	373.4	151.8	95	10	Negative
CUR-D6	373.4	133.8	95	30	Negative
DMC	337.4	216.8	95	6	Negative
DMC	337.4	173.1	95	10	Negative
DMC	337.4	118.9	95	30	Negative
THC	373.4	177	95	3	Positive
THC	373.4	163	95	5	Positive
THC	373.4	137	95	30	Positive
TUR	217.3	118.9	70	15	Positive
TUR	217.3	91	70	55	Positive

Other parameters: collision gas temperature and flow rate, nebulizer pressure, sheath gas temperature and flow rate, and capillary and nozzle voltages, can also be optimized on an Agilent 6460 triple quadrupole mass spectrometer to ensure the largest analyte response.

Table 3.4: Aggregate optimization parameters for curcuminoids: curcumin, tetrahydrocurcumin, demethoxycurcumin, bisdemethoxycurcumin, and S-turmerone for detection on an Agilent 6460 triple quadrupole mass spectrometer.

Parameter	Optimization
Gas Temperature	330 ˚C
Gas Flow Rate	10 L/min
Nebulizer Pressure	45 PSI
Sheath Gas Temperature	400 ˚C
Sheath Gas Flow Rate	12 L/min
Capillary Voltage	5000 V
Nozzle Voltage	2000 V

Separation was achieved on a Supelco Ascentis Express RP-Amide HPLC Column 10cm x 2.1mm, 5µm column (**Table 3.5**).

Table 3.5: Final separation method for curcuminoids: curcumin, tetrahydrocurcumin, demethoxycurcumin, bisdemethoxycurcumin, and S-turmerone on a Supelco Ascentis Express RP-Amide HPLC Column 10cm x 2.1mm, 5µm column.

Time (Min)	H_2O %	Acetonitrile %	Flow (mL/min)
0	60	40	1.0000
1	60	40	1.0000
4	50	50	1.0000
5	40	60	1.0000
6	0	100	1.0000
7	0	100	1.0000
7.1	60	40	1.0000

This liquid chromatography method gave baseline separation and gaussian peaks of all analytes: CUR THC, DMC, DBMC, and TUR (**Figure 3.4**).

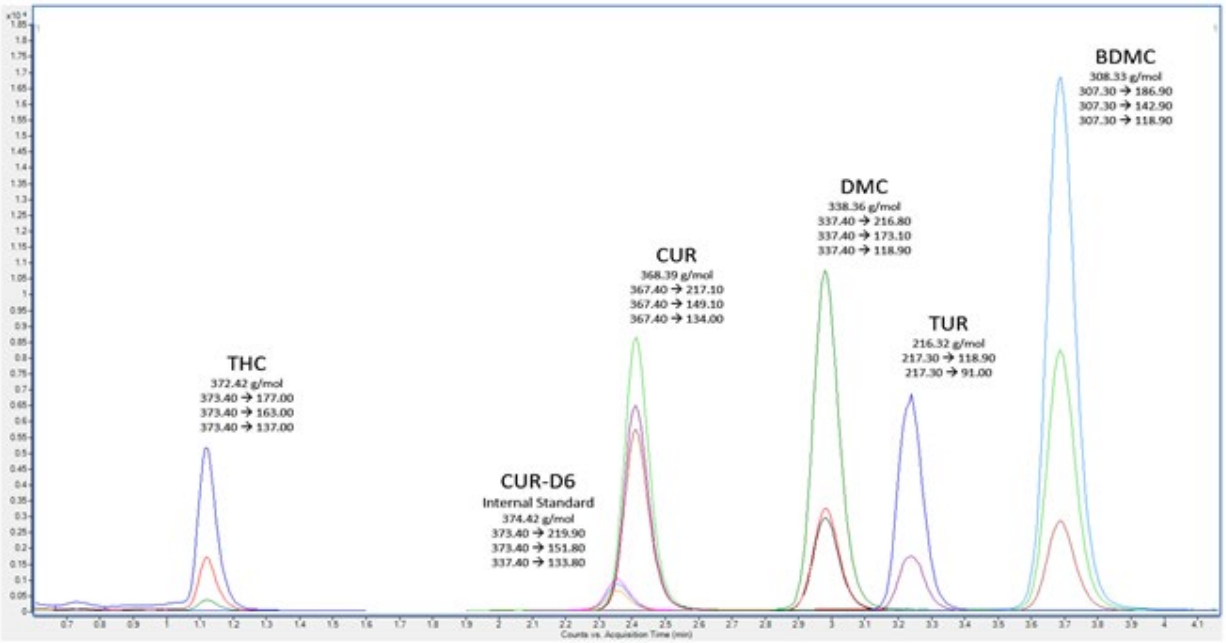

Figure 3.4. Final separation of curcuminoids: curcumin (CUR), tetrahydrocurcumin (THC), demethoxycurcumin (DMC), bisdemethoxycurcumin (BDMC), and S-turmerone (TUR) on a Supelco Ascentis Express RP-Amide HPLC Column 10cm x 2.1mm, 5µm column detected on an Agilent 6460 triple quadrupole mass spectrometer. Molecular weights and mass transitions are listed.

Prior to testing on patient samples, extraction, separation, and detection methods were developed and improved upon. The extraction methods and development can be seen below (**Table 3.6**). Due to time constraints of the project, patient blood samples from patient one used the Modified extraction procedure. Patient blood samples from patients two and three as well as all cerebrospinal fluids used the Final Modified Extraction Procedure, which was shown to have an increased extraction response.

Table 3.6: Evolution of extraction protocol[66] in serum and cerebrospinal fluid for curcuminoids: curcumin, tetrahydrocurcumin, demethoxycurcumin, bisdemethoxycurcumin, and S-turmerone. The final modified extraction procedure was utilized for patients 01-03 in this portion of the study.

Extraction Procedure from Literature[66]		Modified Extraction Procedure*		Final Modified Extraction Procedure**	
Reagent	Volume	Reagent	Volume	Reagent	Volume
Serum	100 µL	Standard	10 µL	Standard	10 µL
Standard	10 µL	Internal Standard	10 µL	Internal Standard	10 µL
Internal Standard	10 µL	Vortexed at 3000 RPM for 10 Seconds		Vortexed at 3000 RPM for 10 Seconds	
Vortexed at 3000 RPM for 10 Seconds		Centrifuged at 13500 RPM for 4 Minutes		Centrifuged at 13500 RPM for 4 Minutes	
Ethyl Acetate	3 mL	Ethyl Acetate	1000 µL	Ethyl Acetate	500 µL
Vortexed at 3000 RPM for 30 Seconds		Vortexed at 3000 RPM for 30 Seconds		Vortexed at 3000 RPM for 10 Seconds	
Centrifuged at 6000 RPM for 4 Minutes		Centrifuged at 13500 RPM for 4 Minutes		Centrifuged at 13500 RPM for 4 Minutes	
Removed Supernatant into 5 mL tube		Removed Supernatant into 1.5 mL Tube		Removed Supernatant into 1.5 mL Tube	
Used Nitrogen to Evaporate Ethyl Acetate		Ethyl Acetate	500 µL	Ethyl Acetate	500 µL
		Vortexed at 3000 RPM for 30 Seconds		Vortexed at 3000 RPM for 10 Seconds	
		Centrifuged at 13500 RPM for 4 Minutes		Centrifuged at 13500 RPM for 4 Minutes	
		Placed in Speed Vac at 45 ˚C for 15 minutes and Continued Vacuum for an Additional 45 minutes		Removed Supernatant into 1.5 mL Tube	
				Ethyl Acetate	1000 µL
		Minutes at 5.1 Torr		Vortexed at 3000 RPM for 30 Seconds	
				Centrifuged at 13500 RPM for 4 Minutes	
				Removed Supernatant into 1.5 mL Tube	
				Placed in Speed Vac at 45 ˚C for 15 minutes and Continued Vacuum for an Additional 45 minutes	
				Minutes at 5.1 Torr	
Reconstitution		Reconstitution		Reconstitution	
Acetonitrile	50 µL	Acetonitrile	50 µL	Acetonitrile	50 µL
18 Ω DI Water	50 µL	18 Ω DI Water	50 µL	18 Ω DI Water	50 µL
Formic Acid	0.1 µL	Formic Acid	0.1 µL	Formic Acid	0.1 µL
Vortexed at 3000 RPM for 30 Seconds		Vortexed at 3000 RPM for 30 Seconds		Vortexed at 3000 RPM for 30 Seconds	
Centrifuged at 6000 RPM for 4 Minutes		Centrifuged at 13500 RPM for 4 Minutes		Centrifuged at 13500 RPM for 4 Minutes	
Removed 25 µL for Analysis in LC-MS		Removed 50 µL for Analysis in LC-MS		Removed 50 µL for Analysis in LC-MS	

Once final separation and extraction procedures had been achieved, patient samples were extracted and tested for the curcuminoids. An eleven-point calibration curve was made following United States Food and Drug Administration (FDA) validation protocol, such that at least six could be conserved. All calibration curves were bracketed to correct for instrument drift and included three quality control samples which were also bracketed. Blanks consisting of a 50:50 mixture of water and acetonitrile were also measured several times throughout the

run time to account for any crossover or contamination. A sample workflow could be shown as:

- 11 calibration curve standards run in duplicate
- 3 quality control samples (low, medium, and high) run in duplicate
- 11 patient samples run in quadruplicate
- 3 quality control samples (low, medium, and high) run in duplicate
- 11 calibration curve standards run in duplicate

The concentrations of these calibration curve points, and quality control standards (**Table 3.7**) lists the known concentrations of each standard in patients 01-03.

Table 3.7. Concentrations of curcumin and its analogs in calibration curves, quality control standards, and deuterated internal standard for patients 01-03.

Calibration Level	Concentration of Curcumin and Analogs in Spike (ng/g)	Final Concentration of Curcumin and Analogs in Serum (ng/g)
11	1000	83.33
10	500	41.67
9	250	20.83
8	125	10.42
7	62.5	5.21
6	31.25	2.6
5	15.63	1.3
4	7.81	0.65
3	3.91	0.33
2	1.95	0.16
1	0.98	0.08
Quality Control 3	523.81	43.65
Quality Control 2	261.9	21.83
Quality Control 1	130.95	10.91
Internal Standard in All Samples	100	8.33

These standards were used to produce the following calibration curves (**Figure 3.5**) for potential quantification of any detected curcuminoids. Based on these calibration curves, a limit of detection of 5.0 ng/mL and a limit of quantitation of 15.1 ng/mL was calculated. Despite these relatively low limits, no quantitation of any curcuminoids in any sample was achieved, though repeated detection was observed in several samples.

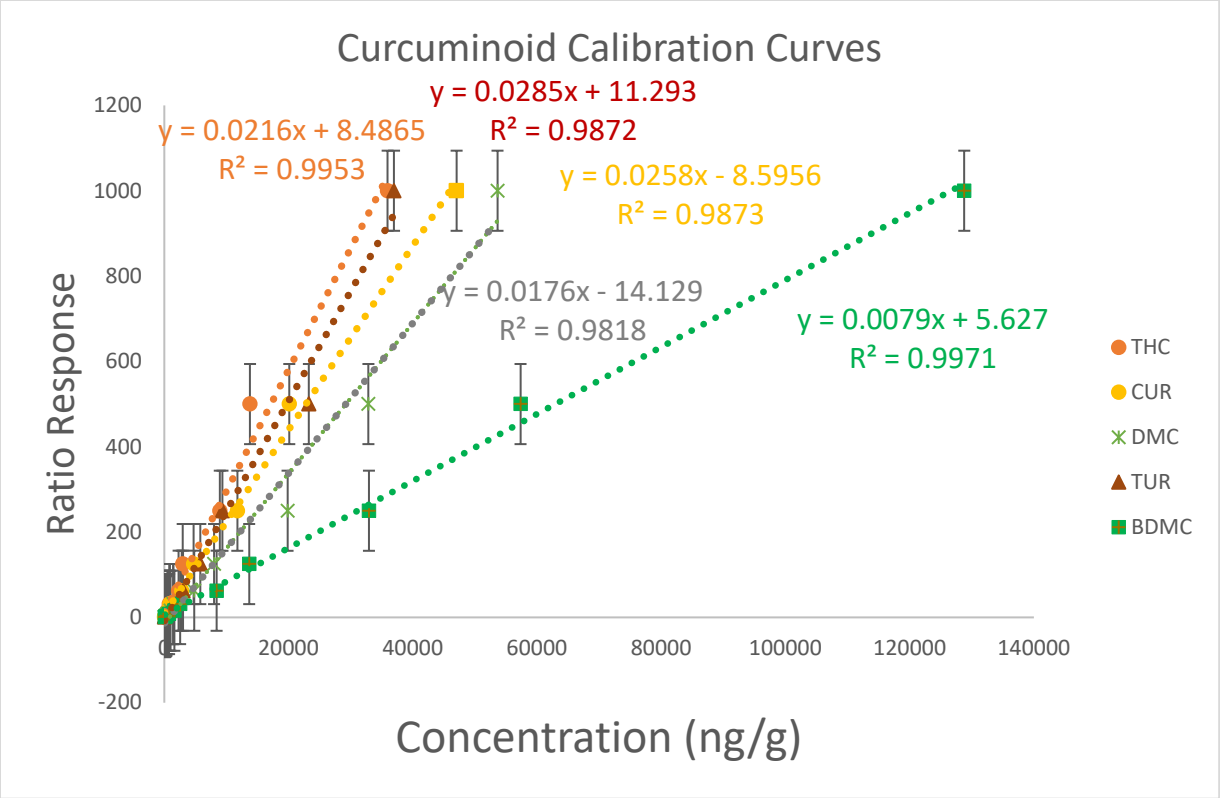

Figure 3.5: Combined calibration curves of curcuminoids: curcumin (CUR), tetrahydrocurcumin (THC), demethoxycurcumin (DMC), bisdemethoxycurcumin (BDMC), and S-turmerone (TUR) with accompanying linearity for patients 01-03.

3.4 Results and Discussion of Patient 01-03

Determination of the efficacy of curcumin extraction and dosing required analytical quantitation of curcuminoids. Extractions were performed and quantitation was attempted via the use of calibration curves (**Figure 3.5**). Results of extraction and processing of samples (**Table 3.8**) were catalogued, and it was determined that, while analytes of THC, DMC, TUR and BDMC were observed qualitatively, they were at an insufficient level to be quantitated. Due to qualitative THC being observed in all samples, including those taken prior to dosing of the patients with medication, it was believed that these either represented an unknown molecule of similar mass transitions or

potential contamination of samples prior to delivery to Duquesne University. As no appreciable amount of DMC, TUR, or BDMC were present in samples prior to dosing, it was determined that these were more worthy of consideration as being the analytes of interest. However, TUR and BDMC only appeared in one of the three patients each. This could potentially be caused by different absorption and metabolic rates of patients as they were only observed in the serum of patient one. More consistently, DMC was observed in serum and cerebrospinal fluid of all patients beginning at the third collection time. Prior to analysis, it was theorized that analyte levels would increase as they passed from the gastrointestinal tract into the body and then decrease as they were cleared. This would eventually plateau on the final draw, Day 7, after the patient had been dosed consistently for a week. However, once absorbed, DMC remained in the body for the duration of the first dosing showing a potential longer half-life within the body than other analytes of CUR. Chromatograms of analytes THC in serum (**Figure 3.6**), TUR in serum (**Figure 3.7**), THC in cerebrospinal fluid (**Figure 3.8**), BDMC in cerebrospinal fluid (**Figure 3.9**), and an overlay of all patient samples, both serum and cerebrospinal fluid (**Figure 3.10**) to show the observed analytes in relation to the signal to noise ratio are presented.

Table 3.8: Complied results for patients 01-03 for all serum and cerebrospinal fluid samples. Where ND stands for no detection and NQ stands for not quantifiable.In sample tube 6 of Patient 01, in one of the four replicates, a large amount of curcumin was observed. This was not seen again in any of the other three repicates or in any of the other time samples before or after, this replicate was discarded as an instrument error.

Patient	Vial	THC	CUR	BDMC	TUR	DMC
1	1	NQ	ND	ND	ND	ND
1	2	NQ	ND	ND	ND	ND
1	3	NQ	ND	ND	ND	ND
1	4	NQ	ND	NQ	ND	NQ
1	5	NQ	ND	ND	ND	ND
1	6	NQ	ND*	ND	ND	NQ
1	7	NQ	ND	NQ	NQ	NQ
1	8	NQ	ND	ND	ND	NQ
1	9	NQ	ND	ND	ND	ND
1	10	NQ	ND	ND	ND	ND
1	11	NQ	ND	ND	ND	NQ
2	1	NQ	ND	ND	ND	ND
2	2	NQ	ND	ND	ND	ND
2	3	NQ	ND	ND	ND	ND
2	4	NQ	ND	ND	ND	NQ
2	5	NQ	ND	ND	ND	NQ
2	6	NQ	ND	ND	ND	NQ
2	7	NQ	ND	ND	ND	NQ
2	8	NQ	ND	ND	ND	NQ
2	9	NQ	ND	ND	ND	NQ
2	10	NQ	ND	ND	ND	NQ
2	11	NQ	ND	ND	ND	NQ
3	1	NQ	ND	ND	ND	ND
3	2	NQ	ND	ND	ND	ND
3	3	NQ	ND	ND	ND	NQ
3	4	NQ	ND	ND	ND	NQ
3	5	NQ	ND	ND	ND	NQ
3	6	NQ	ND	ND	ND	NQ
3	7	NQ	ND	ND	ND	NQ
3	8	NQ	ND	ND	ND	NQ
3	9	NQ	ND	ND	ND	NQ
3	10	NQ	ND	ND	ND	NQ
3	11	NQ	ND	ND	ND	NQ
1	CSF	NQ	ND	ND	ND	NQ
2	CSF	NQ	ND	ND	ND	NQ
3	CSF	NQ	ND	ND	ND	NQ

THC was theoretically quantitatively observed in all levels of patient samples including a pre-dosed blood sample. As such, it was questioned whether these repeated observations were authentic, or an artifact.

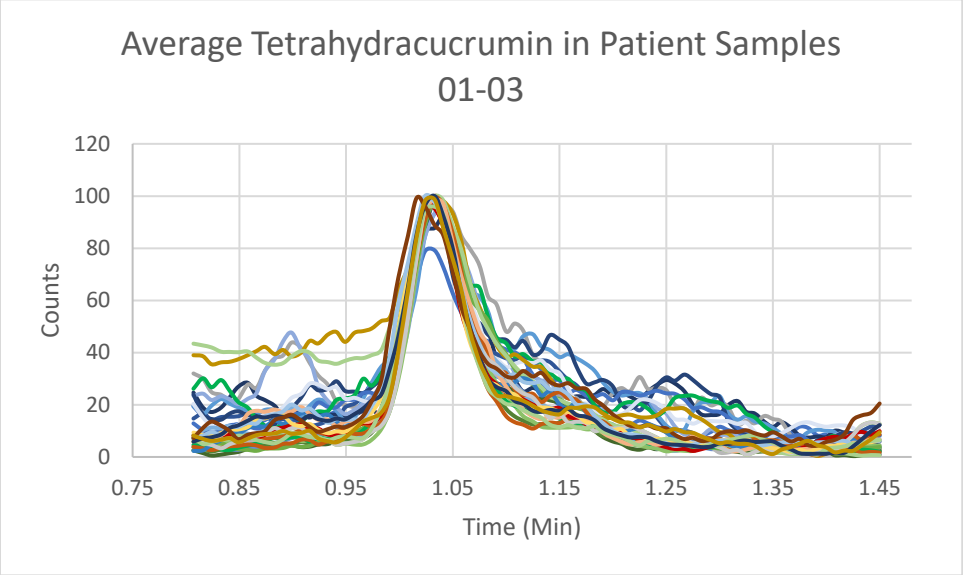

Figure 3.6: Overlaid replicates of all patients showing possible positive response for tetrahydrocucumin in serum samples of patients 01-03 With blue being Patient 01, green Patient 02, and brown Patient 03.

DMC was observed in the serum of all patients throughout the study, starting with the third blood draw. Thus, it is likely this analyte was present, just in a concentration too low for quantitation.

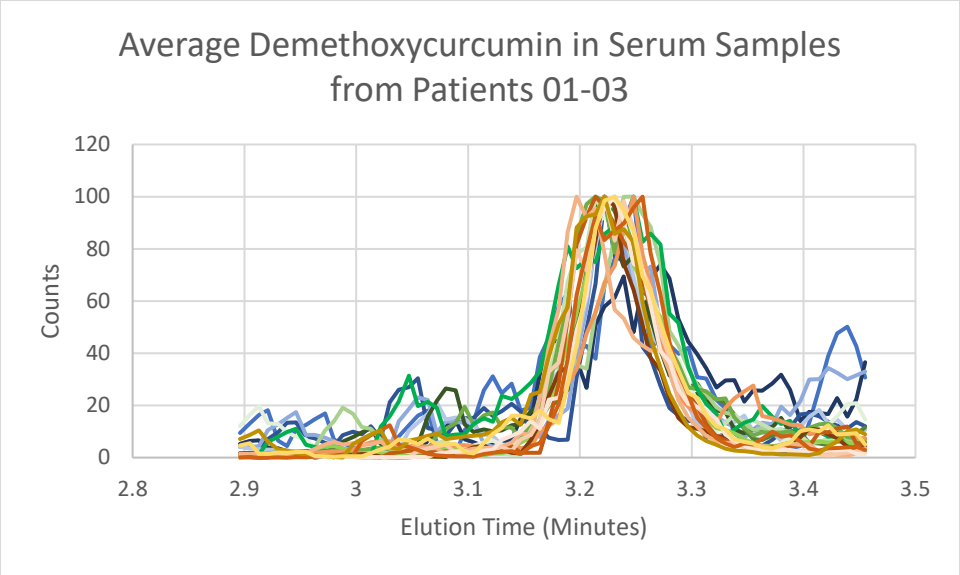

Figure 3.7: Average overlaid replicates of all patients showing possible positive response for demethoxycurcumin in serum samples with Patient 01 in blue, Patient 02 in green, and Patient 03 in brown.

THC was observed in cerebrospinal fluid, but due to its ubiquity in the study it remains to be determined if the analyte was present, or an artifact.

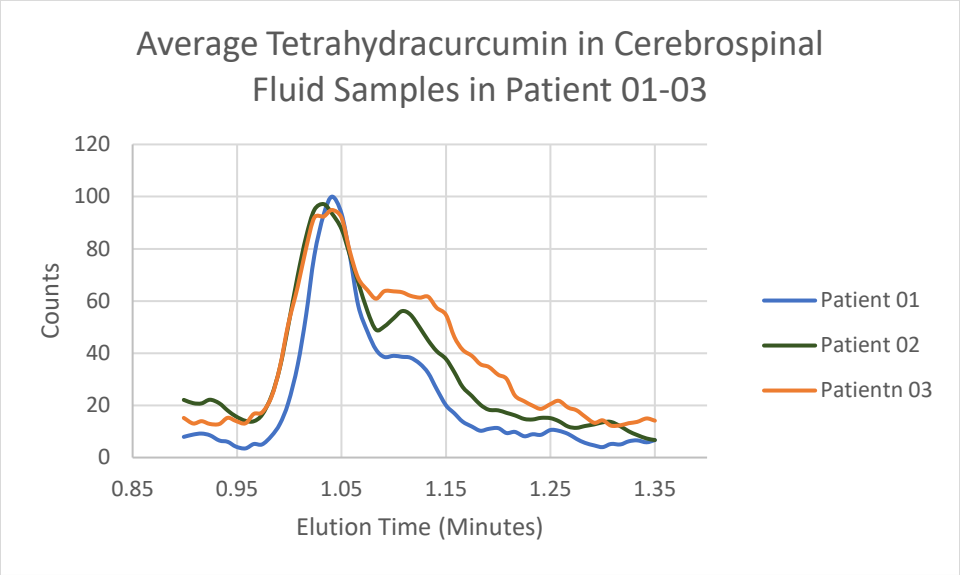

Figure 3.8: Overlaid replicates showing possible positive response for tetrahydrocucumin in cerebrospinal fluid samples, where Patient 01 is blue, Patient 02 is green, and Patient 03 is brown.

DMC was observed in the cerebrospinal fluid of all patients, as well as the provided serum. Due to the nature of its appearance in serum samples, it was determined that DMC was present, but in a concentration too low to be quantitated using traditional calibration curves.

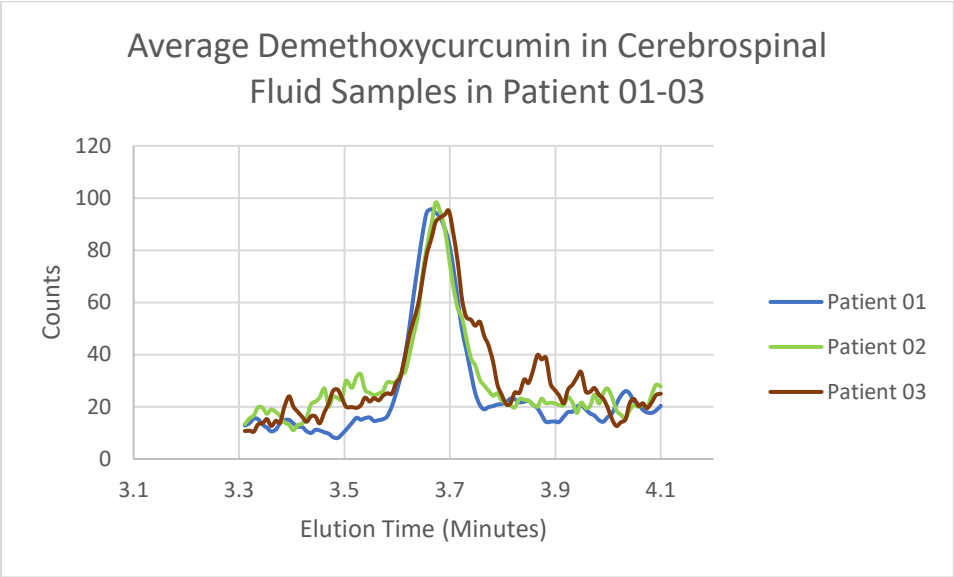

Figure 3.9: Overlaid replicates showing possible positive response for demethoxycurcumin in cerebrospinal fluid samples where Patient 01 is blue, Patient 02 is green, and Patient 03 is brown.

When determining whether a peak can be quantified or even said to be there the signal to noise ratio must be determined. All patient samples, for both blood and cerebrospinal fluid were taken and overlaid. While no peaks were large enough to reach the requisite ten times signal to noise ratio for quantification, or indeed even the 3.3 times to allow for qualitative results, these peaks are above the baseline noise and replicated among different attempts and samples.

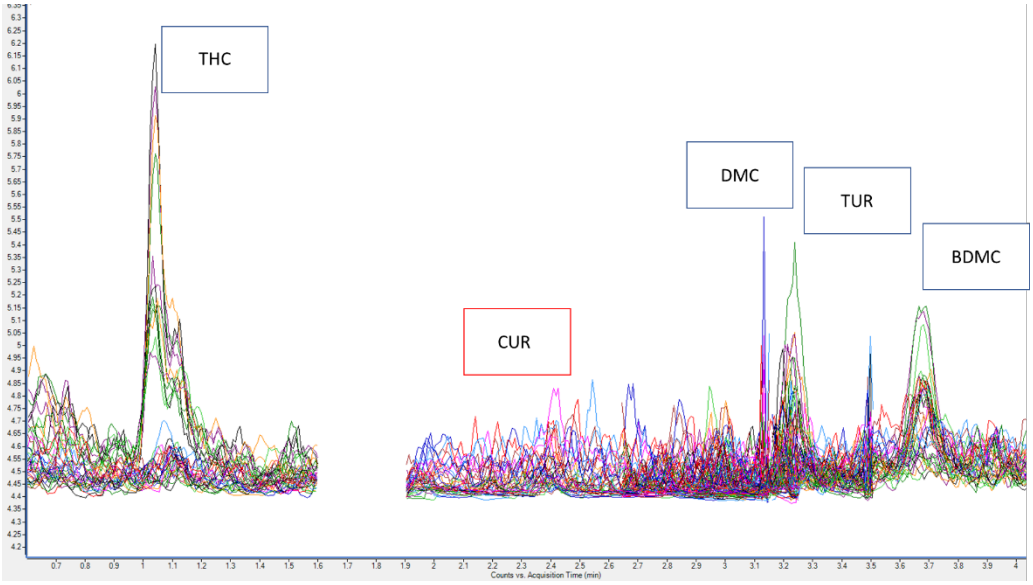

Figure 3.10: Overlapping spectra of all measurments in cerebrospinal fluid for three patients (01-03) in part I of the experiment. Potentially observed analytes are surrounded by a blue box, those that are not present are surrounded by a red box.

3.5 Conclusions of Patient 01-03 Dosing Trials

It was determined that the analyte BDMC was present in both serum and cerebrospinal fluid due to the repeated observations of peaks between patients as well as its absence in the first two blood draws, indicating a time delay for absorption. THC was observed in all patient samples and cerebrospinal fluid including a pre-dose measurement. Thus, it was unclear whether this analyte was present in the patient's pre-dose or was an artifact. No quantitation was possible due to the low levels of analyte and lack of isotopically enhanced spikes for any curcuminoid other than CUR, which was not observed. The physician increased the dose for the next round of patients, and it was decided levels of these analytes as well as GLU-CUR (**Figure 3.11**) to determine if any of the absorbed CUR had been metabolized and was no longer viable as an active ingredient.

3.6 Patients 04-06 Materials and Methods

3.6.1 Reagents and Materials

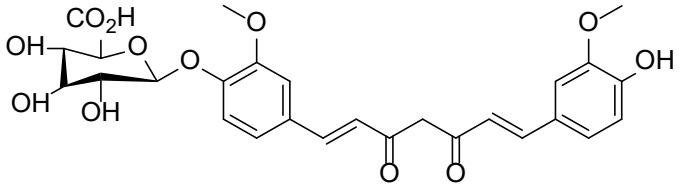

Curcumin-beta-D-Glucuronide (GLU-CUR)
Mass: 544.5090
$C_{27}H_{28}O_{12}$

Figure 3.11: Chemical structure, exact mass, and molecular formula of glucouronidated curcumin (Curcumin-beta-D-Glucu ronide)

3.6.2 Instrumentation

The same instruments and chemicals were utilized as in the first part of the experiment except for the Ascentis Express RP-Amide HPLC Column 10 cm x 2.1 mm, 5 µm column, which had been degraded due to method development with peaks beginning to disappear, be cut off, or run together. The degradation of the column is shown in **Figure 3.12**. A new column was purchased from a new lot (S14047). When this new column was used, the liquid chromatography method that had previously been developed could not be fully transferred with incomplete separation of peaks (**Figure 3.13**). An unscheduled MRM was then run to see more precisely where the analytes eluted before further method development was attempted but it was determined that the column was insufficient for the needs of the project and was replaced with a third column. When the third column was purchased, an attempt was made to acquire one with the same lot number as the first (S14013), but this lot had been sold out. As such, an additional column of the second lot (S14047) was purchased. Additionally, GLU-CUR was added to the analytes of interest attempt to elucidate any metabolism of CUR which may have occurred, and its fragmentation parameters (**Table 3.9**) were added to the overall methodology. After method development, the final separation method was used (**Table 3.10**).

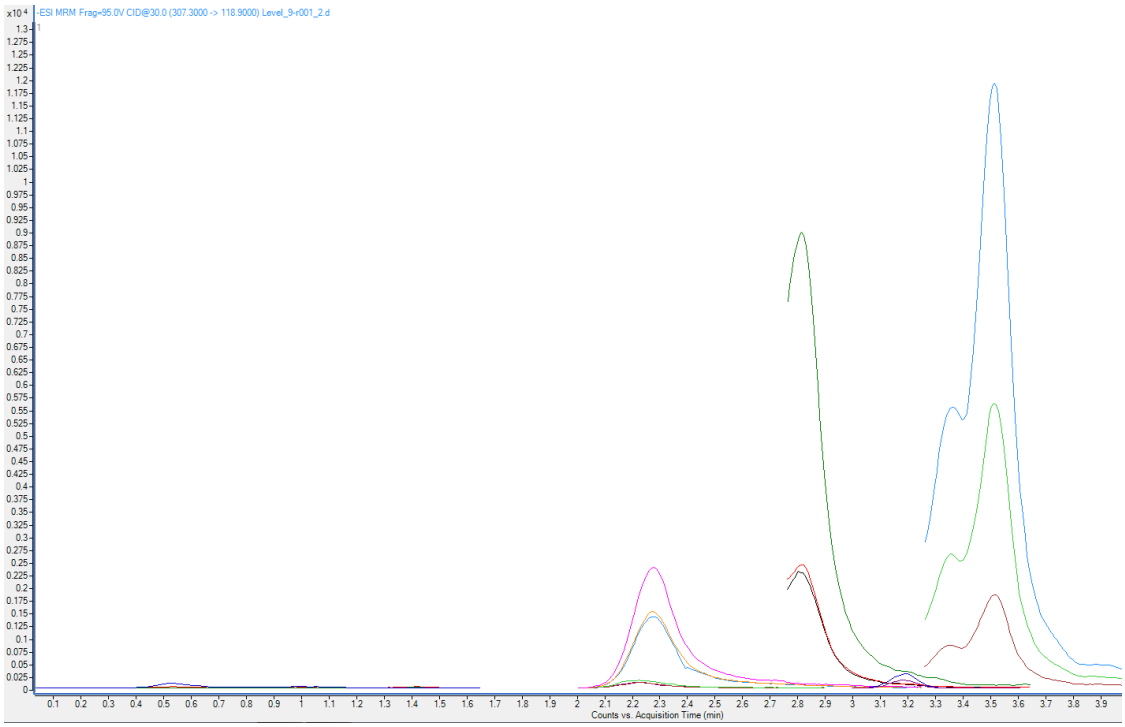

Figure 3.12: Degradation of first purchased column: Supelco Column Ascentis Express RP-Amide HPLC Column 10 cm x 2.1 mm, 5 µm Lot S140413 on calibration curve standard.

Despite being the same model of column, separation proved difficult on the replacement Supelco Column due to a change in lot number. When separation of the same chemicals was attempted incomplete and overlapping peaks were detected. This required further method development for complete separation of all analytes.

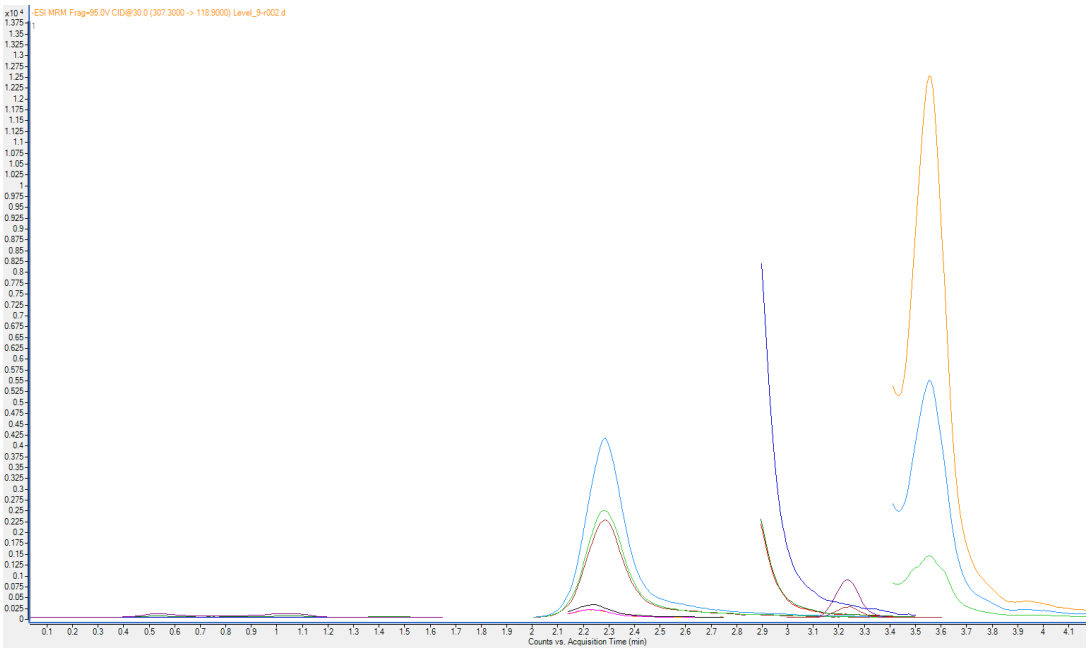

Figure 3.13: Previously developed method when run through new Supelco Column Ascentis Express RP-Amide HPLC Column 10 cm x 2.1 mm, 5 µm Lot S14047 on calibration curve standard.

The addition of GLU-CUR to the list of curcuminoids for detection required the addition of analytes of interest on the mass spectrometer.

Table 3.9: Fragmentation weights, energies, and polarity for detection of curcumin-beta-D-glucuronide for detection on an Agilent 6460 triple quadrupole mass spectrometer.

Analyte	Weight (DA)	Fragment Weight (DA)	Fragmentor Energy (V)	Collision Energy (V)	Polarity
GLU-CUR	545.5	369	160	3	Negative
GLU-CUR	545.5	285	160	6	Negative
GLU-CUR	545.5	245	160	11	Negative
GLU-CUR	545.5	177	160	17	Negative

Separation was achieved using the method described in **Table 3.10**, which allowed full baseline separation of all analytes.

Table 3.10: Final separation method curcuminoids: curcumin, tetrahydrocurcumin, demethoxycurcumin, bisdemethoxycurcumin, S-turmerone, and curcumin-beta-D-glucuronide on a Supelco Ascentis Express RP-Amide HPLC Column 10cm x 2.1mm, 5µm column for detection on an Agilent 6460 triple quadrupole mass spectrometer.

Time (Min)	H_2O %	Acetonitrile %	Flow (mL/min)
0	60	40	1.0000
0.5	60	40	1.0000
4	58	42	1.0000
6.5	54	46	1.0000
7.5	2	98	1.0000
8.5	2	98	1.0000
8.6	60	40	1.0000

The full chromatographic separation of curcuminoids: GLU-CUR, THC, CUR, DMC, TUR, and DBMC can be seen in in **Figure 3.14**.

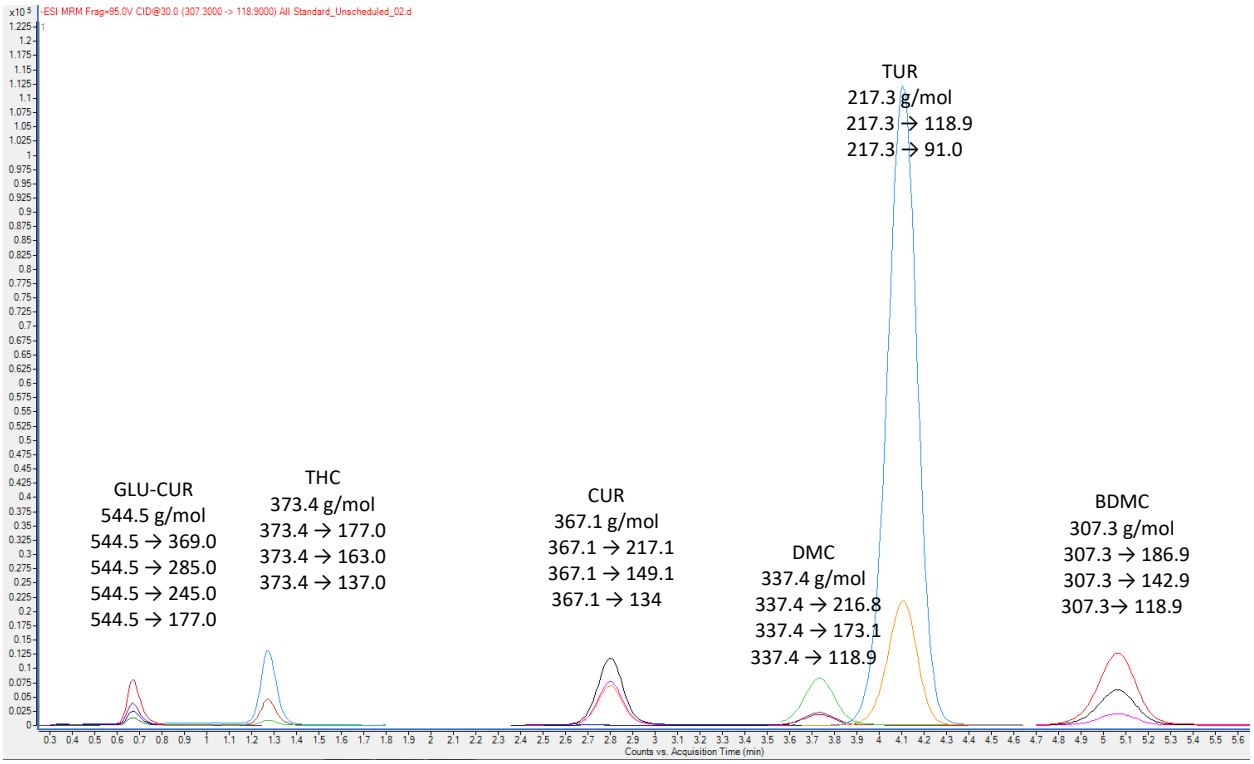

Figure 3.14: Chromatogram of final separation method for curcuminoids: curcumin, tetrahydrocurcumin, demethoxycurcumin, bisdemethoxycurcumin, S-turmerone, and curcumin-beta-D-glucuronide on a Supelco Ascentis Express RP-Amide HPLC Column 10cm x 2.1mm, 5µm column for detection on an Agilent 6460 triple quadrupole mass spectrometer

3.6.3 Extraction Methods

Due to the lack of quantifiable analytes in the first patients (01-03) it was determined that a new extraction method should be developed to extract as much of the analyte as possible and, thus, achieve a greater signal. This was done by changing the extraction solvent from ethyl acetate to ethanol (**Table 3.11**). The new extraction method was then tested against the previous extraction method. The new extraction method appeared to more than double the extracted material from the previous extracted method, Final Modified Extraction Procedure (**Figure 3.15**). The Ethanol Extraction Procedure was tested for its extraction efficiency by extracting three separate samples. The first sample contained 50 µL of bovine serum which was spiked with 2 µL of the highest level of calibration curve standards. This was extracted three times using the Ethanol Extraction Method,

dried in the speed vac, reconstituted with a 50:50 mixture of acetonitrile and 18.2 Ω deionized water and an addition of 0.1% formic acid. The second trial fully extracted 50 µL of bovine serum three times, it was dried and reconstituted and then 2 µL of the highest level of calibration curve standards were added. The third and final sample contained 50 µL of bovine serum, which was extracted, but no calibration curve standard was added to test for a blank. It was determined that the extraction efficiency of the Ethanol Extraction Method was determined to be 63.09%

Table 3.11: Ethanol extraction method for curcuminoids: curcumin, tetrahydrocurcumin, demethoxycurcumin, bisdemethoxycurcumin, S-turmerone, and curcumin-beta-D-glucuronide

Ethanol Extraction Procedure		
Reagent	Volume	
Serum	50 µL	
Standard	2 µL	
Internal Standard	2 µL	
Vortexed at 3000 RPM for 10 seconds		
Ethanol	50 µL	
Vortexed at 3000 RPM for 60 seconds		
Centrifuged at 13500 RPM for 10 minutes		
Removed supernatant into 2 mL tube		
Ethanol	50 µL	
Vortexed at 3000 RPM for 10 seconds		
Centrifuged at 13500 RPM for 10 minutes		
Removed supernatant into 2 mL tube		
Ethanol	50 µL	
Vortexed at 3000 RPM for 30 seconds		
Centrifuged at 13500 RPM for 10 minutes		
Removed supernatant into 2 mL tube		
Placed collected supernatant in centrifuge		
Centrifuged at 13500 RPM for 10 minutes		
Removed supernatant and placed in LC vial		
Reconstitution		
Acetonitrile	50 µL	
18 Ω DI Water	50 µL	
Formic Acid	0.1 µL	
Vortexed at 3000 RPM for 30 seconds		
Centrifuged at 13500 RPM for 4 minutes		
Removed 50 µL for analysis in LC-MS		

The newly developed method, the Ethanol Extraction Method, was compared to the previously used method, Final Modified Extraction Procedure, by extracting the highest level of calibration curve and plotting them in the same graph. Below the difference in counts can be seen.

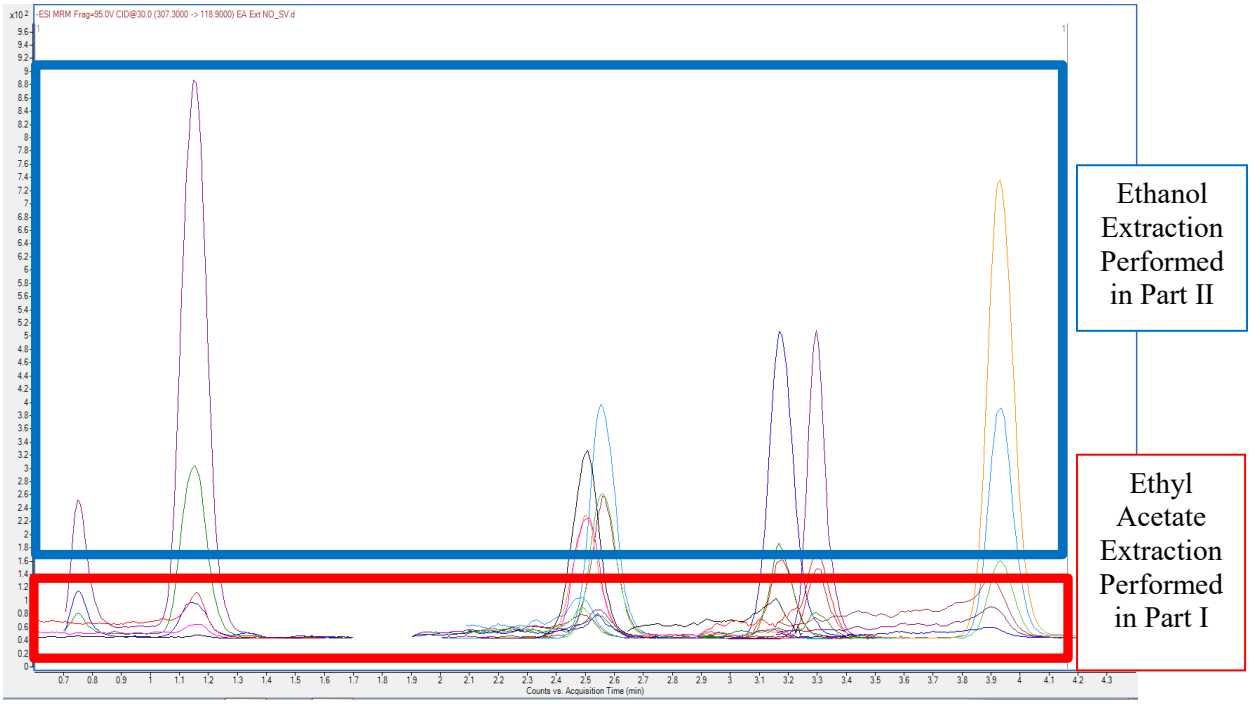

Figure 3.15. Results of comparison of final ethyl acetate extraction and ethanol extraction of curcuminoids

3.6.4 Calibration Curves

Although FDA validation protocol recommends a ten-to-twelve-point calibration curve, such that at least six can be conserved, it was observed that the highest and lowest levels in the calibration curve were rejected in many cases owing to the sensitivity of the instrument. It was determined that a nine-point calibration curve could be utilized with six points still maintained. All calibration curves were bracketed to correct for instrument drift and included three quality control samples which were also bracketed. Blanks were also measured several times throughout the run time to account for any crossover or contamination. Blanks consisted of a 50:50 mixture of water and acetonitrile. A sample workflow could be shown as:

- 9 calibration curve standards run in duplicate

- 3 quality control samples (low, medium, and high) run in duplicate
- 11 patient samples run in triplicate
- 3 quality control samples (low, medium, and high) run in duplicate
- 9 calibration curve standards run in duplicate

Calibration curve levels were made by taking stock solutions of natural analytes: CUR, THC, DMC, BDMC, and TUR with concentration of approximately 11,000 ng/g and performing serial dilutions in methanol as well as a constant level of deuterated internal standard: CUR-D6. GLU-CUR was not extracted well with the current method and, therefore, was excluded from calibration curves. These dilutions can be seen in **Table 3.12**. All samples were prepared by spiking 50 µL of bovine serum with 2 µL of internal standard and 2 µL of spike from the corresponding calibration level, except for Calibration Level 9, where 3 µL of spike was used due to previously diluted sample strength.

Table 3.12. Concentrations of curcumin and its analogues in calibration curves, quality control standards, and deuterated internal standard.

Calibration Level	Concentration of Curcumin and Analogs in Spike (ng/g)	Final Concentration of Curcumin and Analogs in Serum (ng/g)
9*	1000	160.98
8	1000	107.84
7	500	53.92
6	250	26.96
5	125	13.48
4	62.5	7.74
3	31.25	3.37
2	15.63	1.68
1	7.81	0.84
Quality Control 3	523.81	17.97
Quality Control 2	261.9	8.99
Quality Control 1	130.95	4.49
Internal Standard in All Samples**	100	11.76

*3 µL of spike was used due to previously diluted sample strength

** Due to total volume of Calibration Level 9, Internal Standard was calculated to be 11.71 ng/g

Once the samples had been run, data was analyzed and quantified using Agilent Technologies MassHunter software (version B.06.00 SP1) that was loaded on a computer onto which Windows 7 operating system had been installed calibration curves were constructed. An example of the following calibration curves lines of regression can be seen in **Figure 3.16** which is a conglomerate average of all points on te calibration curves.

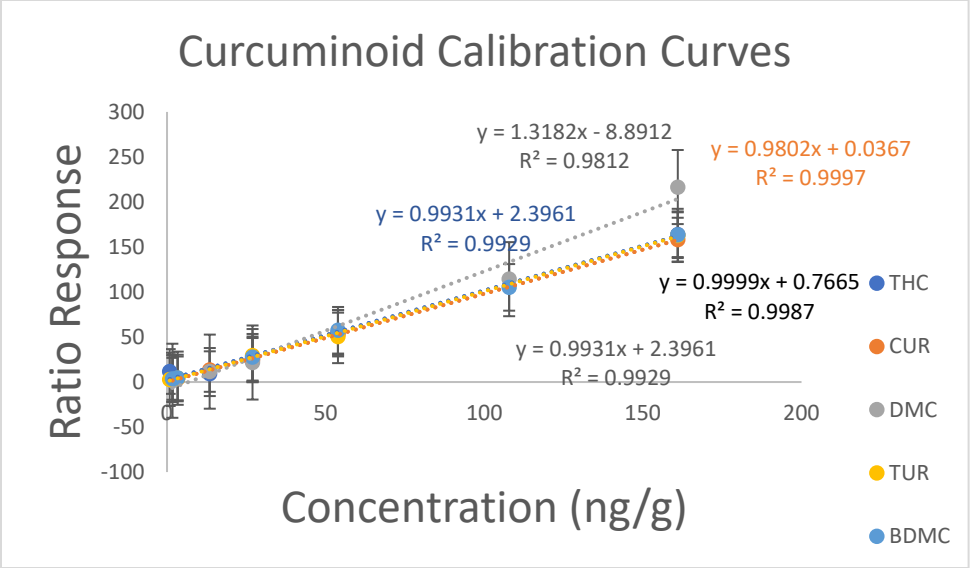

Figure 3.16: Combined calibration curves of curcuminoids: curcumin (CUR), tetrahydrocurcumin (THC), demethoxycurcumin (DMC), bisdemethoxycurcumin (BDMC), and S-turmerone (TUR) with accompanying linearity for patients 04-06.

3.7 Patient 04-06 Results and Discussion

After performing extractions on each of the patient samples and ran the methodologies on the instruments and attempting to quantify the data as described above, the results are catalogued in **Table 3.13**. The limit of quantification was estimated to be approximately 5 ng/ml with a limit of quantitation estimated to be 13.1 ng/mL. In all cases the analytes were below the limit of quantification and in many below the limit of detection. Despite the better extraction protocols and increased dosing of the patients, no increase in analyte detection occurred from patients 01-03. The only detection in cerebrospinal fluid was observed to be TUR, but upon comparison to a blank, it was deemed not appreciable. **Figure 3.17** shows TUR in cerebrospinal fluid with no blanks present and **Figure 3.18** shows TUR with blanks overlaid.

Table 3.13: Complied results for patients 04-06 for all serum and cerebrospinal fluid samples. Where ND stands for no detection and NQ stands for not quantifiable, as the concentration was too low to be quantfied using calibration curves.

Patient	Vial	THC	CUR	GLU-CUR	BDMC	TUR	DMC
4	1	NQ	ND	ND	ND	ND	ND
4	2	NQ	ND	ND	ND	ND	ND
4	3	NQ	ND	ND	ND	ND	ND
4	4	NQ	ND	ND	ND	ND	ND
4	5	NQ	ND	ND	ND	ND	ND
4	6	NQ	ND	ND	ND	ND	ND
4	7	NQ	ND	ND	ND	NQ	ND
4	8	NQ	ND	ND	ND	NQ	ND
4	9	NQ	ND	ND	ND	NQ	ND
4	10	NQ	ND	ND	ND	NQ	ND
4	11	NQ	ND	ND	ND	NQ	ND
5	1	NQ	ND	ND	ND	ND	ND
5	2	NQ	ND	ND	ND	ND	ND
5	3	NQ	ND	ND	ND	ND	ND
5	4	NQ	ND	ND	ND	ND	ND
5	5	NQ	ND	ND	ND	ND	ND
5	6	NQ	ND	ND	ND	ND	ND
5	7	NQ	ND	ND	ND	ND	ND
5	8	NQ	ND	ND	ND	ND	ND
5	9	NQ	ND	ND	ND	ND	ND
5	10	NQ	ND	ND	ND	ND	ND
5	11	NQ	ND	ND	ND	ND	ND
6	1	NQ	ND	ND	ND	ND	ND
6	2	NQ	ND	ND	ND	ND	ND
6	3	NQ	ND	ND	ND	ND	ND
6	4	NQ	ND	ND	ND	ND	ND
6	5	NQ	ND	ND	ND	ND	ND
6	6	NQ	ND	ND	ND	ND	ND
6	7	NQ	ND	ND	ND	ND	ND
6	8	NQ	ND	ND	ND	ND	ND
6	9	NQ	ND	ND	ND	ND	ND
6	10	NQ	ND	ND	ND	ND	ND
6	11	NQ	ND	ND	ND	ND	ND
4	CSF	ND	ND	ND	ND	ND	ND
5	CSF	ND	ND	ND	ND	ND	ND
6	CSF	ND	ND	ND	ND	ND	ND

Potential peaks for TUR were seen in cerebrospinal fluid, giving a gaussian response curve with a signal-to-noise ratio too low to be quantitated.

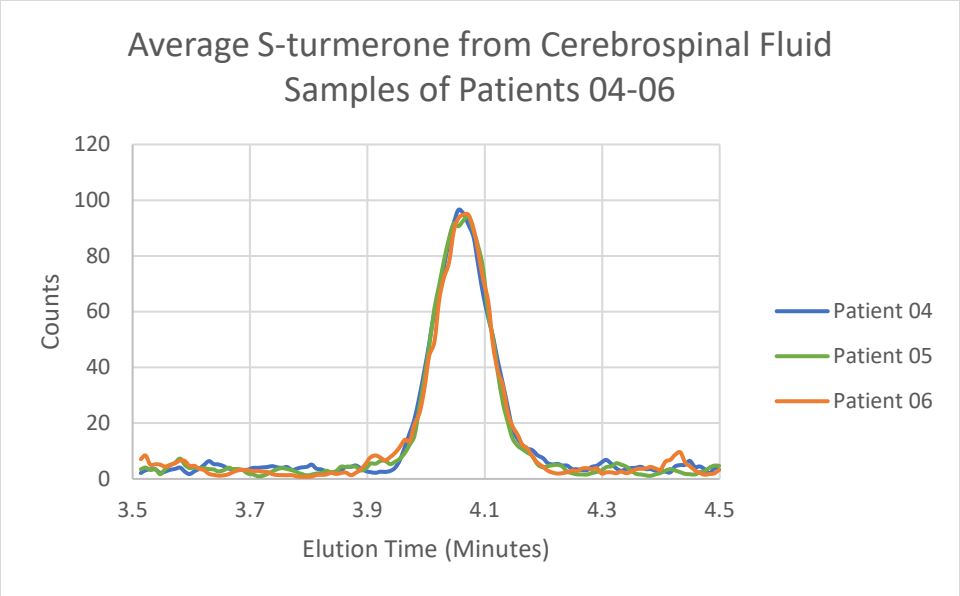

Figure 3.17: Average S-turmerone extracted from cerebrospinal fluid samples from: Patient 04 in blue, Patient 05 in green, and Patient 06 in brown

However, when TUR signal in the sample was compared to the blanks run before and after the sample, similar sized peaks were seen representing potential cross contamination from book-ended calibration curves or an artifact from the extraction process.

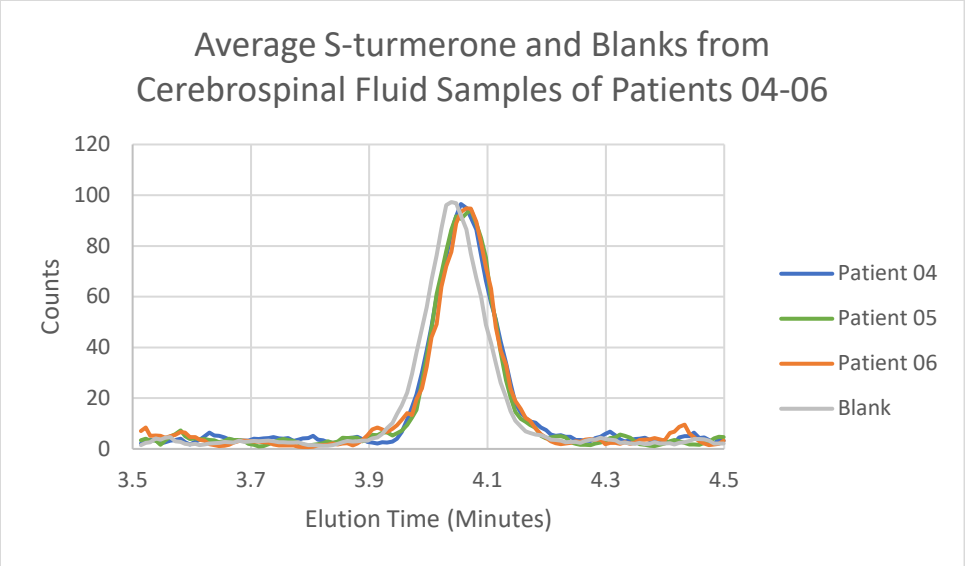

Figure 3.18: Average S-turmerone extracted from cerebrospinal fluid samples from: Patient 04 in blue, Patient 05 in green, and Patient 06 in brown, as well as Blanks in Grey.

3.8 Conclusions

Initial patient samples, Patients 01-03, were run with an ethyl acetate extraction. Most of the analytes were below the limit of detection in all samples. THC was the only analyte observed consistently throughout all patient samples. The analogue DMC was also observed in several patient samples. For the following set of patient samples, Patients 04-06, an improved extraction technique using ethanol was employed achieving a 63.09% extraction efficiency, however, was not effective in extracting the additional curcumin analogue, GLU-CUR. The first purchased column ceased to function properly and was replaced, but the second column was defective causing a loss of six weeks of time. Once a third column was obtained, a new chromatography method was developed, and the samples were processed. However, despite the improved extraction and increased patient dose, the only curcumin metabolite found in cerebrospinal fluid was TUR, which was also observed in comparable counts in the blank. This proves the need for a novel method to

be developed which allows for accurate quantitation at levels below what would be considered possible using traditional calibration curves.

3.9 Sensitive Quantification Improvements as a Foundation for Future Research

These medical quantifications demonstrated the critical need for more and better sensitive quantification beyond the capabilities of the current mass spectrometers used in standard configurations. This was a reduction to practice of a new patented method for quantification which is digital and does not use the analogue calibration curve methods described in this research for quantification. These research development applied to ultra-sensitive mass spectrometry quantification are discussed elsewhere in this dissertation. However, it was these critical medical examples that demonstrated the need that for the research enabling quantification issues in subsequent chapters that are part of this dissertation.

3.10 References

1. Hatcher, H.; Planalp, R.; Cho, J.; Torti, F. M.; Torti, S. V., Curcumin: from ancient medicine to current clinical trials. *Cell Mol Life Sci* **2008,** *65* (11), 1631-52.

2. Lestari, M. L.; Indrayanto, G., Curcumin. *Profiles Drug Subst Excip Relat Methodol* **2014,** *39*, 113-204.

3. Sharma, R. A.; Gescher, A. J.; Steward, W. P., Curcumin: the story so far. *Eur J Cancer* **2005,** *41* (13), 1955-68.

4. Cheng, A. L.; Hsu, C. H.; Lin, J. K.; Hsu, M. M.; Ho, Y. F.; Shen, T. S.; Ko, J. Y.; Lin, J. T.; Lin, B. R.; Ming-Shiang, W.; Yu, H. S.; Jee, S. H.; Chen, G. S.; Chen, T. M.; Chen, C. A.; Lai, M. K.; Pu, Y. S.; Pan, M. H.; Wang, Y. J.; Tsai, C. C.; Hsieh, C. Y., Phase I

clinical trial of curcumin, a chemopreventive agent, in patients with high-risk or pre-malignant lesions. *Anticancer Res* **2001,** *21* (4b), 2895-900.

5. Youssef, K. M.; El-Sherbeny, M. A., Synthesis and antitumor activity of some curcumin analogs. *Arch Pharm (Weinheim)* **2005,** *338* (4), 181-9.

6. Brouet, I.; Ohshima, H., Curcumin, an anti-tumour promoter and anti-inflammatory agent, inhibits induction of nitric oxide synthase in activated macrophages. *Biochem Biophys Res Commun* **1995,** *206* (2), 533-40.

7. Reddy, A. C.; Lokesh, B. R., Studies on spice principles as antioxidants in the inhibition of lipid peroxidation of rat liver microsomes. *Mol Cell Biochem* **1992,** *111* (1-2), 117-24.

8. Huang, M. T.; Lysz, T.; Ferraro, T.; Abidi, T. F.; Laskin, J. D.; Conney, A. H., Inhibitory effects of curcumin on in vitro lipoxygenase and cyclooxygenase activities in mouse epidermis. *Cancer Res* **1991,** *51* (3), 813-9.

9. Duvoix, A.; Blasius, R.; Delhalle, S.; Schnekenburger, M.; Morceau, F.; Henry, E.; Dicato, M.; Diederich, M., Chemopreventive and therapeutic effects of curcumin. *Cancer Lett* **2005,** *223* (2), 181-90.

10. Garg, A. K.; Buchholz, T. A.; Aggarwal, B. B., Chemosensitization and radiosensitization of tumors by plant polyphenols. *Antioxid Redox Signal* **2005,** *7* (11-12), 1630-47.

11. Hour, T. C.; Chen, J.; Huang, C. Y.; Guan, J. Y.; Lu, S. H.; Pu, Y. S., Curcumin enhances cytotoxicity of chemotherapeutic agents in prostate cancer cells by inducing p21(WAF1/CIP1) and C/EBPbeta expressions and suppressing NF-kappaB activation. *Prostate* **2002,** *51* (3), 211-8.

12. Li, M.; Zhang, Z.; Hill, D. L.; Wang, H.; Zhang, R., Curcumin, a dietary component, has anticancer, chemosensitization, and radiosensitization effects by down-regulating the MDM2 oncogene through the PI3K/mTOR/ETS2 pathway. *Cancer Res* **2007,** *67* (5), 1988-96.

13. Jagetia, G. C., Radioprotection and radiosensitization by curcumin. *Adv Exp Med Biol* **2007,** *595*, 301-20.

14. Chendil, D.; Ranga, R. S.; Meigooni, D.; Sathishkumar, S.; Ahmed, M. M., Curcumin confers radiosensitizing effect in prostate cancer cell line PC-3. *Oncogene* **2004,** *23* (8), 1599-607.

15. Arbiser, J. L.; Klauber, N.; Rohan, R.; van Leeuwen, R.; Huang, M. T.; Fisher, C.; Flynn, E.; Byers, H. R., Curcumin is an in vivo inhibitor of angiogenesis. *Mol Med* **1998,** *4* (6), 376-83.

16. Mohan, R.; Sivak, J.; Ashton, P.; Russo, L. A.; Pham, B. Q.; Kasahara, N.; Raizman, M. B.; Fini, M. E., Curcuminoids inhibit the angiogenic response stimulated by fibroblast growth factor-2, including expression of matrix metalloproteinase gelatinase B. *J Biol Chem* **2000,** *275* (14), 10405-12.

17. Bhandarkar, S. S.; Arbiser, J. L., Curcumin as an inhibitor of angiogenesis. *Adv Exp Med Biol* **2007,** *595*, 185-95.

18. Baeuerle, P. A.; Henkel, T., Function and activation of NF-kappa B in the immune system. *Annu Rev Immunol* **1994,** *12*, 141-79.

19. Barnes, P. J.; Karin, M., Nuclear factor-kappaB: a pivotal transcription factor in chronic inflammatory diseases. *N Engl J Med* **1997,** *336* (15), 1066-71.

20. Aggarwal, S.; Ichikawa, H.; Takada, Y.; Sandur, S. K.; Shishodia, S.; Aggarwal, B. B., Curcumin (diferuloylmethane) down-regulates expression of cell proliferation and antiapoptotic

and metastatic gene products through suppression of IkappaBalpha kinase and Akt activation. *Mol Pharmacol* **2006,** *69* (1), 195-206.

21. Balogun, E.; Hoque, M.; Gong, P.; Killeen, E.; Green, C. J.; Foresti, R.; Alam, J.; Motterlini, R., Curcumin activates the haem oxygenase-1 gene via regulation of Nrf2 and the antioxidant-responsive element. *Biochem J* **2003,** *371* (Pt 3), 887-95.

22. Bush, J. A.; Cheung, K. J., Jr.; Li, G., Curcumin induces apoptosis in human melanoma cells through a Fas receptor/caspase-8 pathway independent of p53. *Exp Cell Res* **2001,** *271* (2), 305-14.

23. Dickinson, D. A.; Iles, K. E.; Wigley, A. F.; Forman, H. J., Analysis of Transcription Factor Remodeling in Phase II Gene Expression with Curcumin. In *Methods in Enzymology*, Academic Press: 2004; Vol. 378, pp 302-318.

24. Bharti, A. C.; Donato, N.; Aggarwal, B. B., Curcumin (diferuloylmethane) inhibits constitutive and IL-6-inducible STAT3 phosphorylation in human multiple myeloma cells. *J Immunol* **2003,** *171* (7), 3863-71.

25. Yang, X.; Thomas, D. P.; Zhang, X.; Culver, B. W.; Alexander, B. M.; Murdoch, W. J.; Rao, M. N.; Tulis, D. A.; Ren, J.; Sreejayan, N., Curcumin inhibits platelet-derived growth factor-stimulated vascular smooth muscle cell function and injury-induced neointima formation. *Arterioscler Thromb Vasc Biol* **2006,** *26* (1), 85-90.

26. Korutla, L.; Kumar, R., Inhibitory effect of curcumin on epidermal growth factor receptor kinase activity in A431 cells. *Biochim Biophys Acta* **1994,** *1224* (3), 597-600.

27. Ng, T. P.; Chiam, P. C.; Lee, T.; Chua, H. C.; Lim, L.; Kua, E. H., Curry consumption and cognitive function in the elderly. *Am J Epidemiol* **2006,** *164* (9), 898-906.

28. Pandav, R.; Belle, S.; DeKosky, S., Apolipoprotein E polymorphism and Alzheimer's disease: The Indo-US cross-national dementia study. *Arch Neurol* **2000,** *57*, 824-30.

29. Chen, M.; Du, Z. Y.; Zheng, X.; Li, D. L.; Zhou, R. P.; Zhang, K., Use of curcumin in diagnosis, prevention, and treatment of Alzheimer's disease. *Neural Regen Res* **2018,** *13* (4), 742-752.

30. Farkhondeh, T.; Samarghandian, S.; Pourbagher-Shahri, A. M.; Sedaghat, M., The impact of curcumin and its modified formulations on Alzheimer's disease. *J Cell Physiol* **2019,** *234* (10), 16953-16965.

31. Zhang, L.; Fiala, M.; Cashman, J.; Sayre, J.; Espinosa, A.; Mahanian, M.; Zaghi, J.; Badmaev, V.; Graves, M. C.; Bernard, G.; Rosenthal, M., Curcuminoids enhance amyloid-beta uptake by macrophages of Alzheimer's disease patients. *J Alzheimers Dis* **2006,** *10* (1), 1-7.

32. Ambegaokar, S. S.; Wu, L.; Alamshahi, K.; Lau, J.; Jazayeri, L.; Chan, S.; Khanna, P.; Hsieh, E.; Timiras, P. S., Curcumin inhibits dose-dependently and time-dependently neuroglial cell proliferation and growth. *Neuroendocrinology Letters* **2003,** *24* (6), 469-469.

33. Fiala, M.; Liu, P. T.; Espinosa-Jeffrey, A.; Rosenthal, M. J.; Bernard, G.; Ringman, J. M.; Sayre, J.; Zhang, L.; Zaghi, J.; Dejbakhsh, S., Innate immunity and transcription of MGAT-III and Toll-like receptors in Alzheimer's disease patients are improved by bisdemethoxycurcumin. *Proceedings of the National Academy of Sciences* **2007,** *104* (31), 12849-12854.

34. Yang, F.; Lim, G. P.; Begum, A. N.; Ubeda, O. J.; Simmons, M. R.; Ambegaokar, S. S.; Chen, P. P.; Kayed, R.; Glabe, C. G.; Frautschy, S. A., Curcumin inhibits formation of amyloid β oligomers and fibrils, binds plaques, and reduces amyloid in vivo. *Journal of Biological Chemistry* **2005,** *280* (7), 5892-5901.

35. Pendurthi, U. R.; Rao, L. V. M., Suppression of Transcription Factor Egr-1 by Curcumin. *Thrombosis Research* **2000,** *97* (4), 179-189.

36. Kim, G.-Y.; Kim, K.-H.; Lee, S.-H.; Yoon, M.-S.; Lee, H.-J.; Moon, D.-O.; Lee, C.-M.; Ahn, S.-C.; Park, Y. C.; Park, Y.-M., Curcumin inhibits immunostimulatory function of dendritic cells: MAPKs and translocation of NF-κB as potential targets. *The Journal of Immunology* **2005,** *174* (12), 8116-8124.

37. Giri, R. K.; Rajagopal, V.; Kalra, V. K., Curcumin, the active constituent of turmeric, inhibits amyloid peptide-induced cytochemokine gene expression and CCR5-mediated chemotaxis of THP-1 monocytes by modulating early growth response-1 transcription factor. *Journal of neurochemistry* **2004,** *91* (5), 1199-1210.

38. Rathore, P.; Dohare, P.; Varma, S.; Ray, A.; Sharma, U.; Jaganathanan, N.; Ray, M., Curcuma oil: reduces early accumulation of oxidative product and is anti-apoptogenic in transient focal ischemia in rat brain. *Neurochemical research* **2008,** *33* (9), 1672-1682.

39. Jiang, J.; Wang, W.; Sun, Y. J.; Hu, M.; Li, F.; Zhu, D. Y., Neuroprotective effect of curcumin on focal cerebral ischemic rats by preventing blood–brain barrier damage. *European journal of pharmacology* **2007,** *561* (1-3), 54-62.

40. Calabrese, V.; Butterfield, D. A.; Stella, A., Nutritional antioxidants and the heme oxygenase pathway of stress tolerance: novel targets for neuroprotection in Alzheimer's disease. *The Italian journal of biochemistry* **2003,** *52* (4), 177-181.

41. Scapagnini, G.; Foresti, R.; Calabrese, V.; Stella, A. G.; Green, C.; Motterlini, R., Caffeic acid phenethyl ester and curcumin: a novel class of heme oxygenase-1 inducers. *Molecular Pharmacology* **2002,** *61* (3), 554-561.

42. Biswas, S. K.; McClure, D.; Jimenez, L. A.; Megson, I. L.; Rahman, I., Curcumin induces glutathione biosynthesis and inhibits NF-κB activation and interleukin-8 release in alveolar epithelial cells: mechanism of free radical scavenging activity. *Antioxidants & redox signaling* **2005,** *7* (1-2), 32-41.

43. DAI, X.; SUN, Y., JIANG. Zhaofeng Copper (2) potentiation of Alzheimers A-(beta) 1-40 cytotoxicity and transition on its secondary structure. *Acta Biochimica et Biophysica Sinica* **1938,** *11*, 765-72.

44. Perry, G.; Sayre, L. M.; Atwood, C. S.; Castellani, R. J.; Cash, A. D.; Rottkamp, C. A.; Smith, M. A., The role of iron and copper in the aetiology of neurodegenerative disorders. *CNS drugs* **2002,** *16* (5), 339-352.

45. Garcia-Nino, W. R.; Pedraza-Chaverri, J., Protective effect of curcumin against heavy metals-induced liver damage. *Food Chem Toxicol* **2014,** *69*, 182-201.

46. Puglielli, L.; Tanzi, R. E.; Kovacs, D. M., Alzheimer's disease: the cholesterol connection. *Nature neuroscience* **2003,** *6* (4), 345-351.

47. Rao, D. S.; Sekhara, N. C.; Satyanarayana, M.; Srinivasan, M., Effect of curcumin on serum and liver cholesterol levels in the rat. *The Journal of nutrition* **1970,** *100* (11), 1307-1315.

48. Lesne, S.; Koh, M. T.; Kotilinek, L.; Kayed, R.; Glabe, C. G.; Yang, A.; Gallagher, M.; Ashe, K. H., A specific amyloid-beta protein assembly in the brain impairs memory. *Nature* **2006,** *440* (7082), 352-7.

49. Piller, C. Blots on a field?

A neuroscience image sleuth finds signs of fabrication in scores of Alzheimer's articles, threatening a reigning theory of the disease. https://www.science.org/content/article/potential-fabrication-research-images-threatens-key-theory-alzheimers-disease (accessed July 25, 2022).

50. Anand, P.; Kunnumakkara, A. B.; Newman, R. A.; Aggarwal, B. B., Bioavailability of curcumin: problems and promises. *Mol Pharm* **2007,** *4* (6), 807-18.

51. Pan, M.-H.; Huang, T.-M.; Lin, J.-K., Biotransformation of curcumin through reduction and glucuronidation in mice. *Drug metabolism and disposition* **1999,** *27* (4), 486-494.

52. Lin, J.-K.; Pan, M.-H.; Lin-Shiau, S.-Y., Recent studies on the biofunctions and biotransformations of curcumin. *Biofactors* **2000,** *13* (1-4), 153-158.

53. Ravindranath, V.; Chandrasekhara, N., Absorption and tissue distribution of curcumin in rats. *Toxicology* **1980,** *16* (3), 259-265.

54. Sharma, R. A.; Euden, S. A.; Platton, S. L.; Cooke, D. N.; Shafayat, A.; Hewitt, H. R.; Marczylo, T. H.; Morgan, B.; Hemingway, D.; Plummer, S. M., Phase I clinical trial of oral curcumin: biomarkers of systemic activity and compliance. *Clinical Cancer Research* **2004,** *10* (20), 6847-6854.

55. Perkins, S.; Verschoyle, R. D.; Hill, K.; Parveen, I.; Threadgill, M. D.; Sharma, R. A.; Williams, M. L.; Steward, W. P.; Gescher, A. J., Chemopreventive efficacy and pharmacokinetics of curcumin in the min/+ mouse, a model of familial adenomatous polyposis. *Cancer Epidemiology Biomarkers & Prevention* **2002,** *11* (6), 535-540.

56. Garcea, G.; Berry, D. P.; Jones, D. J.; Singh, R.; Dennison, A. R.; Farmer, P. B.; Sharma, R. A.; Steward, W. P.; Gescher, A. J., Consumption of the putative chemopreventive agent curcumin by cancer patients: assessment of curcumin levels in the colorectum and their pharmacodynamic consequences. *Cancer Epidemiology Biomarkers & Prevention* **2005,** *14* (1), 120-125.

57. Maiti, K.; Mukherjee, K.; Gantait, A.; Saha, B. P.; Mukherjee, P. K., Curcumin–phospholipid complex: preparation, therapeutic evaluation and pharmacokinetic study in rats. *International journal of pharmaceutics* **2007,** *330* (1-2), 155-163.

58. Ravindranath, V.; Chandrasekhara, N., Metabolism of curcumn-studies with [3H] curcumin. *Toxicology* **1981,** *22* (4), 337-344.

59. Esatbeyoglu, T.; Ulbrich, K.; Rehberg, C.; Rohn, S.; Rimbach, G., Thermal stability, antioxidant, and anti-inflammatory activity of curcumin and its degradation product 4-vinyl guaiacol. *Food Funct* **2015,** *6* (3), 887-93.

60. Kharat, M.; Du, Z.; Zhang, G.; McClements, D. J., Physical and Chemical Stability of Curcumin in Aqueous Solutions and Emulsions: Impact of pH, Temperature, and Molecular Environment. *J Agric Food Chem* **2017,** *65* (8), 1525-1532.

61. Lee, B. H.; Choi, H. A.; Kim, M.-R.; Hong, J., Changes in chemical stability and bioactivities of curcumin by ultraviolet radiation. *Food Science and Biotechnology* **2013,** *22* (1), 279-282.

62. Mondal, S.; Ghosh, S.; Moulik, S. P., Stability of curcumin in different solvent and solution media: UV-visible and steady-state fluorescence spectral study. *J Photochem Photobiol B* **2016,** *158*, 212-8.

63. Price, L. C.; Buescher, R. W., Decomposition of Turmeric Curcuminoids as Affected by Light, Solvent and Oxygen. *Journal of Food Biochemistry* **1996,** *20* (5), 125-133.

64. Thakare, V. N.; Osama, M. M.; Naik, S. R., Therapeutic potential of curcumin in experimentally induced allergic rhinitis in guinea pigs. *Int Immunopharmacol* **2013,** *17* (1), 18-25.

65. Pumps, A. O. Preparation of Artificial CSF. https://www.alzet.com/guide-to-use/preparation-of-artificial-csf/ (accessed 06/28/2022).

66. Kim, H. J.; Jang, Y. P., Direct analysis of curcumin in turmeric by DART-MS. *Phytochem Anal* **2009,** *20* (5), 372-7.

Chapter 4: Development of Novel Accurate Quantification Technique of Methylmalonic Acid Below the Instrument Manufacturer's Lower Limit of Quantitation Known as Thor's Hammer Isotope Dilution Mass Spectrometry.

4.1. Introduction

As technology has increased, detections of analytes have matched its pace throughout scientific disciplines. Techniques as varied as epiflorescence microsopy,[1] the incorporation of an Orbitrap into mass spectrometry,[2] and the use of ion mobility chromatography[3] have been used to detect various analytes in concentrations well below what was possible in just a decade past. In the field of proteomics alone, researchers propose the existence of between 10,000 and several billion different protein species in the human body.[4-6] According to the Plasma Proteome Database, 10.5 thousand blood-plasma proteins have been detected and less than 10% have been measured in a quantitative manner.[6, 7] One of the major challenges in protein quantitation is detecting ultralow-abundance species with concentrations $<10^{-12}$ M in the presence of high-copied protein molecules at concentrations $>10^{-6}$ M.[8] The increased frequency of protein detection and isolation has been a potential boon for the discovery and characterization of biomarkers for various disease states which may aid in future treatment and patient monitoring.[9] However, due to the absence of, or poor quality, of quantitation for these potential biomarkers, physicians are unable to utilize them to their fullest extent.[10] Thus, the future of medicine requires not only greater tool to determine and categorize potential biomarkers, but to quantitate them by lowering the lower limit of quantitation (LLOQ).

The development of potential quantitative techniques to decrease the LLOQ and allow for quantitation of low levels of analytes can follow two potential routs in mass spectrometry.[11] The

first is by decreasing the signal to noise ratio or increasing the sensitivity of the instrument, which typically requires utilization of highly purified chemicals and advanced and expensive instrumentation.[12-14] The second is signal amplification of the analyte, which typically utilizes the reduction of a large volume of matrix to quantitate a small concentration of analyte,[15] adding a known concentration of analyte to the sample via standard addition,[16] or through derivatization.[17] These techniques may be difficult or impossible to perform due to sample size limitations or lack of functionalization sites of the analyte of interest. Thus, from the perspective of an analyst, it would be beneficial to produce a robust quantitation method which could be utilized across many platforms without being cost prohibitive.

In addition to the LLOQ, the lower limit of detection (LLOD) and limit of the blank (LOB) are required for analytical determinations utilizing mass spectrometry prior to the beginning of testing. When utilizing calibration curves, the LOB is 1.3 times the standard deviation of the signal response over the slope of the calibration curve, the LLOD is 3.3 times the standard deviation of the signal response over the slope of the calibration curve, and the LLOQ is 10 times the standard deviation of the signal response over the slope of the calibration curve.[18] This is, traditionally, the most widely utilized form of lower limit determination due to the ubiquity of calibration curves in quantitation as well as its relative simplicity.[19] However, this is by no means the only accepted method of determination of the limits of calibration curves.[20, 21] There is currently no universally accepted definition of the LLOD and LLOQ let alone standard on how to determine them.[22-24]

One frequently used method to determine the LLOD and LLOQ utilizes signal to noise ratio of the blank to determine the signal to noise ratio which analyte can be reliably distinguished from the noise of the sample.[21] In this determination, a series of blanks are processed first to determine the LOB which is the highest *apparent* analyte concentration expected to be found when

replicates of a blank sample containing no analyte are tested.[21] The LOB is determined by means of the blank plus 1.645 times the standard deviation of the blank.[21] This limit is then used to determine the LLOD, which is the lowest analyte concentration likely to be reliably distinguished from the LOB and at which detection is feasible, by taking this number and adding 1.645 times the standard deviation of a low concentration sample.[21] Finally, the LLOQ, the lowest concentration at which the analyte can not only be reliably detected but at which some predefined goals for bias and imprecision are met, may be equivalent or higher than to the LLOD.[21] This methodology was utilized to determine the LLOD and LLOQ as isotope dilution mass spectrometry (IDMS) does not utilize calibration curves. While statistical determinations have been proposed, there is no defined method for determination of LLOD and LLOQ utilizing IDMS.[25]

IDMS is a quantification technique developed by George de Hevesy which won a Nobel Prize in 1943.[26] IDMS allows for accurate quantitation without the use of a calibration curve by means of isotopic measurement, or perhaps it is better explained as the use of a one-point internal calibration curve. A heavy isotopic labeled version of the analyte in question, which does not exist in high quantity in the natural world, is purchased or synthesized and added to a sample and equilibrated. Once equilibrated, the foreknowledge of the weight and concentration of this isotopically labeled molecule allows for accurate quantitation without the use of a calibration curve using the IDMS equation (Equation 1). This combined with the knowledge that the chemistry of the isotopes is identical, meaning the rate of ionization of the added spike and the natural chemical are similar in most cases, allow for quantitation to be based on ratio without time constraints of using calibration coves. Compared to traditional calibration curves, both accuracy and precision are increased even at low levels. IDMS is designated by the International Union of Pure and

Applied Chemistry as one of the definitive methods for the certification of a reference material.[27] Professor Kingston teaches that calibration curves are an analog method while IDMS is a digital method of quantifying concentrations.

Proper application of isotopic spike to sample is determined by the error propagation factor (Equation 1.2).[28] This is dependent on the isotopic enhancement of the spike and isotopic abundances of the natural sample.[28] The error propagation factor equation is applied to avoid pitfalls of the application of the isotopic spike, namely the spiked sample ratio approaching the spike ratio, known as overspiking, or approaching the natural isotopic ratio, known as underspiking.[28] The effect of the error propagation factor is dependent on the mass spectrometric precision, and the relative enrichment of the spike isotope and natural isotope.[28] Optimal spiking ratio can is determined utilizing the equation, but the associated error can be low over orders of magnitude. For carbon the optimal spiking ratio close to 1:1, but error remains low from a ratio of carbon 13/12 ranging from 0.01 to 10 (**Figure 4.2**).

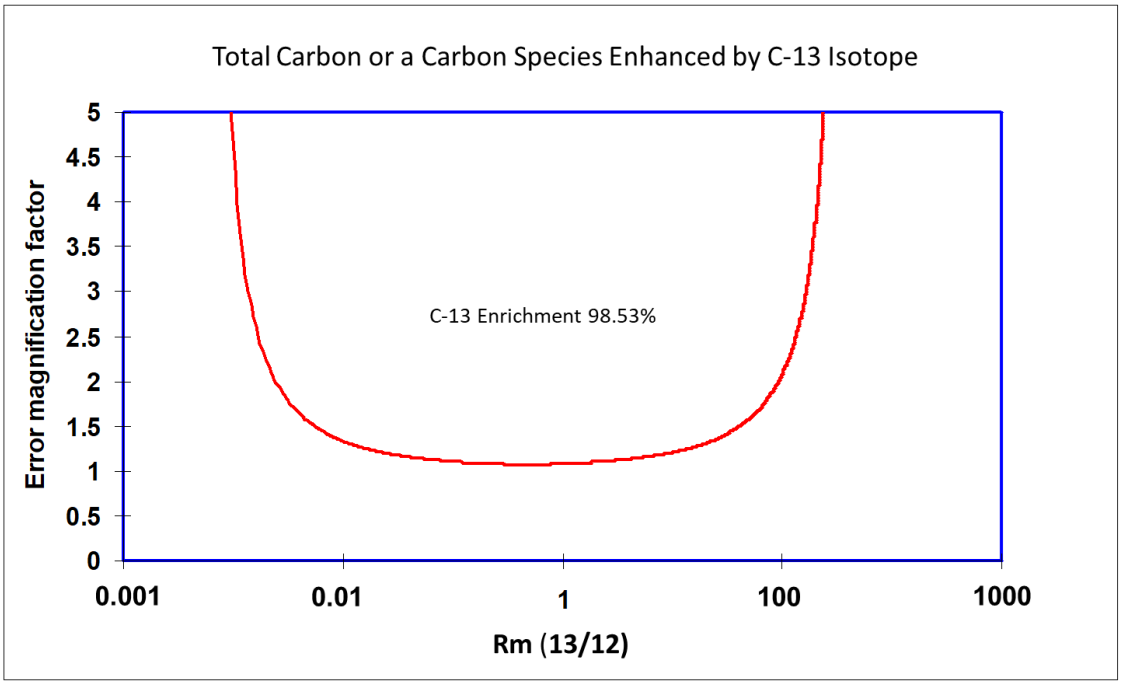

Figure 4.1. Calculated and plotted error propagation factor for use in carbon isotope 13/12 for use in determining the optimum spiking ratio for isotope dilution mass spectrometry and acceptable error window for MetaSpike™ use in Thor's Hammer isotope dilution mass spectrometry.

This range of relatively low error can be exploited by expanding on one of the natural features of IDMS, namely the presence of a small concentration of natural in the isotopically enriched standards. As an example, carbon has two stable isotopes, carbon-12 and 13. Carbon naturally has an isotopic ratio of 98.93% carbon-12 and 1.07% carbon-13 (**Figure 4.2**).

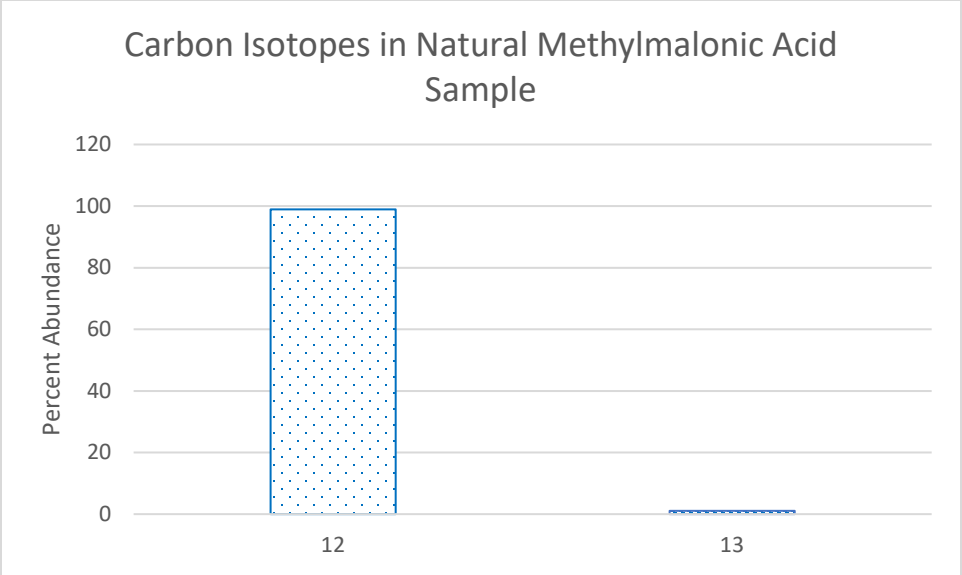

Figure 4.2. Natural isotopic abundance of carbon in methylmalonic acid. Naturally, carbon has a 98.89% carbon-12 isotope and a 1.11% carbon-13 isotopic distribution. Methylmalonic acid has four carbons and standards were measured to have an isotopic distribution of 99.41% which would fall into the mass transition of 117→73 and 0.59% in the isotopically enhanced mass transition of 121→76.

In contrast, isotopically enriched standards of MMA can be purchased for quantification utilizing both calibration curves as an internal standard and IDMS for the enabling spike. This standard has four carbons, each of which were enriched to carbon-13, which has a mass transition of 121→76. These mass transitions are unique and do not overlap with any known isobar. Abundances of isotopes are published by the manufacturer (**Figure 4.3**) and must be considered when utilizing IDMS for quantitation.

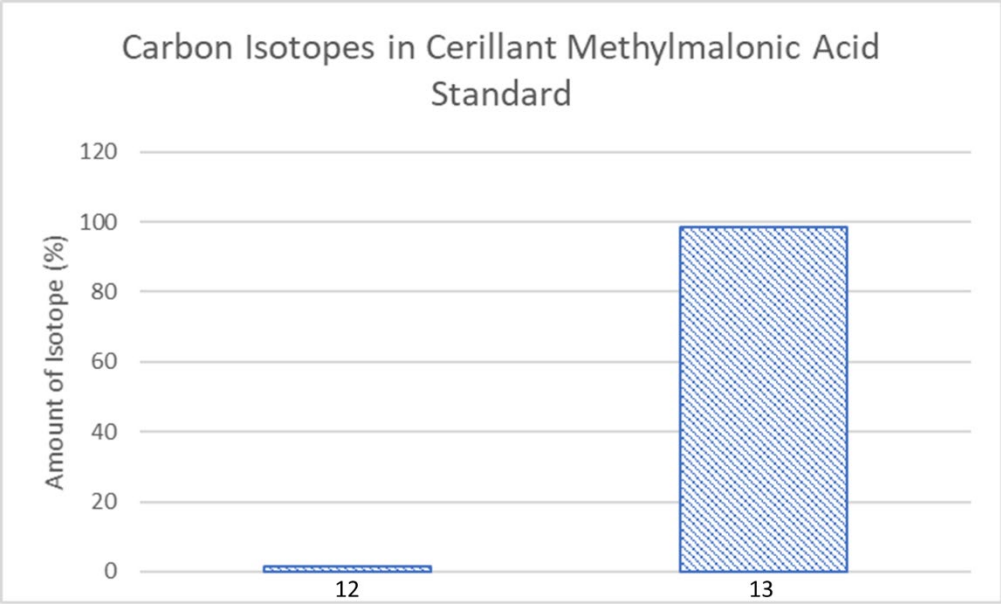

Figure 4.3. Isotopic abundance of carbon in methylmalonic acid purchased from Cerilliant (Lot FN06121302). This lot was reported to have a carbon isotopic abundance of 1.47% carbon-12 isotope and a 98.53% carbon-13 isotopic distribution. Standards were measured to have an isotopic distribution of 2.13% carbon-12 and 97.87% carbon-13.

This impurity is a known value in isotopic standards and is reported by the manufacturer. The knowledge of the isotopic abundances in the natural sample and spike is what allows for deconvolution in IDMS and speciated isotope dilution mass spectrometry (**Figure 4.4**).[29] Given that the optimal spiking ratio of heavy to light isotopes can have a relatively large range in which error associated with spiking is low, this can be utilized to enhance the purchased spike with natural sample to create a new MetaSpike™ which will increase the signal of the analyte and allow for quantitation at levels below the LLOQ (**Figure 4.5**).

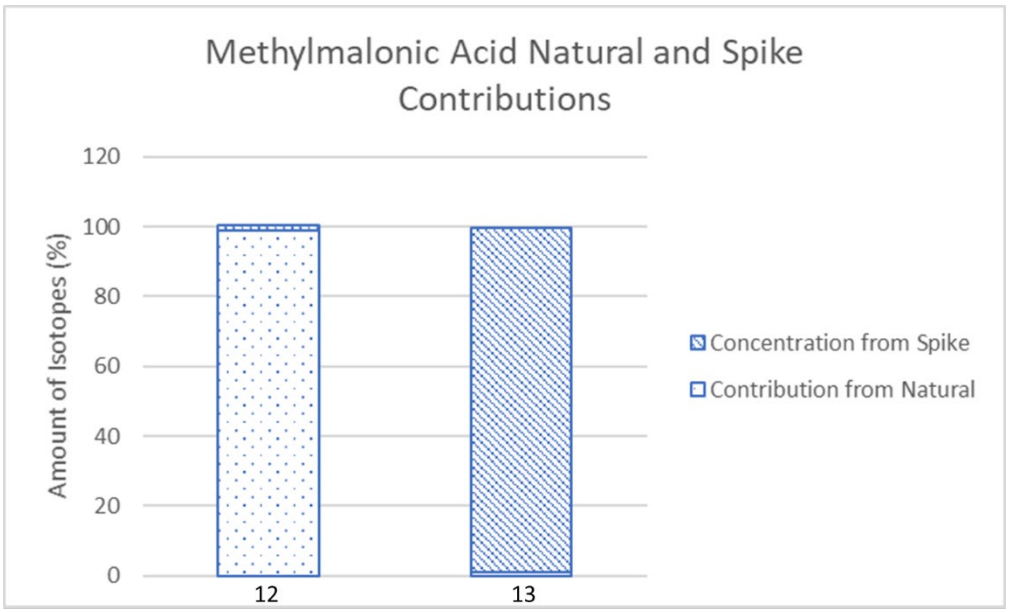

Figure 4.4. Optimal isotopic abundance of carbon in methylmalonic acid of an isotope dilution mass spectrometry spike based on the error propagation factor curve. These curves are unique to the element of interest for isotope dilution mass spectrometry but have not been prepared for more complex molecules. This represents how spike for traditional isotope dilution mass spectrometry is utilized. By the nature of the spike, a small percentage of natural isotope is added to the sample which is deconvoluted in the isotope dilution mass spectrometry equation (Equation 1.1).

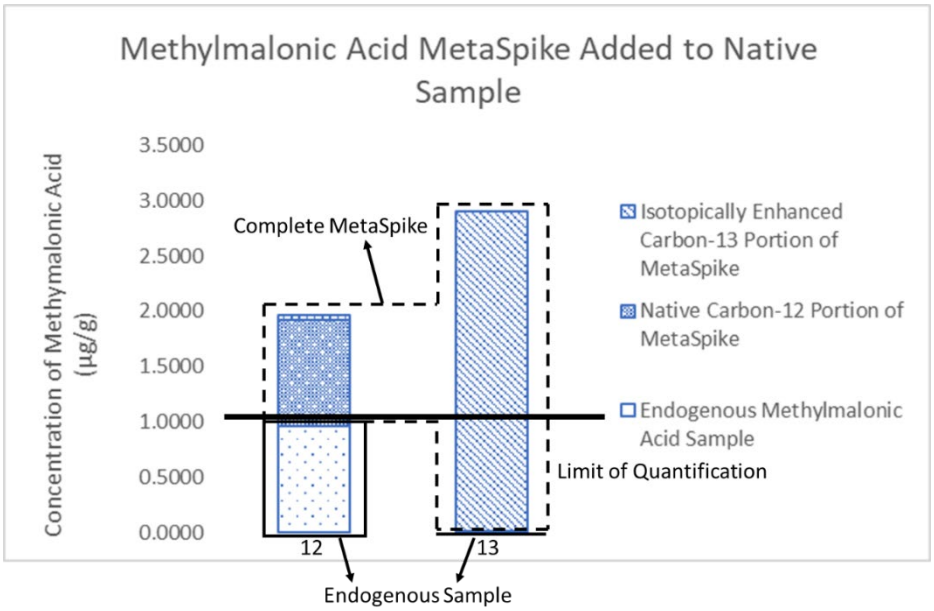

Figure 4.5. The completed MetaSpike™ which is ready to add to the sample to enable Thor's Hammer isotope dilution mass spectrometry. The natural addition of a small concentration of analyte through the traditional isotope dilution mass spectrometry spike has been expanded upon to create a unique isotope found nowhere else on the planet. There is, so far, no literature which investigates the creation of such a spike for signal enhancement.

Elevated methylmalonic acid (MMA) is seen at levels of one in 48,000 patients in North America, and at a level of one in 26,000 patients in China.[30] The accepted normal range of MMA is between 70 and 270 nmol/L,[31-33] however some conditions, such as a genetic deficiency in MCEE, the gene on chromosome 2 which controls the enzyme methylmalonyl-CoA epimerase, is seen in concentration of only 7 nmol/L.[34] This concentration is too far below the calculated LLOQ for MMA to be quantitated by calibration curves. For this reason, MMA was chosen as a proof of concept to enable a new quantification technique known as Thor's Hammer isotope dilution mass spectrometry (TH-IDMS).

4.2. Materials and Methods

4.2.1 Chemicals and Preparation of samples

MMA purchased from Sigma Aldrich (Lot STBB4671) and SUC purchased from Alfa Aesar (Lot Y12A042) were purchased and made into standards of approximately 1 µg/g being dissolved in 15-mL Fisher Scientific (Lot 035329) in Fisherbrand metal free disposable centrifuge tubes (Lot 26920041) utilizing 18.2 MΩ deionized water was which was made in lab using a 7146 Barnstead NANOpure system (Model 251115-102), which was then passed through a D7035 Easypure II water filtration system (Model 1305080906425). These solutions were allowed to mix on a Vortex Genie 2 Digital Serial (Model A3-1896) for 30 seconds at 5000 RPM. The samples were then filtered via a 10-mL Norm-Ject luer lock solo syringe (Lot 20F01C8) and passed through a 0.22 µm pore size polypropylene Agilent technologies filter (Lot FG4627). Solutions of MMA, SUC, and a combination of the two were made and used for liquid chromatography separation and mass spectrometry optimization. A 4C13 isotopically enriched standard of MMA which was

purchased from Cerilliant (Lot FN06121302) which had been enriched to 98.53% and was diluted with 18.2 MΩ deionized water to create an 84.037 ng/g isotopically enriched standard which would be utilized as an internal standard for calibration curve measurements as well as heavy isotopic standards for IDMS quantification.

Abundance testing was performed on samples of MMA, both isotopically enhanced and natural, which were diluted to approximately 1mL of 8.4 ng/mL in 1 mL Agilent amber glass liquid chromatography vials (Lot 18154222). These samples were made in triplicate and then directly injected onto an Agilent triple quadrupole system with five replicates.[35, 36] Mass transitions ranging from 117 → 68-78 and 121 → 68-78 were monitored for each sample to determine the extent of full enrichment of MMA in the isotopic and natural analogs. Three levels of MMA spike concentrations were tested. First was natural MMA with no isotopically enriched analog added. The second was the isotopically enriched analog to which no natural MMA had been added. The third and final sample was the MetaSpike™ for use in TH-IDMS quantitation which had be reconstituted to roughly 30% natural and 70% isotopically enriched MMA.

Calibration curve and TH-IDMS quantitation levels were made in 18.2 MΩ deionized water and which were serial diluted prior to the addition of internal standard of 4C13 enriched MMA purchased from Cerilliant for the calibration curve quantitation and the MetaSpike™ which had been prepared prior to the experimentation which were added to each sample, respectively. After dilution and addition of the respective spikes, new concentrations for each level of quantitation were recalculated to account for this further dilution. These spikes weighed approximately 0.025 g for each sample and consisted of an isotopically enriched MMA with a concentration of 5.9127 µg/g for the calibration curves and a MetaSpike™ which contained a concentration of roughly 30% natural and 70% isotopically enriched MMA made from mixture of

1.9845 µg/g natural and 5.9127 µg/g isotopically enriched analogs. These samples were prepared in triplicate and tested in replicates of five to ensure precision and repeatability of the method.

Comparison samples of TH-IDMS to traditional IDMS were performed by the addition of natural MMA as well as the IDMS standard and MetaSpike™ to bovine blood samples to which Ethylenediaminetetraacetic acid had been added which were purchased from Lampire on 11/29/2016 which had been stored in a -80 °C freezer until needed and was then thawed overnight on ice which had been spiked with MMA. Blood card testing was application of 20 µL of spiked bovine blood samples to cellulose Whatman C-Pak cards (Lot ET7059416). These blood samples were created with a concentration of roughly 0.15 µg/g of natural MMA and 0.025 g of 5.9127 µg/g isotopically enriched MMA and a separate sample to which 0.025 g of roughly 30% natural and 70% isotopically enriched MMA made from mixture of 1.9845 µg/g natural and 5.9127 µg/g isotopically enriched analogs for the Meta Spike and allowed to dry on the Whatman C-Pack blood cards for 24 hours. These samples were then desorbed using the method developed on the Gerstel SPExos system as well as the liquid chromatography separation achieved on the Agilent 1200 liquid chromatography system and the optimization parameters which were determined on the Agilent 6460 triple quadrupole mass spectrometer. Samples which were quantitated through traditional IDMS were then compared to those who were quantitated using TH-IDMS.

4.2.2 Instrumentation

Detection was achieved using an Agilent 6460 triple quadruple mass spectrometer (Model US92170174) in negative mode selecting for an ion of mass/charge (m/z) of 117 in the first quadrupole and 73 in the third through multiple reaction monitoring for natural MMA and 121 in the first quadrupole and 76 in the third quadrupole for the isotopically enriched MMA.[37-39] While

many of the literature values for determining MMA in the MS have derivatized the molecule to aid in detection and analysis, one of the goals of the experiment was to automate the process as much as possible.[40-42] As such, it was determined that no additional derivatization should be performed on the MMA and all detection and quantification would occur for the natural state of the organic acid. This may potentially decrease the sensitivity of detection, however the increase of detection through instrumental optimization should overcome this discrepancy.

An Agilent 1200 Liquid Chromatography System comprised of a G13798B degasser, a G1312B binary pump, a G1367D high performance autosampler, a G1330B thermostat, and a G1316B column compartment, was utilized for separation which was then ionized via electrospray using a G1958-65138 Agilent Jet-Stream Electrospray Ionization source. Samples were separated on a Phenomenex Synergi 4 μm Hydro-RP 80 Å 150 x 4.6 mm column (Lot 00F-475-F0) was used for successful peak separation. A flow rate of 1.000 mL/min was utilized with a mobile phase consisting of 18.2 Ω deionized water from a Barnstead NANOpure system manufactured by Thermo Scientific (Model 7146) which was then passed through an Easypure II water filtration system manufactured by Thermo Scientific (Model D7035) and HPLC grade acetonitrile purchased from Fisher Scientific (Lot 190931) to both of which 0.1% optima grade formic acid from Fisher Chemical (Lot 173815) had been applied to aid in the ionization process.[43] The complete method can be seen below (**Table 4.1**).

Table 4.1. Final LC-MS method for separation of methylmalonic acid and succinic acid on an Agilent 1200 liquid chromatography system through a Phenomenex Synergi 4 µm Hydro-RP 80 Å 150 x 4.6 mm column for detection on an Agilent 6460 triple quadrupole mass spectrometer. This method resulted in complete baseline separation with Gaussian peaks.

Time (Min)	H_2O %	Acetonitrile %
0.00	99.0	1.0
4.00	90.0	10.0
4.50	35.0	65.0
4.75	5.0	95.0
5.75	5.0	95.0
5.80	99.0	1.0

The Agilent 6460 triple quadrupole mass spectrometer was optimized for the detection of MMA over SUC by utilizing the source optimization program in Agilent's software. The optimal factors are shown below in **Table 4.2**.

Table 4.2. Optimization parameters for the detection of methylmalonic acid on an Agilent 6460 triple quadrupole mass spectrometer which was run in negative mode.

Parameter	Optimization
Gas Temperature	230 ˚C
Gas Flow	4 L/min
Nebulizer	45 PSI
Sheath Gas Temp	300 ˚C
Sheath Gas Flow	9 L/min
Capillary Voltage	4000 V
Nozzle Voltage	500 V

A Gerstel Inc. DBSA SPExos Automated Blood Card system comprised of a model 730 high pressure dispenser, a model 725 automated cartridge extraction system, a model 410 dried blood spot desorption unit, and a model 014-02A multipurpose sampler arm was used. This was controlled by Maestro software (Version 1.4.25.1) was utilized for this purpose and samples were applied to Whatman FTA DMPK-C Card with a nitrocellulose membrane and a 0.1-12.0 µm pore

size and analytes were collected on Spark Holland SPExos strong hydrophobic styrene-divinylbenzene polymer resin (Lot 86.329) single use cartridges before being injected into the liquid chromatography system and further detection on the mass spectrometer. First, the pure MMA sample was tested, then the mixed MMA and SA sample, next the spiked blood sample, and finally the isotopically spiked blood sample. Twenty µL of sample was added to each of the four spots on the card and allowed to dry overnight. Once dried, the blood card was inserted into the Gerstel SPExos and a method was developed for detection and quantification. It began by conditioning a Gerstel SPExos cartridge with a strong hydrophobic resin (styrene-divinylbenzene) inside. The desorption hot cap was set to 80 ˚C (which aids in the removal of analyte from DBS) and the flow rate was set to 4000 µL/min with a 1000 µL/min dispense, which was then optimized to 250 µL/min. After detection of the analyte, it was necessary to determine if the analyte had been lost in the washing step of the MMA elution for a possible increase in response from MMA. The complete method for desorption can be seen below (**Table 4.3**).

Table 4.3. Method for desorption of methylmalonic acid from a quantitative dried blood spot using a Gerstel SPExos system onto strong hydrophobic resin (styrene-divinylbenzene) cartridges. All solvents contained 0.1% formic acid except the clean mix (acetonitrile, methanol, isopropanol, and 18.2 Ω deionized water in a 3:3:2:2 Ratio) which had 0.05% formic acid.

	Cartridge Conditioning		Wash			Desorption
Solvent	Methanol	H_2O	0.1% NH_4OH	Clean Mix	H_2O	H_2O
Dispense Rate	1000 µL/min	1000 µL/min	1000 µL/min	1000 µL/min	1000 µL/min	250 µL/min
Dispense Volume	1000 µL	2000 µL	2000 µL	1000 µL	1000 µL	250 µL

4.2.3 MetaSpike™ Preparation

Once the dynamic range of isotopic error had been determined, the MetaSpike™ standard was created by mixing standards of the purified analyte of interest at natural isotopic abundances. A natural MMA standard, purchased from Fisher Chemical, and enriched 4C13 labeled MMA, purchased from Cerilliant, were utilized to create a unique isotopic spike of MMA. The ratio of natural and enriched mixture standard depends on factors such as the natural abundance of isotopes, the desired signal amplification, the error propagation factor curves, and the LLOD and LLOQ of the analyte. The isotopic standards should be mixed in such a way that the altered isotopic abundance profile of the newly created MetaSpike™ which reduces imprecision by boosting the signal to quantifiable levels above the LLOQ. The MetaSpike™ can be mixed in any ratio but works best if the natural analyte is between 20 and 80% of the spike which enables quantitation at levels below the LLOQ.

The MetaSpike™ is applied to the sample in the same way as spike is applied in IDMS, measured by mass, and thoroughly equilibrated. The MetaSpike™ must have the correct

concentration, as an excessive spike will overwhelm the signal from the sample and a low concentration will not aid in quantitation. Thus, prior to application, concentration of the MetaSpike™ should be determined through experimentation and should attempt to be slightly below the LLOQ or LLOD. For the determination of MMA at or below the LLOQ, a MetaSpike™ was prepared from solutions of 1.984 µg/g natural and 5.926 µg/g enriched MMA into a single solution which had a concentration of 0.333 µg/g natural and 0.995 µg/g isotopically enriched MMA. This MetaSpike™ was utilized for all TH-IDMS experiments. However, the roughly 30% natural and 70% isotopically enriched MetaSpike™ is only one possible concentration and can be altered to increase signal and enable quantitation at lower levels of analyte concentration.

4.2.4 Isotope Dilution Mass Spectrometry Sample Preparation

For IDMS quantitation at or below the calculated LOQ, samples of natural MMA were made starting at 1.912 µg/g of solution and diluted for six data points such that. These samples were then spiked with 0.995 µg/g of 4C13 enriched MMA purchased from Cerilliant which acted as an internal standard. These samples were prepared in 18.2 MΩ deionized water and in 1 mL Agilent amber glass liquid chromatography vials to decrease overall waste of solution. These samples were separated by an Agilent 1200 liquid chromatography system after being passed through a Phenomenex Synergi Hydro RP column and detected on an Agilent 6460 triple quadrupole mass spectrometer. Abundances were then calculated and used for future IDMS quantitation.

Table 4.4. Concentration and responses for isotope dilution mass spectrometry quantitation of methylmalonic acid for quantitation at or below lower limit of quantitation.

Calibrant Level	1	2	3	4	5	6
Concentration (µg/g)	1.912	0.962	0.492	0.245	0.128	0.067
Natural Methylmalonic Acid Counts	23401	12683	7121	4437	2484	1474
Natural Methylmalonic Acid Standard Deviation	489.1	222.0	212.4	182.0	77.3	294.8
Natural Methylmalonic Acid 95% Confidence Interval	162.0	73.6	70.4	60.27	25.6	97.6
Enriched Methylmalonic Acid Counts	10400	11369	13083.6	15563	17027	17632
Enriched Methylmalonic Acid Standard Deviation	963.1	706.8	133.2	407.9	372.4	123.3
Enriched Methylmalonic Acid 95% Confidence Interval	319.0	234.1	44.1	135.1	123.4	40.8

IDMS quantitation was then applied to determine accurate concentration levels at or below LLOQ.

4.2.5 Thor's Hammer on Dried Blood Spot Preparation

Blood samples were made first from bovine whole blood with Ethylenediaminetetraacetic acid purchased from Lampire on 11/29/2016 which had been stored in a -80 °C freezer until needed and was then thawed overnight on ice which had been spiked with MMA and SUC. Blood card testing was application of 20 µL of spiked bovine blood samples to cellulose Whatman C-Pak cards (Lot ET7059416). These blood samples were created with a concentration of 0.155 µg/g MMA and either 0.9828 µg/g of Cerilliant 4C13 enriched MMA for IDMS samples or a MetaSpike™, which was comprised of concentration of 0.3333 µg/g natural and 0.9949 µg/g isotopically enriched MMA for TH-IDMS. 20 µL of these samples were pipetted onto each of the four blood spots and allowed to dry in a clean room on Whatman C-Pack blood cards for 24 hours.

Once dried, these samples were passed through the method developed on the Gerstel SPExos system as well as the liquid chromatography separation achieved on the Agilent 1200 liquid chromatography system and the optimization parameters which were determined on the Agilent 6460 triple quadrupole mass spectrometer.

4.3 Discussion

4.3.1 Determination of Lower Limit of Detection and Quantification

Before TH-IDMS utilizing MetaSpike™ technology can be employed, the LLOD and LLOQ must be established for the analyte of interest on the instrument that is to be utilized. There is currently no universally accepted mathematical determination of the LLOQ,[44] however, there are three widely utilized methods of determination, those which stem from a calibration curve, signal to noise ratios, and those which stem from the measured blank.[18, 21, 45] However, the LLOQ is generally accepted to be 10 times the standard deviation of the signal to noise ratio of the blank.[46] Experimentally, 20 blanks were run and the signal to noise ratio was recorded for both tracked mass transitions of MMA and SUC (**Table 4.5**). Note that these experimental methods of establishing measurement parameters are instrument and method dependent. As any peaks were indistinguishable from the noise, SUC and MMA peaks were taken from the elution time of the analytes for separation method, 4.5 minutes, and 5.1 minutes respectively. This experiment was repeated three separate times to ensure consistency and repeatability.

Table 4.5. Average peak areas and standard deviations of methylmalonic acid and succinic acid taken from twenty blank samples an Agilent 1200 liquid chromatography system through a Phenomenex Synergi 4 µm Hydro-RP 80 Å 150 x 4.6 mm column for detection on an Agilent 6460 triple quadrupole mass spectrometer.

	Mass Transition 117-73				Mass Transition 121-76			
	Succinic Acid		Methylmalonic Acid		Succinic Acid		Methylmalonic Acid	
	S/N	Peak Area	S/N	Peak Area	S/N	Peak Area	S/N	Peak Area
Average Counts	3.4	15.3	3.3	13.0	4.3	5.9	4.3	4.8
Standard Deviation	1.4	6.4	1.4	4.2	1.7	3.3	1.7	2.4

From these results, the LOB, LLOD, and LLOQ were calculated for SUC and MMA using the previously developed methodology for detection and quantification on an Agilent 1200 liquid chromatography system through a Phenomenex Synergi 4 µm Hydro-RP 80 Å 150 x 4.6 mm column for detection on an Agilent 6460 triple quadrupole mass spectrometer (**Table 4.6**).[21]

Table 4.6. Calculated results for limit of the blank, lower limit of detection, and lower limit of quantification of succinic and methylmalonic acid utilizing blank-derived methodology on an Agilent 1200 liquid chromatography system through a Phenomenex Synergi 4 µm Hydro-RP 80 Å 150 x 4.6 mm column for detection on an Agilent 6460 triple quadrupole mass spectrometer.

	Mass Transition 117-73		Mass Transition 121-76	
	Succinic Acid	Methylmalonic Acid	Succinic Acid	Methylmalonic Acid
Average Counts	15.3	13.0	5.9	4.8
Standard Deviation	6.4	4.2	3.3	2.4
Limit of Blank	25.8	19.9	11.3	8.7
Limit of Detection	51.0	41.3	21.0	16.6
Limit of Quantitation	51.0	41.3	21.0	16.6

Thus, the LLOD and LLOQ based on signal to noise ratio for methylmalonic acid based on the employed sample preparation technique and separated on an Agilent 1200 liquid chromatography system through a Phenomenex Synergi 4 µm Hydro-RP 80 Å 150 x 4.6 mm

column and detected on an Agilent 6460 triple quadrupole mass spectrometer should be greater than 41.3 for accurate quantitation.

4.3.2 Analyte and Isotopic Spike Abundance Testing

The final step prior to quantitation testing using TH-IDMS is to determine an accurate abundance of each of the isotopes which are being measured. In this case, the analytes were natural MMA and 4C13 isotopically enriched isotopes purchased from Cerilliant which was reported to be enriched to 98.53%. Abundance testing was performed on an Agilent 6530 quadrupole time of flight mass spectrometer to which samples of each analyte which had been dissolved in 18.2 MΩ deionized water to approximately 1mL of 5.4 µg/mL in 1 mL Agilent amber glass liquid chromatography vials. These samples were separated by an Agilent 1200 liquid chromatography system after being passed through a Phenomenex Synergi Hydro RP column and detected on an Agilent 6460 triple quadrupole mass spectrometer. Abundances were then calculated (**Table 4.7**) and used for future IDMS and TH-IDMS quantitation.

Table 4.7. Calculated abundances of isotope transitions 117 → 73 and 121 → 76 natural methylmalonic acid, 4C13 enriched methylmalonic acid purchased from Cerilliant, and for the MetaSpike™ which enables Thor's Hammer isotope dilution mass spectrometry for use in accurate quantitation.

	Natural Methylmalonic Acid Abundance	**^{13}C Enriched Methylmalonic Acid Abundance**
Natural Standard	0.9941	0.0059
IDMS Standard	0.0216	0.9784
Thor's Hammer Standard	0.2911	0.7089

Calculated abundances were then used in the IDMS equation for both the spike (IDMS standard and Thor's Hammer standard respectively) and the sample (Natural standard) to allow more accurate quantitation.

4.3.3 Thor's Hammer Quantitation and Validation as Compared to Traditional Isotope Dilution Mass Spectrometry

While quantitation utilizing calibration curves is the gold standard of metrology, it is not appropriate to utilize this quantitative tool below the established LLOQ. As this exceeds the definition of the calibration curve, any resultant data would be meaningless. Thus, validation and comparison must be performed utilizing IDMS, a quantitative tool with no universally defined LLOQ, but instead one with only limits which are dependent on observation. Methylmalonic acid is a stable organic molecule and there should be no difficulty in quantitating it at levels above the LLOQ, Chapter 2, however, this changes at lower concentrations where calibration curves begin to falter the standard of metrology is to be replaced with an IUPAC gold method for standard certification. To preform analogous testing and allow a direct comparison between methodologies, a serial dilution for methylmalonic acid was prepared which began above the limit of detection of MMA, which was determined to be approximately 1.9 µg/g of analyte. While this quantitation would not normally be possible utilizing calibration curves, a comparison of IDMS was used for method validation. This solution was serial diluted for six levels to experimentally determine the LLOQ for MMA based on IDMS as well as TH-IDMS. Samples were prepared with natural MMA and 4C13 enriched MMA in 18.2 MΩ deionized water. Samples underwent chromatographic separations on an Agilent 1200 liquid chromatography system and were passed through a Phenomenex Synergi Hydro RP column before being detected on an Agilent 6460 triple

quadrupole mass spectrometer. Samples were run in replicates of five before quantitation was attempted with IDMS as well as TH-IDMS. Using the prepared samples above, attempts were made to quantitate samples of MMA (**Table 4.8**).

Table 4.8. Calculated concentration of methylmalonic acid at or below the lower limit of detection from isotope dilution mass spectrometry along with the confidence interval and error.

Sample Level	1	2	3	4	5	6
Known MMA Concentration (µg/g)	1.912	0.962	0.492	0.245	0.128	0.067
Calculated MMA Concentration (µg/g)	1.870	0.898	0.425	0.189	0.060	0.002
95% Confidence Interval (µg/g)	0.100	0.011	0.018	0.010	0.033	0.039
Associated Error (%)	2.4	6.7	13.6	22.9	53.1	97.0

The associated error of at or below the LLOQ of MMA as quantified by IDMS was successful at three levels below the traditional LLOQ with ≤15 % error to 0.492 µg/g before levels exceeded the ≤20 % error as defined by the FDA's Bioanalytical Method Validation Guidance for Industry. The 95% confidence limits did encompass the known concentration of the analyte for the first three data points but failed to overlap in the lowest three levels. (**Figure 4.6**). These points did not overlap, however, meaning they were statistically different.

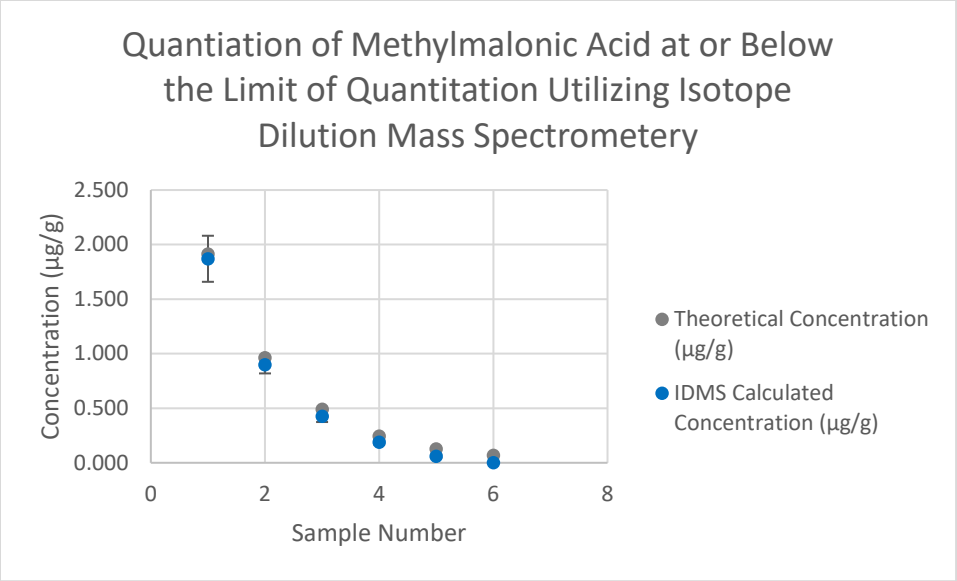

Figure 4.6. Graphical representation of isotope dilution mass spectrometry quantitated data points at or below the limit of quantitation. All 95% confidence intervals overlap, meaning samples were not statistically different.

This data is representative of the reason which the LLOQ is calculated, at certain concentration of low-level quantitation calibration curves are no longer reliable. This leads to a blind spot in quantitation which may lead to limitations in diagnosis and care from physicians. Through the application of the MetaSpike™ and quantitation using TH-IDMS, the signal from the analyte is increased in and accurate quantitation is possible below the LLOQ as determined for a calibration curve.

A second set of samples had the MetaSpike™ applied, and the known concentrations of MMA were recalculated to reflect the change in mass of the sample. The MetaSpike™ acts as a single-point calibration curve inside each sample which can utilize the IDMS equation to allow for accurate quantitation. These samples were introduced in replicates of five through the same methodology and instrumentation as the calibration curve quantitated samples, the results of which were quantitated using the IDMS equation with the abundances of the spike updated to reflect the concentration of the MetaSpike™ (**Table 4.9**).

Table 4.9. Calculated concentration of methylmalonic acid at or below the lower limit of detection from Thor's Hammer isotope dilution mass spectrometry along with the confidence interval and error.

Sample Level	1	2	3	4	5	6
Known MMA Concentration (µg/g)	1.912	0.962	0.452	0.208	0.088	0.020
Calculated MMA Concentration (µg/g)	1.952	0.927	0.492	0.245	0.128	0.067
95% Confidence Interval (µg/g)	0.211	0.079	0.051	0.021	0.017	0.001
Associated Error (%)	1.5	3.7	8.0	15.0	31.3	70.8

Quantitation was successful and within acceptable error using TH-IDMS up to the fourth dilution below the LLOQ, which was 0.208 µg/g of sample, one order of magnitude below the calculated LLOQ. While quantitation exceeded the acceptable error of ± 20% at the LLOQ as stipulated by the Food and Drug Administration.[47] When viewed graphically, no overlap of error bars on any level are observed, meaning the samples are statistically distinct from one another at the 95% confidence interval (**Figure 4.7**). These confidence intervals do not overlap with the known concentration at the lowest levels, suggesting that there is a limit to the potential extension of TH-IDMS below the L-LOQ. These errors may potentially be overcome by altering the MetaSpike™ such that it has a greater percentage of natural analyte which could increase the signal from the mass spectrometer further and allow quantitation at even lower levels.

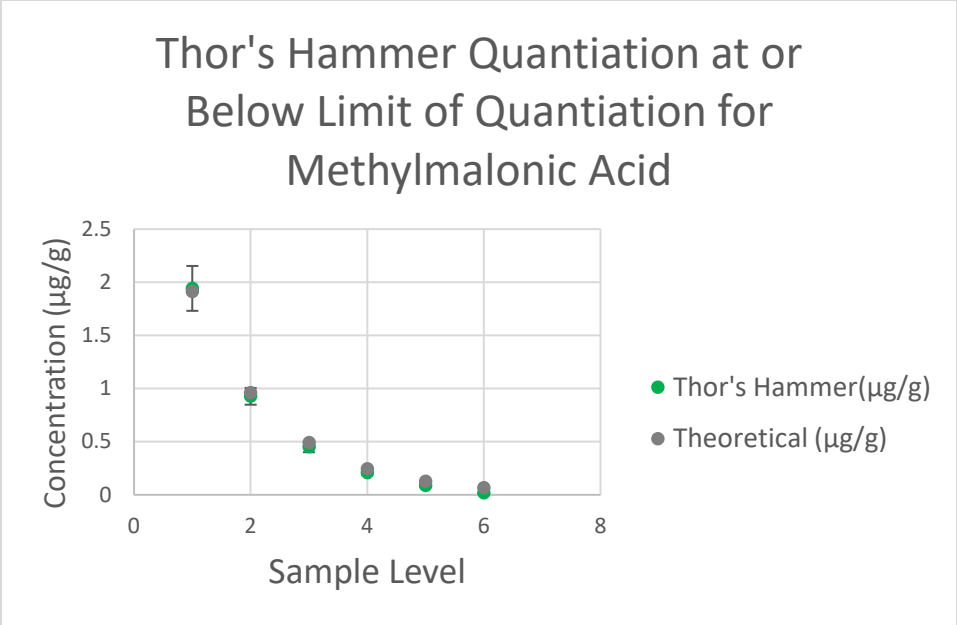

Figure 4.7. Graphical representation of Thor's Hammer isotope dilution mass spectrometry quantification. No 95% confidence intervals overlap other samples and are accurate up to one order of magnitude below the previously determined limit of quantitation.

At every level of the data set, the errors were reduced (**Figure 4.8**) including the levels in which TH-IDMS could no longer accurately be applied with a reduction of error by greater than 50% in all cases. This indicates creating a MetaSpike™ with a greater percentage of natural MMA may be able to increase the signal to allow for accurate quantitation at even lower concentrations of analyte.

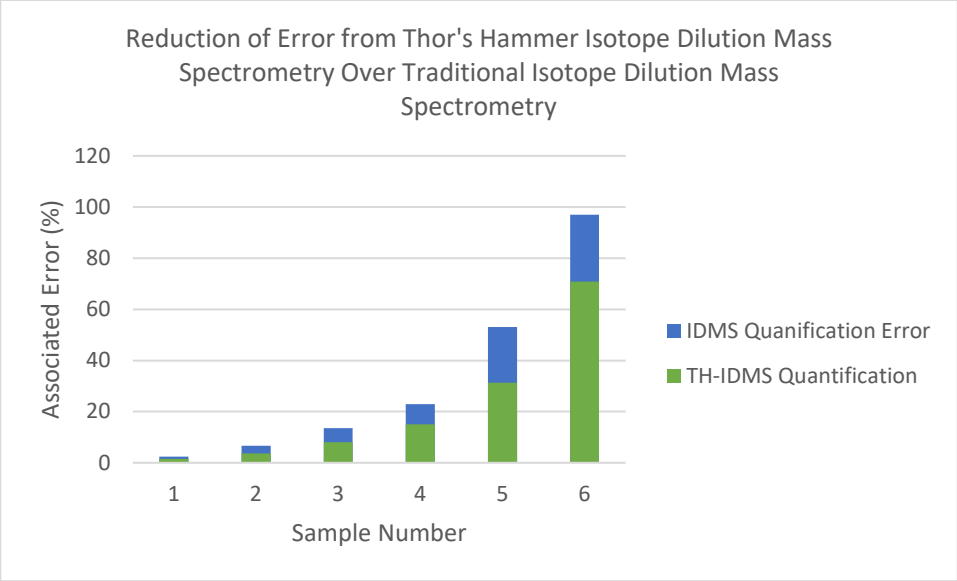

Figure 4.8. Decrease in error of each sample compared from isotope dilution mass spectrometry and Thor's Hammer isotope dilution mass spectrometry. The error was decreased by 0.9%, 3.0% 5.6%, 7.9%, 21.8%, and 26.2% respectively.

4.3.4 Thor's Hammer Isotope Dilution Mass Spectrometry Compared to Traditional Isotope Dilution Mass Spectrometry on Dried Blood Spots

Quantitation utilizing TH-IDMS had proven a superior method to calibration curves below the previously established LLOQ. Previously, traditional IDMS had been proven a successful quantitation tool for MMA on DBS cards and it was determined to test TH-IDMS in a similar manner and as a comparison tool to traditional IDMS. As TH-IDMS utilizes the same equation as traditional IDMS but includes the MetaSpike™ which increases signal from the mass spectrometer, TH-IDMS should allow for accurate quantitation at lower levels than traditional IDMS. Neither IDMS nor TH-IDMS utilize calibration curves, however, instead rely on the single point calibration curve of the spike that is digitally applied. IDMS is one of the IUPAC definitive methods analytically.[27] Thus, no calibration curves were created, and a single MMA concentration was applied to bovine blood which was then spiked with either 4C13 which was purchased from Cerilliant, or from the MetaSpike™ which had been previously utilized. These blood samples were

then applied to Whatman-C Pak blood cards and allowed to dry overnight in a clean room. These cards were then desorbed using a fully automated Gerstel SPExos system and the results were quantitated (**Table 4.10**). Due to the loss of potential signal from analytes when utilizing this system, it was determined that quantitation below the LLOQ should be tested utilizing the automated system and desorbed from DBS in order to compare these two metrology techniques on a matrix where TH-IDMS may be the most beneficial. As each blood spot can only be tested once, all blood spots were utilized in order for the maximum statistical benefit.

Table 4.10. Comparison of quantitation methods isotope dilution mass spectrometry and Thor's Hammer isotope dilution mass spectrometry of methylmalonic acid which had been desorbed from a Whatman C-Pack dried blood spot card using a Gerstel SPExos system and was retained on a on Spark Holland SPExos strong hydrophobic resin single use cartridge by an Agilent 1200 liquid chromatography system through a Phenomenex Synergi 4 µm Hydro-RP 80 Å 150 x 4.6 mm column as seen on an Agilent 6460 triple quadrupole mass spectrometer

IDMS		TH-IDMS	
Volume (µL)	20	**Volume (µL)**	20
Replicates	4	**Replicates**	4
Known Concentration of MMA (µg/g)	0.1544	**Known Concentration of MMA (µg/g)**	0.1569
Calculated Concentration of MMA (µg/g)	0.1922 ± 0.1505	**Calculated Concentration of MMA (µg/g)**	0.1672 ± 0.0550
Associated Error (%)	19.7	**Associated Error (%)**	9.9

Quantitation utilizing IDMS and TH-IDMS were both within acceptable (≤20%) error and had overlapping confidence intervals at the 95% level (**Figure 4.9**) at over an order of magnitude below the previously established LLOQ. However, TH-IDMS had a superior performance with <10% error and smaller confidence intervals. As the error associated with TH-IDMS for MMA on DBS cards was superior even to traditional IDMS, it suggested that accurate quantitation could be performed at an even lower level and possibly up to two orders of magnitude below the calculated

LLOQ. Introducing a new MetaSpike™ with a unique ratio of natural to isotopically enriched analyte, which would enhance the signal further, would allow an even lower LLOQ.

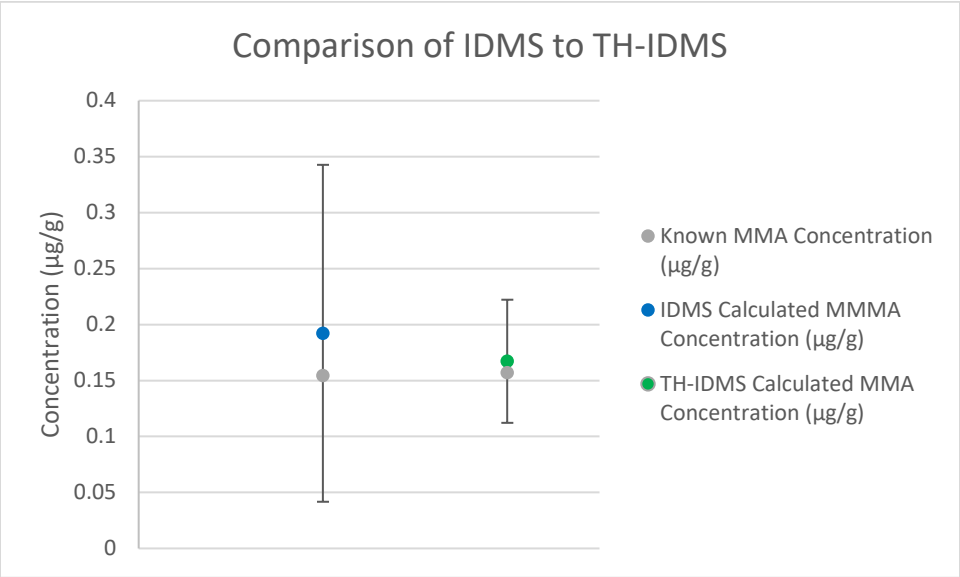

Figure 4.9. Graphical comparison of quantitation methods isotope dilution mass spectrometry and Thor's Hammer isotope dilution mass spectrometry of methylmalonic acid which had been desorbed from a Whatman C-Pack dried blood spot card using a Gerstel SPExos system and was retained on a on Spark Holland SPExos strong hydrophobic resin single use cartridge by an Agilent 1200 liquid chromatography system through a Phenomenex Synergi 4 µm Hydro-RP 80 Å 150 x 4.6 mm column as seen on an Agilent 6460 triple quadrupole mass spectrometer.

Overall error reduction of TH-IDMS as compared to traditional IDMS was reduced by 49.5%, (**Figure 4.10**) to enable accurate quantitation at levels an order of magnitude below the LLOQ. When utilizing a DBSA system, signal is naturally lost as the analyte is desorbed from a DBS on a cellulose card, retained on a cartridge, and finally eluted from the cartridge.

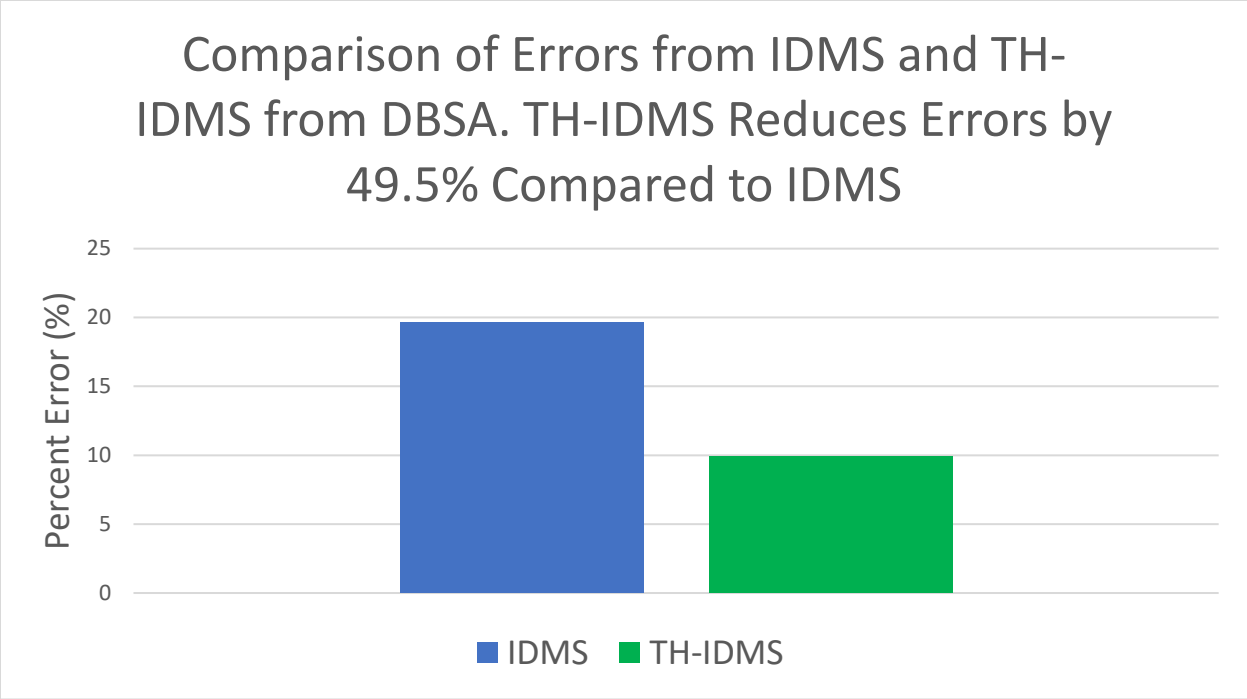

Figure 4.10. Comparison of errors of quantitation methods isotope dilution mass spectrometry and Thor's Hammer isotope dilution mass spectrometry of methylmalonic acid which had been desorbed from a Whatman C-Pack dried blood spot card using a Gerstel SPExos system and was retained on a on Spark Holland SPExos strong hydrophobic resin single use cartridge by an Agilent 1200 liquid chromatography system through a Phenomenex Synergi 4 µm Hydro-RP 80 Å 150 x 4.6 mm column as seen on an Agilent 6460 triple quadrupole mass spectrometer. Error was reduced by 49.5%.

4.4 Conclusions and Future Development

One significant issue with performing accurate quantitation on dried bloods spots is the loss of analyte and signal which is inherent when processing the sample. Loss of signal can be partially attributed to analyte loss in three major steps in processing blood cards on a fully automated solid phase extraction system: the desorption of analyte from the blood card, cartridge retention, cartridge elution. Not all analytes may be completely desorbed from the blood card, not all analytes may be retained on the cartridge, and not all analytes may be eluted from the cartridge into the liquid chromatography system. An even greater loss of analyte may be seen in manual punch and desorption from blood cards. Due the loss of signal, and trace analyte concentration in

the body, many analytes need signal enhancement before any quantification can occur. Currently derivatization to enhance signal output is widely utilized, but this approach using calibration curve quantitation falls short of the desired levels of data quality. The use of MetaSpike™ invention allows for accurate quantitation without derivatization of analyte at even the lowest levels of quantitation.

Optimally, MetaSpike™ concentrations for the more abundant isotope of the natural sample should be close to the LLOQ, thus a 1:1 ratio of the naturally occurring isotopic portion of the MetaSpike™ and isotopically labeled portion of the MetaSpike™ would be inappropriate as both isotopes must be above the LLOQ for quantitation. The optimal spike would have a higher concentration of the isotopically labeled portion of the MetaSpike™, by three to four times for methylmalonic acid. Once the MetaSpike™ has been mixed with endogenous sample, the outcome should be quantifiable and should consist of the sample, which has a natural isotopic distribution ratio, and the MetaSpike™, which consists of both natural isotopic distribution ratios as well as an isotopically enhanced standard designed to raise the signal to quantifiable levels without masking the original sample. The concentrations of both isotopic signatures within the MetaSpike™, as well as the MetaSpike™ itself, can be adjusted to fit the lab's needs with nothing more complicated than isotopic abundance testing. With the signal raised about the LLOQ, and with concentrations and abundances known, a simple IDMS or SIDMS calculation can be performed for accurate quantitation that has been shown to lower the LLOQ by almost two orders of magnitude as compared to calibration curves.

Proper medical diagnosis and health assessment require accurate metrology, with some conditions presenting symptoms associated with the concentration of and endogenous analyte that may be too low to measure with classical mass spectrometric and IDMS and SIDMS techniques.

Previous attempts to improve quantification at the LLOQ level in a mass spectrometer by engineering augmentation by pushing more ions in the instrument has not addressed the challenge.

TH-IDMS has been shown to effectively lower the limit of quantitation by almost two orders of magnitude compared with the traditional calibration curves methods by implementing MetaSpike™-enabled IDMS without derivatization. Previous successes on quantification from blood cards in Kingston laboratories indicate this invention will be successful in widening the dynamic range and thereby increasing the number of analytes that can be analyzed by quantitative dried blood spot analysis. Further, MetaSpike™ invention has been automated in an integrated sample handling. This work was given a provisional patent WO 2022/086819 A1.[48] This system can be easily scaled up and duplicated in any analytical laboratory.

TH-IDMS is necessary to developed QDBS as the small sample size reduces the amount of analyte. Development of QDBS relying on TH-IDMS could enable world-wide testing and sharing of data and it is our current focus of research.

4.5 References

1. Lepore, A.; Taylor, H.; Landgraf, D.; Okumus, B.; Jaramillo-Riveri, S.; McLaren, L.; Bakshi, S.; Paulsson, J.; Karoui, M. E., Quantification of very low-abundant proteins in bacteria using the HaloTag and epi-fluorescence microscopy. *Sci Rep* **2019,** *9* (1), 7902.

2. Gómez-Pérez, M. L.; Plaza-Bolaños, P.; Romero-González, R.; Martínez-Vidal, J. L.; Garrido-Frenich, A., Comprehensive qualitative and quantitative determination of pesticides and veterinary drugs in honey using liquid chromatography–Orbitrap high resolution mass spectrometry. *Journal of Chromatography A* **2012,** *1248*, 130-138.

3. Wang, S.; Chen, H.; Sun, B., Recent progress in food flavor analysis using gas chromatography–ion mobility spectrometry (GC–IMS). *Food Chemistry* **2020,** *315*, 126158.

4. Adkins, J. N.; Varnum, S. M.; Auberry, K. J.; Moore, R. J.; Angell, N. H.; Smith, R. D.; Springer, D. L.; Pounds, J. G., Toward a human blood serum proteome: analysis by multidimensional separation coupled with mass spectrometry. *Molecular & Cellular Proteomics* **2002,** *1* (12), 947-955.

5. Smith, L. M.; Kelleher, N. L., Proteoform: a single term describing protein complexity. *Nature methods* **2013,** *10* (3), 186-187.

6. Ponomarenko, E. A.; Poverennaya, E. V.; Ilgisonis, E. V.; Pyatnitskiy, M. A.; Kopylov, A. T.; Zgoda, V. G.; Lisitsa, A. V.; Archakov, A. I., The Size of the Human Proteome: The Width and Depth. *Int J Anal Chem* **2016,** *2016*, 7436849.

7. Muthusamy, B.; Hanumanthu, G.; Suresh, S.; Rekha, B.; Srinivas, D.; Karthick, L.; Vrushabendra, B.; Sharma, S.; Mishra, G.; Chatterjee, P., Plasma Proteome Database as a resource for proteomics research. *Proteomics* **2005,** *5* (13), 3531-3536.

8. Schwanhäusser, B.; Busse, D.; Li, N.; Dittmar, G.; Schuchhardt, J.; Wolf, J.; Chen, W.; Selbach, M., Global quantification of mammalian gene expression control. *Nature* **2011,** *473* (7347), 337-342.

9. Liang, Y.; Lehrich, B. M.; Zheng, S.; Lu, M., Emerging methods in biomarker identification for extracellular vesicle-based liquid biopsy. *J Extracell Vesicles* **2021,** *10* (7), e12090.

10. Simpson, K. L.; Whetton, A. D.; Dive, C., Quantitative mass spectrometry-based techniques for clinical use: biomarker identification and quantification. *J Chromatogr B Analyt Technol Biomed Life Sci* **2009,** *877* (13), 1240-9.

11. Sheehan, T.; Yost, R. A., What's the most meaningful standard for mass spectrometry: instrument detection limit or signal-to-noise ratio. *Curr Trends Mass Spectrom* **2015,** *13*, 16-22.

12. Vasconcelos Soares Maciel, E.; de Toffoli, A. L.; Sobieski, E.; Domingues Nazario, C. E.; Lancas, F. M., Miniaturized liquid chromatography focusing on analytical columns and mass spectrometry: A review. *Anal Chim Acta* **2020,** *1103*, 11-31.

13. Annesley, T. M., Ion suppression in mass spectrometry. *Clinical chemistry* **2003,** *49* (7), 1041-1044.

14. Reinecke, T.; Naylor, C. N.; Clowers, B. H., Ion multiplexing: Maximizing throughput and signal to noise ratio for ion mobility spectrometry. *TrAC Trends in Analytical Chemistry* **2019,** *116*, 340-345.

15. Sondergaard, J.; Asmund, G.; Larsen, M. M., Trace elements determination in seawater by ICP-MS with on-line pre-concentration on a Chelex-100 column using a 'standard' instrument setup. *MethodsX* **2015,** *2*, 323-30.

16. Hasegawa, K.; Minakata, K.; Suzuki, M.; Suzuki, O., The standard addition method and its validation in forensic toxicology. *Forensic Toxicology* **2021,** *39* (2), 311-333.

17. Dubland, J. A.; Rakic, B.; Vallance, H.; Sinclair, G., Analysis of 2-methylcitric acid, methylmalonic acid, and total homocysteine in dried blood spots by LC-MS/MS for application in the newborn screening laboratory: A dual derivatization approach. *J Mass Spectrom Adv Clin Lab* **2021,** *20*, 1-10.

18. Long, G. L.; Winefordner, J. D., Limit of detection. A closer look at the IUPAC definition. *Analytical chemistry* **1983,** *55* (7), 712A-724A.

19. Allegrini, F.; Olivieri, A. C., IUPAC-consistent approach to the limit of detection in partial least-squares calibration. *Anal Chem* **2014,** *86* (15), 7858-66.

20. Mocak, J.; Bond, A. M.; Mitchell, S.; Scollary, G., A Statistical Overview of Standard (IUPAC and ACS) and New Procedures for Determining the Limits of Detection and Quantification: Application to Voltammetric and Stripping Techniques. *Pure and Applied Chemistry* **1997,** *69*.

21. Armbruster, D. A.; Pry, T., Limit of blank, limit of detection and limit of quantitation. *Clin Biochem Rev* **2008,** *29 Suppl 1* (Suppl 1), S49-S52.

22. Bernal, E., Limit of Detection and Limit of Quantification Determination in Gas Chromatography. In *Advances in Gas Chromatography*, Guo, X., Ed. IntechOpen: Rijeka, 2014.

23. Currie, L. A., Nomenclature in evaluation of analytical methods including detection and quantification capabilities (IUPAC Recommendations 1995). *Pure and Applied Chemistry* **1995,** *67*, 1699 - 1723.

24. Gold, V., *The IUPAC Compendium of Chemical Terminology*. 2019.

25. Yu, L. L.; Fassett, J. D.; Guthrie, W. F., Detection limit of isotope dilution mass spectrometry. *Anal Chem* **2002,** *74* (15), 3887-91.

26. De Hevesy, G., Some applications of isotopic indicators. *Nobel Lecture* **1944,** *12*.

27. definitive method. In *The IUPAC Compendium of Chemical Terminology*, 2014.

28. Rodríguez-González, P.; Garcia Alonso, J., Isotope Dilution Mass Spectrometry. 2018.

29. Agency, U. E. P., Method 6800: Elemental and speciated isotope dilution mass spectrometry. Agency, U. S. E. P., Ed. Washington DC, 2007.

30. Irini Manoli, J. L. S., and Charles P Venditti, *Isolated Methylmalonic Acidemia*. GeneReviews® [Internet]: 2005 [Updated 2022].

31. Bjorke Monsen, A. L.; Ueland, P. M., Homocysteine and methylmalonic acid in diagnosis and risk assessment from infancy to adolescence. *Am J Clin Nutr* **2003,** *78* (1), 7-21.

32. Kolker, S.; Schwab, M.; Horster, F.; Sauer, S.; Hinz, A.; Wolf, N. I.; Mayatepek, E.; Hoffmann, G. F.; Smeitink, J. A.; Okun, J. G., Methylmalonic acid, a biochemical hallmark of methylmalonic acidurias but no inhibitor of mitochondrial respiratory chain. *J Biol Chem* **2003,** *278* (48), 47388-93.

33. Elghetany MT, S. K., Banki K., Erythrocytic disorders. In *Henry's Clinical Diagnosis and Management by Laboratory Methods*, 23rd ed.; Richard McPherson, M. P., Ed. Elsevier: St. Lous, MO, 2017.

34. Gradinger, A. B.; Bélair, C.; Worgan, L. C.; Li, C. D.; Lavallée, J.; Roquis, D.; Watkins, D.; Rosenblatt, D. S., Atypical methylmalonic aciduria: frequency of mutations in the methylmalonyl CoA epimerase gene (MCEE). *Human mutation* **2007,** *28* (10), 1045-1045.

35. Vocke, R. D., Atomic Weights of the Elements 1997. *Pure and Applied Chemistry* **1999,** *71* (8), 1593-1607.

36. Audi, G.; Wapstra, A. H., The 1993 atomic mass evaluation. *Nuclear Physics A* **1993,** *565* (1), 1-65.

37. Douglas A. Skoog, F. J. H., Stanley R. Crough, *Instrumental Analysis*. 2007; p 3.

38. Petrović, M.; Hernando, M. D.; Díaz-Cruz, M. S.; Barceló, D., Liquid chromatography–tandem mass spectrometry for the analysis of pharmaceutical residues in environmental samples: a review. *Journal of Chromatography A* **2005,** *1067* (1), 1-14.

39. Verkerk, P. K. a. U. H., Electrospray: From Ions in Solution to Ions in the Gas Phase, What We Know Now. *Mass Spectrometry Reviews* **2009,** *28*, 898-917.

40. Windelberg, A.; Arseth, O.; Kvalheim, G.; Ueland, P. M., Automated assay for the determination of methylmalonic acid, total homocysteine, and related amino acids in human

serum or plasma by means of methylchloroformate derivatization and gas chromatography-mass spectrometry. *Clin Chem* **2005,** *51* (11), 2103-9.

41. Ueland, P. M.; Schneede, J., Automated assay of methylmalonic acid in serum and urine by derivatization with 1-pyrenyldiazomethane, liquid chromatography, and fluorescence detection. *Clinical Chemistry* **1993,** *39* (3), 392-399.

42. Schmedes, A.; Brandslund, I., Analysis of methylmalonic acid in plasma by liquid chromatography-tandem mass spectrometry. *Clin Chem* **2006,** *52* (4), 754-7.

43. Wu, Z.; Gao, W.; Phelps, M. A.; Wu, D.; Miller, D. D.; Dalton, J. T., Favorable effects of weak acids on negative-ion electrospray ionization mass spectrometry. *Anal Chem* **2004,** *76* (3), 839-47.

44. Evard, H.; Kruve, A.; Leito, I., Tutorial on estimating the limit of detection using LC-MS analysis, part I: Theoretical review. *Anal Chim Acta* **2016,** *942*, 23-39.

45. Shrivastava, A.; Gupta, V. B., Methods for the determination of limit of detection and limit of quantitation of the analytical methods. *Chron. Young Sci* **2011,** *2* (1), 21-25.

46. Armbruster, D. A.; Pry, T., Limit of blank, limit of detection and limit of quantitation. *Clin Biochem Rev* **2008,** *29 Suppl 1* (Suppl 1), S49-52.

47. Ohtsu, Y.; Tanaka, S.; Igarashi, H.; Kakehi, M.; Mori, T.; Nakamura, T.; Ohashi, R.; Shimizu, H.; Yasuda, Y.; Okayama, T.; Kakuo, H.; Yokoi, H.; Horiuchi, M.; Katashima, M.; Nakamura, R.; Saito, K.; Saito, Y., Analytical method validation for biomarkers as a drug development tool: points to consider. *Bioanalysis* **2021,** *13* (18), 1379-1389.

48. Kingston, H. M. Quantification of previously undetectable quantities cross-referene to related applcation. 2022.

Chapter 5: A Novel Blood Test for Radon Based on Isotopic Abundances and Concentrations of Long Lived Radioactive and Stable Lead Isotopes

5.1 Introduction

Radon is a colorless, odorless, and flavorless inert gas with a half-life of 3.8 days that occurs naturally from the decay of unstable isotopes of uranium or thorium.[1, 2] As radon is heavier than air, it tends to concentrate in enclosed spaces such as underground mines or basements, and is a major contributor to the ionizing radiation to which the general population is exposed.[3] While thorium is several times the concentration of uranium in the Earth's crust, the distribution is not equivalent in all areas. Maps published by the United States Geological Survey, **Figure 5.1** and **Figure 5.2**, shows the inhomogeneous distribution of uranium and thorium, respectively. Uranium and thorium are both unstable elements with long half-lives based on isotopic abundance. They are localized inside the contiguous United States at various approximate concentrations. In western Pennsylvania, radon originating from uranium decay is deposited significantly in the Marcellus Shale region.[4, 5] Roughly 390 million years ago, what is now western Pennsylvania was part of a large inland sea.[4] As the ocean retreated, uranium naturally found in sea water was left behind and salted the land with ocean water from the northern Atlantic containing two to four times more uranium than thorium.[6, 7] Despite remediation efforts developed through the Indoor Radon Abatement Act of 1988, there are still 21,000 small cell lung cancer deaths linked to radon exposure annually. Of these approximately 2,900 of have never smoked.[3, 8, 9] Worldwide total radon related deaths are estimated to be approximately 84,000 yearly, prominently noted in India and Korea. The US accounts for a quarter of these deaths.[3, 8] Currently, Allegheny County has an average indoor radon concentration of 6.5 pCi/L, significantly above the 4.0 pCi/L level deemed safe by the EPA.[10] Elevated radon levels are

estimated to affect 43% of households in Allegheny County and may expose as many as 520,000 individuals.[10] This is a significant issue in this region and, as such, hospital networks in Allegheny County have been searching for diagnostic tests to determine if radon exposure has occurred. Presently, such a test is not available.

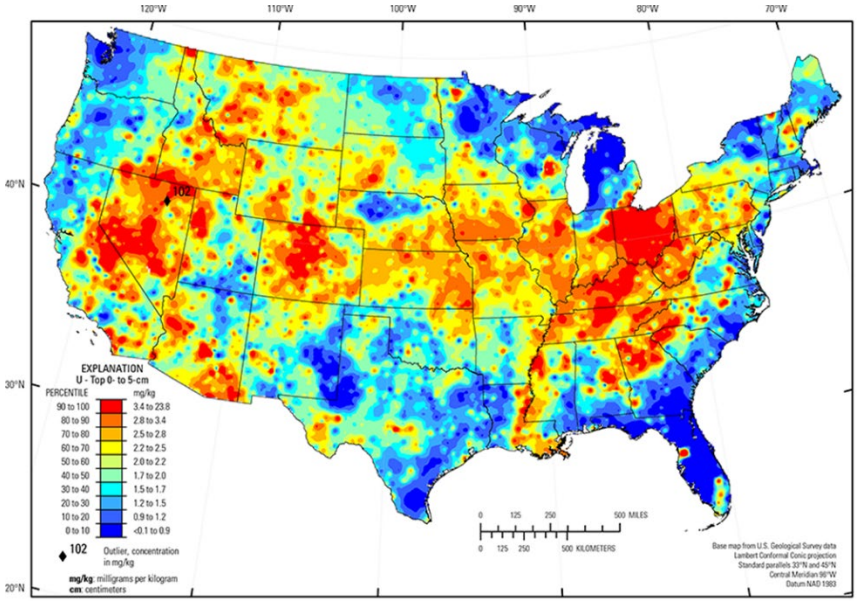

Figure 5.*1.* Map of uranium concentration in the soil of the contiguous United States. Taken from 2014 United States Geological Survey Map.[11]

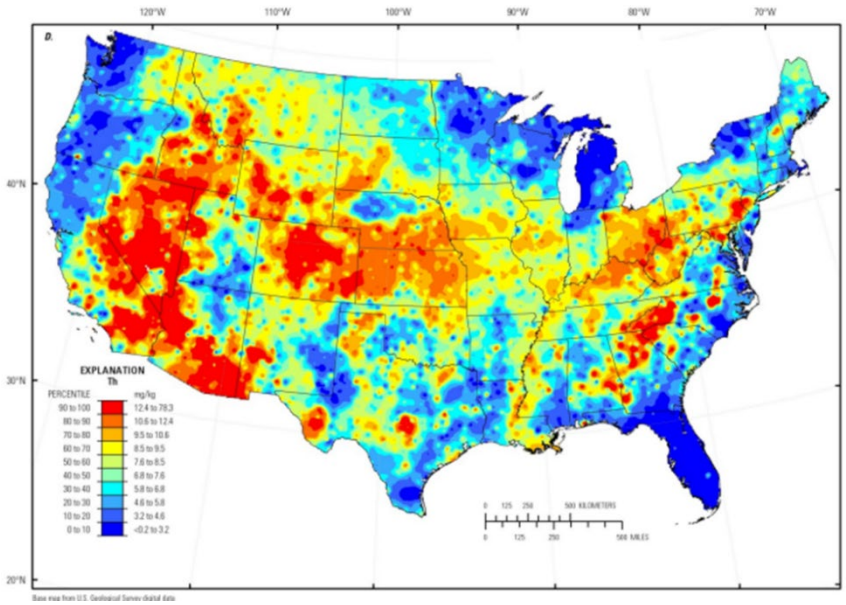

Figure 5.*2*. Map of thorium concentration in the soil of the contiguous United States. Taken from 2014 United States Geological Survey Map.[11]

As inhaled, the air contains some amount of radon and decay products, alpha particles emitted by short-lived decay products of radon, most notably polonium metal ions which can interact with biological tissue in the lungs, leading to DNA damage and potentially cancer.[3] Metal ions tend to attach to moist tissue on contact. Health effects of radon, most notably lung and bronchial cancer, have been investigated for decades with initial investigations focusing on underground miners exposed to high concentrations of radon in their occupational environment.[3] In the early 1980s, radon concentration surveys in homes and other buildings were carried out, and as a result, radon was determined to be a significant cause of lung cancer in the general population.[3] Recent investigations have shown the association between indoor radon and lung cancer even at levels commonly found in buildings.[3] Radon is now recognized as the second most important causal factor of small cell lung cancer after smoking in the general population.[3]

Radon is formed as a decay product primarily from uranium and thorium which will require different analytical assessment targets during testing. The 238, 235, and 234 isotopes of uranium, as

well as the 232 and 230 isotopes of thorium, are the primary naturally occurring radioactive isotopes that have half-lives long enough to pose a prolonged environmental health risk. The decay pathways of 238, 235, and 234 uranium can be seen in **Figure 5.3** and **Figure 5.4**, respectively. Alpha, beta, and gamma radiation is emitted during these radioactive transformation.[12] Among the radon progeny, the alpha emitters polonium 218 and lead 214 contribute to the significance of the radiation dose (over 90%) from exposure to radon.[13] Radon decay products in the air often become attached to dispersed aerosols due to their electrostatics nature.[14] Depending on factors including aerosol concentration of the surrounding environment, electrostatic charge of radon progeny, and humidity of surrounding environment about 80% of the decay products will attach to aerosols which can be inhaled and emit radiation that cause DNA damage in sensitive tissues such as the bronchus and lungs.[15]

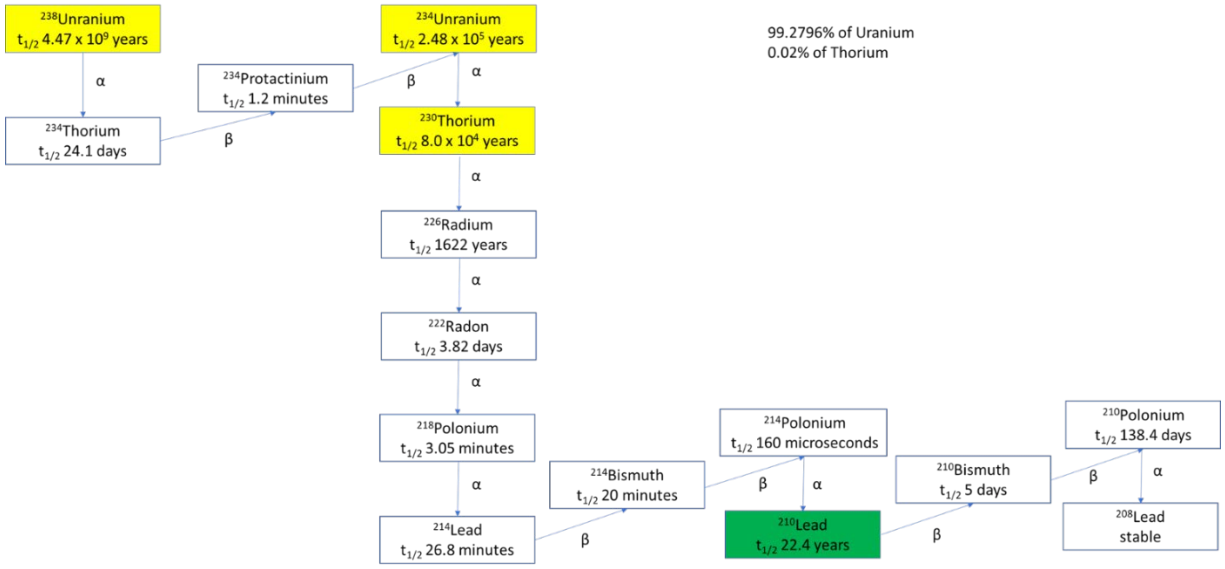

Figure 5.*3*. Decay pathway of ^{238}uranium, ^{234}uranium, and ^{230}thorium. This pathway represents 99.27% of uranium decay and 0.02% of thorium decay. Only the Main decays are shown, no Gamma emitters are represented. Adapted from the US EPA.*[16]*

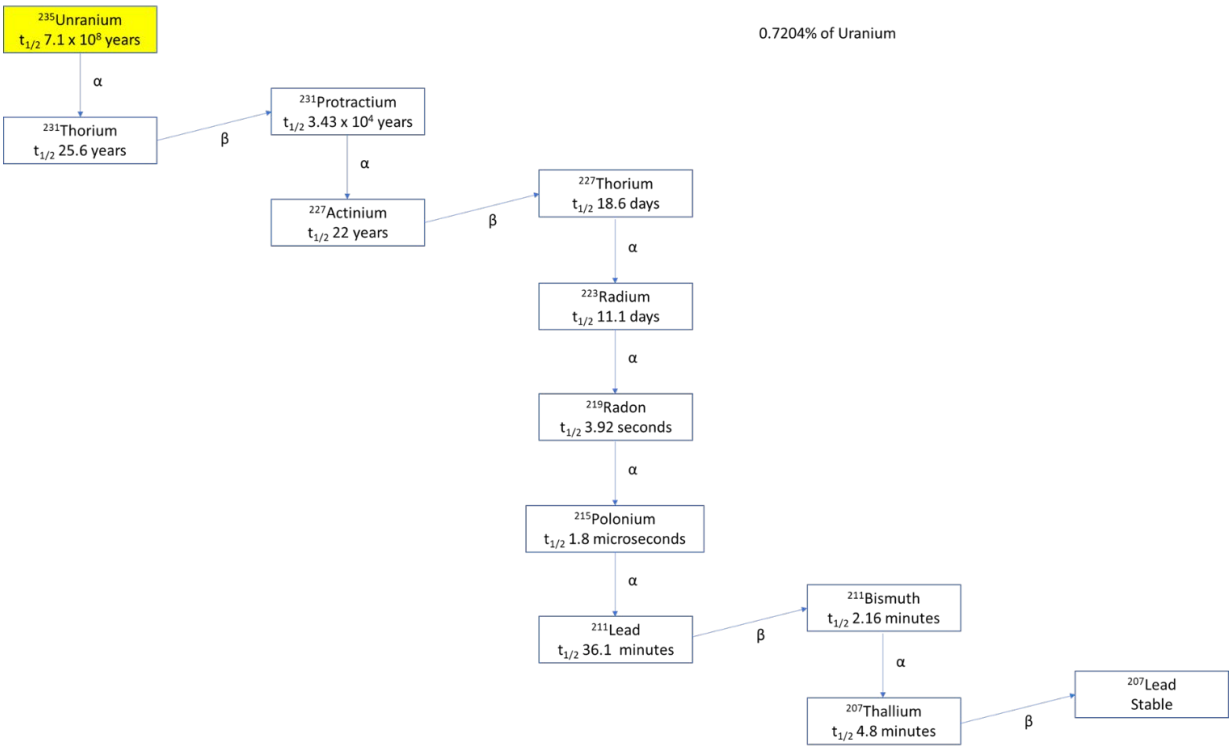

Figure 5.*4*. Decay pathway of ^{235}uranium. This pathway represents 0.72% of uranium decay. Only the main decays are shown, no gamma emitters are represented. Adapted from the US EPA.[*16*]

These pathways prove to be a challenge in the chemical detection of radon in the blood, as many radon progeny, the decay products of radon gas, tend to be short lived. The sole exception is seen in the degradation pathways of uranium-238 and uranium-234, which comprise 99.28% of all uranium species and thorium-230, which comprises only about 0.02%, the lead 210 isotope. Lead-210 is a relatively long-lived radioactive isotope with a half-life of 22.4 years.[16] Lead in the human body is cleared at a variety of rates depending on the specific tissue the molecule has impacted. Averages includes roughly a month in blood, one to one and a half months in soft tissue, and 25-30 years in bone.[17]As lead-210 has a half-life of 22.4 years it makes the isotope a viable target for the testing for radon which comes from uranium decay, as this uranium decay pathway (99.28%) will prove a relatively simple qualitative test for radon exposure.[16] Isobaric interferences of mass 210, as seen in **Table 5.1**, are either in the direct decay pathway of radon or have short enough half-lives so

as to not be present at the time of testing. Polonium-210 is one exception which may be introduced into the body via smoking at a potentially measurable concentration and is downstream in the uranium decay pathway from radon and may constitute a false positive result.[18, 19] Currently, 12.5% of people in the United States are smoker and thus may not be able to take advantage of this potential test.[20] Lead-210 is upstream of ^{210}polonium in the uranium decay pathway and could be tested separately utilizing ion exchange chromatography. Separation of ^{210}lead and the potential confounding elements ^{210}bismuth and ^{210}polonium are routinely performed in ground and sea water utilizing a strontium resin based off of (4,4'(5')-bis-(t-butyl-cyclohexano)-18-crown-6) crown ether.[21]

Table 5.1. Possible interferences for proposed ^{210}lead in radon test from ^{238}uranium pathway

Element	Half-Life
Mercury (Hg) 210	10 minutes
Thallium (Tl) 210*	1.3 minutes
Bismuth (Bi) 210*	5.01 days
Polonium (Po) 210*†	138.28 days
Astatine (At)210*	8.1 hours
Radon (Rn) 210*	2.45 hours
Francium (Fr)210	3.18 minutes
Radium, (Ra) 210*	3.7 seconds
Actinium (Ac) 210	350 milliseconds
Thorium (Th) 210	9 milliseconds

†Polonium-210 is a radioactive material that occurs in nature at very low levels. It is found naturally in the environment, and the general population is internally contaminated with small but measurable amounts of it on a regular basis through food, water, and air. Because tobacco leaves are known to concentrate polonium-210, users of tobacco products are likely to have higher levels of this radioactive element in their bodies.

Testing for radon originating from the degradation of Thorium-232 poses a different challenge. As is seen in **Figure 5.5**, no radon progeny exists with a half-life long enough to be tested until the end of the decay chain at lead-208. Lead-208 as the major isotope of lead in the natural world and thus, its presence is normal in the average patient's blood.

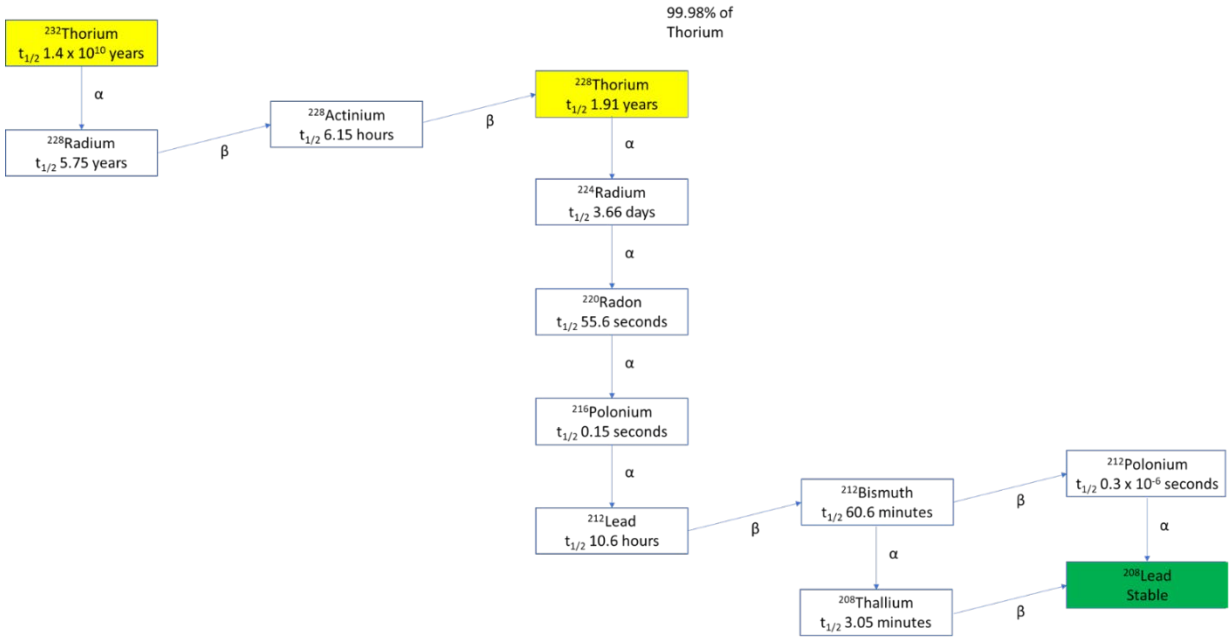

Figure 5.5. Decay pathway of ^{232}thorium. This pathway represents 0.72% of uranium decay. Only the main decays pathways are shown, no gamma emitters are represented. Adapted from US EPA.[16]

The decay pathway of thorium-232 poses a quantitative assessment parameter in differentiating lead inhaled through environmental exposure, such as car exhaust, power plant emissions, or ingestion from food, from the decay of radon-222. Referencing the relative isotopic abundance of lead in nature, which has four naturally occurring isotopes (**Table 5.2.1** and **Table 5.2.2**) may offer a solution to this issue. Three isotopes are unique to lead, while isotopes during measurement of a mass spectrometer for lead-204 are indistinguishable from stable mercury isotope known as an isobar in mass spectrometry. Mercury can be found in small quantities in most patients in the United States and around the world and is introduced to the population through processes such as dietary intake of fish, pollution, and/or dental fillings.[22] The isotopic abundance of mercury-204 is 6.87%, which is significantly greater than the 1.4% of lead isotope at this mass.

Table 5.2.1. Natural isotopic abundances of all stable lead isotopes. Due to the decay of radioactive material, these percentages may change depending on the area in which the lead was acquired.

204	206	207	208
1.4 %	24.1%	22.1%	52.4%

Table 5.2.2. Natural isotopic abundances of all stable lead isotopes, excluding ^{204}lead due to its overlapping mass with ^{204}mercury. Natural abundances were adjusted to reflect the changes after disregarding the 204 Isotope.

206	207	208
24.44%	22.41%	53.14%

As patients are also exposed to mercury environmentally, it would not be suitable to investigate lead-204, however, instead focus on lead-206, lead-207, and lead-208. As radon-222 decays to lead-208, the isotopic makeup of lead isotopes in blood would be altered, resulting in an increased percentage of lead-208 and a decreased percentage of lead-206 and lead-207 (**Figure 5.6**). As lead-207 abundance is affected by the final decay product of uranium-235, which is a small concentration (0.72%) in nature, it could possibly bias results and should not be utilized for concentration determination. Thus, optimal targets for isotopic abundance testing are lead-206 and lead-208 with lead-208 potentially increasing and lead-206 potentially decreasing. Due to the low concentration of environmental radon which can result in negative outcomes, and its comparison to lead concentration in the blood, it is recommended that the isotopic ratio of lead-208 to lead-206 is measured and calculated to extend the difference between the two isotopes and allow statistical differentiation. Due to the increase in abundance of lead-208, it is hypothesized that the isotopic ratio would increase as compared to natural lead standards. It is true that the decay pathway of radon-222, which is the progeny of both the uranium-238 and thorium-230 decay pathway, eventually ends at the stable product of lead-206, which would affect potential ratios. However, once the degradation pathway from radon-222 begins, lead-210 has a 22.4-year half-life and would not substantially further decay until cleared from the blood. Thus, lead which results from the radon-222 decay pathway is not expected to alter the isotopic ratio of lead in the blood in an appreciable way.

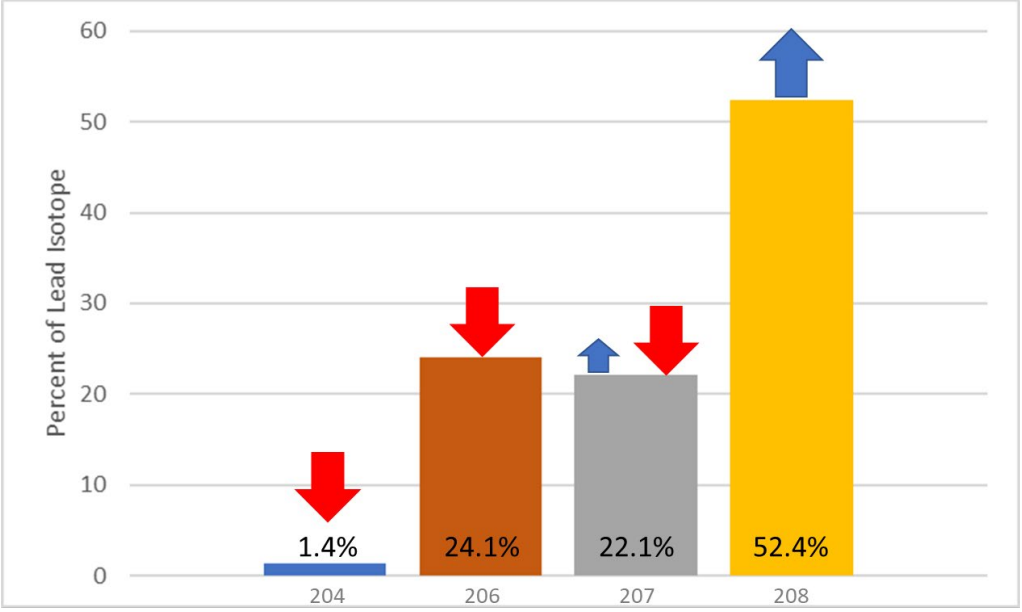

Figure 5.6. Potential shift in lead isotopes 204, 206, 207, and 208 with the introduction of lead from radon decay pathways. Lead which results from radon decay in the thorium-232 pathway will result in lead-208 with consistency and lead which results from radon decay in the uranium-235 pathway will result in lead-207 with consistency.

Thus, if the isotopic abundance of lead in a patient's blood were to be tested against a commercially available naturally occurring lead standard, the indication of radon exposure can be deduced. **Table 5.3** displays the interferences for these masses; however, it should be noted that none of these isotopes listed in this table are naturally occurring and therefore should not be observed in the average patient. While more involved than the test for radon stemming from uranium by testing for lead-210. Testing for lead-206, lead-207, and lead-208 could be performed simultaneously by a mass spectrometrist trained in isotopic assessment using an inductively coupled plasma mass spectrometer (ICP-MS). However, when elements undergo chemical or a physical process, their isotopes will be being treated disproportionally. This results in what is known as isotope fractionation.[23-25]

Table 5.3. Assessment of possible elemental and isotopic interferences when isolating isotopes 206, 207, and 208 of lead. None of these isotopes are naturally occurring, and do not reflect a significant risk for false positive results.

Element	Half-Life	Element	Half-Life	Element	Half-Life
		Actinium (Ac) 207	22 milliseconds	Actinium (AC) 208	95 milliseconds
Radium (Ra) 206	0.24 seconds	Radium (Ra) 207	1.3 seconds	Radium (Ra) 208	1.3 seconds
Francium (Fr) 206	15.9 seconds	Francium (Fr) 207	14.8 seconds	Francium (Fr) 208	59.1 seconds
Radon (Rn) 206	5.67 minutes	Radon (Rn) 207	9.25 minutes	Radon (Rn) 208	24.35 minutes
Astatine (At) 206	30.0 minutes	Astatine (At) 207	1.8 hours	Astatine (At) 208	1.63 hours
Polonium (Po) 206	8.8 days	Polonium (Po) 207	5.8 hours	Polonium (Po) 208	2.898 years
Bismuth (Bi) 206	6.243 days	Bismuth (Bi) 207	31.55 years	Bismuth (Bi) 208	3.68×10^5 years

ICP-MS analysis is ideal for testing elemental isotopes, as organic molecules and complexes are destroyed in the heat of the plasma torch and the associated quadrupoles allow for detection of individual atomic masses.[26] Clinical trials studying isotopic analysis of lead in blood and serum of patients[27] have shown that ICP-MS is sufficiently sensitive to test for lead below the concentration of radon determined to be deleterious to health by the International Commission on Radiological Protection (ICRP) as 0.5 ng/mL.[28] The limit of detection of lead using an ICP-MS has to be determined individually in each lab however from literature the current mass spectrometry studies reported a quantification limit of 0.057 ng/mL,[29] which is an order of magnitude greater sensitivity than required.[29] In addition, the ultra-trace analysis of isotope of lead-210 has already been performed by ICP-MS.[30] Isotopic signatures of lead determined via ICP-MS analysis are precise within approximately 0.5% relative standard deviation from the norm.[31] Finally, utilizing the quadrupole in an ICP-MS, testing for each desired isotopes in the sample could be performed rapidly

in succession and simultaneously in the same analysis session, saving time and allowing for patient tests in a relatively short time. Thus, the ICP-MS is an analytical tool well-suited to determine the concentration of lead isotopes in blood and possibly in urine.

5.2 Materials and Methods

5.2.1 Chemicals

Lead samples were made utilizing lead acetate purchased from Fisher Scientific (Lot 035329) in fisherbrand metal free disposable centrifuge tubes (Lot 26920041), lead standards were made from lead oxide purchased from SPEX (Lot 5-9s 06751) and Applied Isotope Technologies ^{206}Lead-isotopically enhanced lead (Batch 118641 Lot PB010102006A) in 250 mL Thermo Scientific Nalgene flasks (Lot 1140582) flasks. All dilutions and rinses were made by utilizing 18.2 MΩ deionized water was which was made in lab using a 7146 Barnstead NANOpure system (Model 251115-102), which was then passed through a D7035 Easypure II water filtration system (Model 1305080906425). Solutions were allowed to mix on a Vortex Genie 2 Digital Serial (Model A3-1896) for 30 seconds at 5000 RPM. Blood sample digestion was adapted from Yahaya et al by adding lead standards to 0.5 mL whole bovine blood into a polytetrafluoroethylene (PTFE) Teflon flask and inserted into the MAXI-44 (Model MA 179) Milestone rotor. PTFE vessels were cleaned by addition of ten mL of cleaning solution comprised of 65% nitric acid, 7% hydrochloric acid, and 28% 18.2 MΩ deionized water and run through an EPA developed microwave digestion method which began with a 30-minute ramp at 1800 W of power to 180 °C which was maintained at 180 °C for an additional 30-minutes 1800 W, and then allowed to cool to ambient temperature for an hour to remove any organic residue and were rinsed thoroughly with 18.2 MΩ deionized water. Three milliliters of freshly prepared mixture of concentrated nitric acid purchased from Fisher

Scientific (Lot 183460) and hydrogen peroxide purchased from J.T. Baker (Lot 5155-01) in a 2:1 V/V ratio. Extraction techniques and initial quantification were first performed and optimized using synthetic negative blood purchased from Immunalysis (Lot E38284) which had been stored in a -20 °C freezer and, once extraction had been optimized, bovine whole blood with Ethylenediaminetetraacetic acid purchased from Lampire on 11/29/2016 which had been stored in a -80 °C freezer until needed and was then thawed overnight on ice in a 20 °C cold room. Human blood samples were purchased from the Stanford Blood Bank on 08/19/2018 and were stored in a 20 °C cold room in their original containers and packaging. No SPEX lead standard were added to these samples, as human blood has trace levels of lead already in solution this will represent a natural level of isotopic enhancement based on theoretical levels of lead resultant from radon-222 degradation. Ten individual patient samples were utilized (**Table 5.4**) which was believed would show variability between patient blood isotope levels prior to calculation of a ratio and would potentially show regional variability of lead isotopes.

Table 5.4. Patient ID of patient samples for blood purchased from the Stanford Blood Bank for determination of human blood viability of radon-222 degradation testing.

Vial	Patient ID
1	W07051800217000*
2	W070518101769000
3	W070518101775004
4	W070518101776002
5	W070518101777000
6	W070518101781008
7	W070518202169005
8	W07051820217000J
9	W07051820217300D
10	W07051820217400B

5.2.2 Instrumentation

Samples were introduced into an Agilent 7700 ICP-MS (Model G3281A) utilizing a Cetac Autosampler (Model AST-520). The Agilent ICP-MS was cooled by an Agilent Heat Exchanger (G18798) and argon gas was provided by Airgas (Lot UN1951). Quantification was performed using Agilent Technologies MassHunter 4.6 software (Version C.01.06) that was loaded on a computer which Windows 10 pro (Version 1903) operating system had been installed. Optimization parameters for lead response on an Agilent 7700 ICP-MS were taken from Agilent technical note which can be seen in **Table 5.5**.[32] Mass difference was performed on an Agilent 6530 quadrupole time of flight mass spectrometer (Model G6530B) which was run in positive mode. Samples were introduced through electrospray ionization (Model G1958-652 68) on an Agilent direct injection on an Agilent 1100 liquid chromatography system utilizing an Agilent G1312A binary pump which introduced a solution of 18.2 MΩ deionized water solution which had 0.1% optima grade formic acid from Fisher Chemical (Lot 173815) had been applied to aid in the ionization process as the mobile phase. Samples were injected utilizing an Agilent G1367A auto injector which was programed to introduce 10 µL of solution for each sample. Chromatograms were extrapolated using Agilent Technologies MassHunter software (Version B.06.00 SP1) that was loaded on a computer which Windows 10 Pro (Version 1909, OS build 18363.1139) operating system had been installed. Closed Vessel microwave digestion was performed in a Milestone EthosUp microwave (Model MA 182).

Table 5.5. Optimization parameters for stable lead isotopes, 204, 206, 207, and 208 on an Agilent 7700 ICP-MS system

Parameter	
RF Power (W)	1250
RF Matching (V)	1.70
Sample Depth (mm)	7.0
Nebulizer Gas Flow (L/min)	0.40
Nebulizer Pump (rps)	0.10
Skimmer Cone Temperature (°C)	2
Makeup Gas Flow (L/min)	0.90
Lenses	
Extract 1 (V)	-75.0
Extract 2 (V)	-155.0
Omega Bias (V)	-100.0
Omega Lens (V)	4.2
Cell Entrance (V)	-30
Cell Exit (V)	-55
Deflect (V)	-0.4
Plate Bias (V)	-60
Cell	
He Gas Flow (mL/min)	6.0
Octupole Bias (V)	-18.0
Octupole Rf (V)	200
Energy Discrimination (V)	4.0

5.2.3 Sample Preparation

Three milliliters of a freshly prepared mixture of concentrated nitric acid and hydrogen peroxide (2:1V/V) were added the 500 µL blood sample and allowed to stand for 10 minutes to react. These samples were mineral acid decomposed following EPA method 3052. They were heated in a three-stage microwave mineral acid digestion procedure which began with a ten-minute ramp up to 140 °C at 1800 W Power, then a 5-minute ramp up to 180 °C at 1800 W power. That

temperature was then held steady for ten minutes before allowing the samples to cool. The total run time of the method was 40 minutes. Samples were then placed into 15-mL fisherbrand metal free disposable polypropylene centrifuge tubes (Lot 30720140) and centrifuged in an Eppendorf 5810 R 15-amp version centrifuge for 30 minutes at 3000 rpm with a constant temperature of 22 °C. Two-mL of these samples were then removed from their 15-mL tubes via a 10-mL Norm-Ject luer lock solo syringe (Lot 20F01C8) and passed through a 0.22 µm pore size polypropylene Agilent technologies filter (Lot FG4627) before being placed in 50-mL fisherbrand metal free disposable polypropylene centrifuge tubes and diluted to 20-mL with 18.2 MΩ deionized water. Samples were run in replicates of 5 on an ICP-MS with blanks of 18.2 MΩ deionized water in between each replicate to allow for the subtraction of signal from blanks. Additionally, samples with no lead added and samples of only lead and no blood were processed and analyzed in the same manor. Prior to each use of the ICP, tuning was performed utilizing an Agilent Technologies tuning solution for ICP-MS comprised of 1 µg/L concentrations of cerium, cobalt, lithium, magnesium, thallium, and yttrium in 2% nitric acid (Lot 39-22GSX2) to ensure proper instrument response.

Bovine blood standards were prepared in triplicate in five levels by adding either 0 µL, 50 µL, 100 µL, 500 µL, or 1000 µL of 2.89 µg/g solution of SPEX purchased lead standard with the balance being supplemented with nitric acid to ensure a consistent volume for microwave digestion. Another set of standards was made in the same manner with the addition of 14.66 µL of 0.7545 µg/g lead-206 enhanced isotopic standard. These samples were digested and run on the ICP in replicated of five for each sample prepared. Patient samples were prepared with no addition of lead standard for any level, with a second sample set being prepared with the addition of 14.66 µL of 0.7545 µg/g lead-206 enhanced isotopic standard. Due to the limited supply of patient blood, these samples were not prepared in triplicate, but were still run in a replicate of five.

5.3 Discussion

5.3.1. Determination of Isotopic Lead Ratio and Associated Correction Factor

While the Indoor Radon Abatement Act of 1988, cut deaths caused by radon approximately in half, however 21,000 citizens of the United States still die annually of lung and bronchial cancers which are linked to radon, with greater than 10% never having used tobacco products.[3, 8] Allegheny County is especially vulnerable due to its soil make up, with regional hospital systems searching for a rapid and accurate diagnostic test. The first step was to create a lead standard at roughly physiological concentration. It was determined that the samples should be made as close as possible to the average lead concentration to attempt to isolate isotopic fluctuations at exposure concentration of radon gas. As Allegheny County as a higher than average concentration of lead,[33] it was determined to test at the CDC limit of lead in blood, of 5.0 μg/dL.[17] Samples were made from lead acetate and, when tested on an Agilent 7700 ICP-MS, it was determined that the isotopic ratios were not consistent with National Institute of Standards and Technology (NIST) defined lead isotopes (**Table 5.6**). This could be caused by the sourcing of the lead, as radioactive isotopes degrade to lead.[34] This is a documented difficulty in determining lead isotopic abundances and has been used in forensic determination for the origin of lead.[35, 36]

Table 5.6. Isotopic abundances of lead 204, 206, 207, and 208 from Fisher Scientific lot number 035329 as determined by an Agilent 7700 inductively coupled plasma mass spectrometer. It is statistically different from the accepted isotopic abundances from the National Institute of Standards and Technology and will require a mass bias correction.

Pb Isotopes	204	206	207	208
Average %	1.1%	24.7%	20.9%	53.2%
St Dev	0.5%	0.6%	0.4%	0.4%
95% CI	0.180%	0.200%	0.122%	0.144%
Natural %	1.4%	24.1%	22.1%	52.4%
Difference	0.3%	0.6%	1.2%	0.8%

This can be better viewed graphically, as there is no overlap of the 95% confidence intervals (**Figure 5.7**).

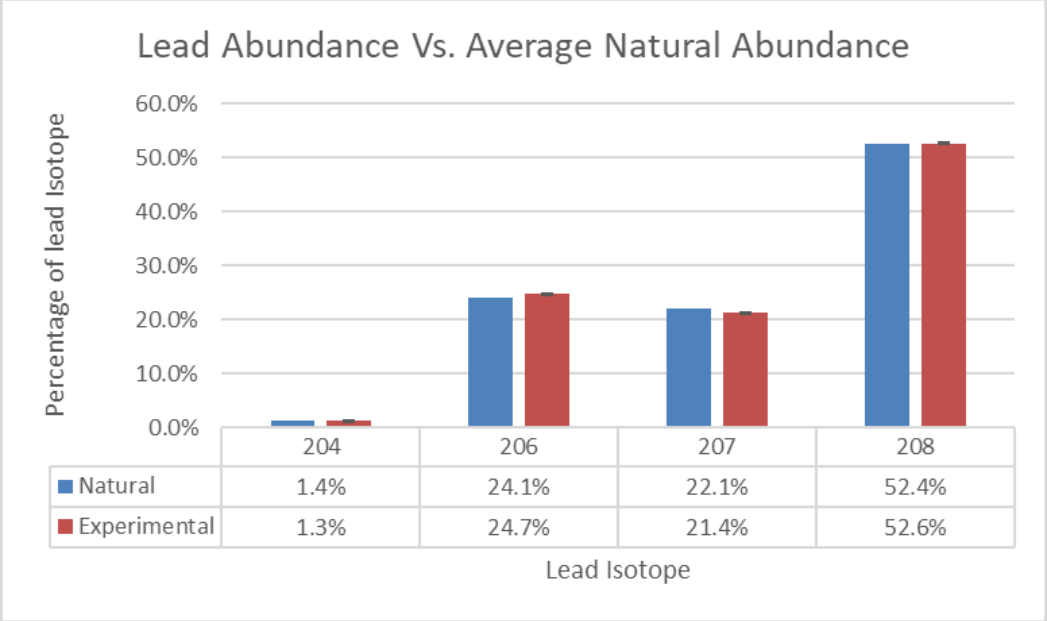

Figure 5.7. Isotopic abundances of lead 204, 206, 207, and 208 from Fisher Scientific lot number 035329 as determined by an Agilent 7700 inductively coupled plasma mass spectrometer plotted graphically with no 95% confidence interval overlap of National Institute of Standards and Technology values.

Once the lead isotope 204, which is an isobar of mercury, had been removed, this did not solve the discrepancy (**Table 5.7**).

Table 5.7. Isotopic abundances of lead 206, 207, and 208, with removal of isobar mass 204, from Fisher Scientific lot number 035329 as determined by an Agilent 7700 inductively coupled plasma mass spectrometer. It is statistically different from the accepted isotopic abundances from the National Institute of Standards and Technology and will require a mass bias correction.

Pb Isotopes	**206**	**207**	**208**
Average %	25.02%	21.19%	53.79%
Standard Deviation	0.58%	0.33%	0.42%
95% Confidence Interval	0.19%	0.11%	0.14%
Natural %	24.44%	22.41%	53.14%
Difference	0.58%	1.22%	0.65%

This can be better viewed graphically, as there is no overlap of the 95% confidence intervals (**Figure 5.8**).

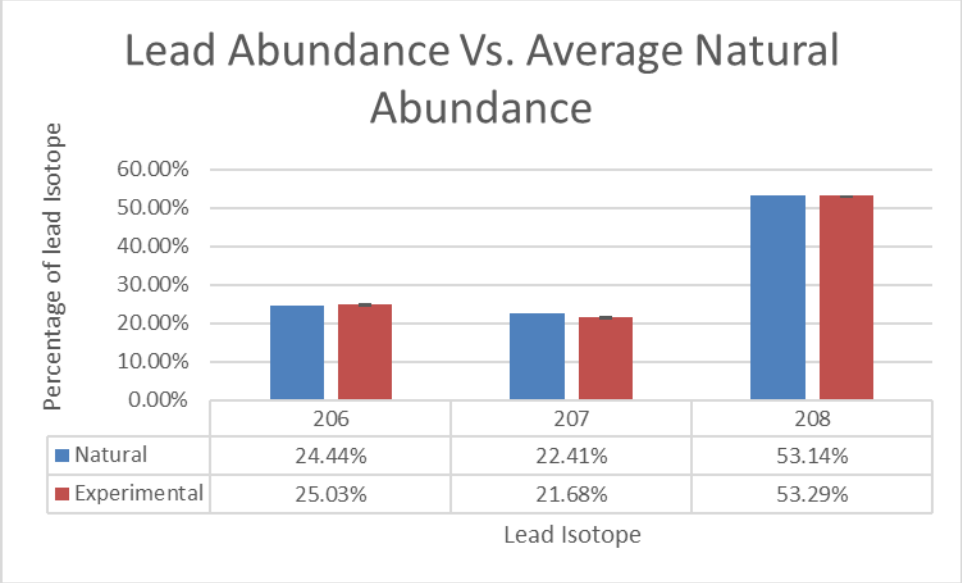

Figure 5.8. Isotopic abundances of lead 206, 207, and 208, with removal of isobar mass 204, from Fisher Scientific lot number 035329 as determined by an Agilent 7700 inductively coupled plasma mass spectrometer plotted graphically with no 95% confidence interval overlap of National Institute of Standards and Technology values.

A correction factor for lead isotope detection must be applied to the lead standard.[37-39] This is performed by a series of equations, which begins with a determination of mass difference of the

lead isotopes on a time of flight mass spectrometer which is compared to NIST values (**Table 5.8**).[38] The NIST values must be compared to calculated values for lead based on the sum of its subatomic particles.[38] Lead having 82 protons with a mass of 1.67262 x 10^{-27} kg, or 1.00728 amu, 82 electrons weighing 9.10938 x 10^{-31} kg, or 0.00054858 amu, and a range of 122 to 126 neutrons with a mass of 1.67492 x 10^{-27} kg, or 1.00866 amu. A small correction factor was applied to the accepted mass difference formula in that the molecule was positively charged and, therefore, had one fewer electron. Thus, the predicted mass was calculated from 81 electrons rather than 82.

Table 5.8. Measured values for exact masses of stable lead isotopes 204, 206, 207, and 208 on an Agilent 6530 quadrupole time of flight mass spectrometer as compared to the calculated value based on the mass of subatomic particles as compared to National Institute of Standards and Technology (NIST) determined values.

Lead Isotope	Calculated Mass (amu)	NIST Mass (amu)	Difference (amu)	Measured Mass (amu)	Difference (amu)
204	205.697915	203.973044	1.724871	203.90784	1.790079
206	207.715235	205.974466	1.740769	205.98494	1.730293
207	208.723895	206.975898	1.747997	206.78240	1.941499
208	209.732555	207.976653	1.755902	207.98139	1.751167

The ratios of these differences are then calculated so that they can be compared to one another both intra and inter sample (**Table 5.9**) for adjustment and future calculation.

Table 5.9. Calculated lead isotopic ratios for stable lead isotopes 204, 206, 207, and 208 on an Agilent 6530 quadrupole time of flight mass spectrometer as compared to the calculated value based on the mass of subatomic particles as compared to National Institute of Standards and Technology (NIST) determined values.

Lead Isotope	NIST Lead Isotopic Ratio	Lead Isotopic Ratio
208/204	1.01799	1.01954
207/204	1.01472	1.01103
206/204	1.00922	1.01841
208/206	**1.00869**	**1.00111**
207/206	1.00415	1.00842

5.3.2. Determination of Lead Isotopic Ratio in Negative Synthetic Blood After Microwave Digestion

Measurements of lead isotopic samples were then normalized against isotopic ratios of 208/206 of a NIST traceable lead standard and corrected based on variances of this standard from published isotopic abundance values. It was also determined that research should focus on the ratios of isotopic mass 208/206 as this represented the largest isotopic shift with the addition of the lead-206 isotope without the confounding factors of isobars or a potential interference of competing isotopic shifts due to nuclear decay pathways. Lead standard samples with a concentration of 31.62 ng/mL as well as those to which a 0.318 ng/mL lead-206 have been added were prepared in a synthetic blood solution, which were prepared in triplicate. These samples then underwent microwave digestion, following EPA method 3052 authored by Professor Kingston, and were measured on an Agilent 7700 ICP-MS with five replicates of each sample. Once these samples were averaged and corrected, they showed promising results of statistically differentiated values (**Table 5.10**).

Table 5.10. The corrected ratio of lead 208/206 with 95% confidence intervals of National Institute of Standards and Technology traceable SPEX lead standard which was made to 31.62 ng/mL as compared to the same standard with the addition of a 0.318 ng/mL lead-206 Oak Ridge National Laboratory traceable standard from Applied Isotope Technologies.

208/206	Corrected Ratio
NIST Lead Standard	0.965706 ± 0.00065
206 Enhanced Lead	0.961506 ± 0.00522

When plotted graphically, these ratios prove to be statistically independent showing a depression in the ratio of lead 208/206 after the introduction of a 99.77% pure isotopic lead-206 spike **(Figure 5.9)**. It is theorized that testing results for lead which originates in the degradation of radon-222 would show an increase of this ratio due to the final degradation product being lead-208. However, a statistical difference can be observed at physiological concentrations of lead and the potential change in the ratio due to radon-222 degradation contribution.

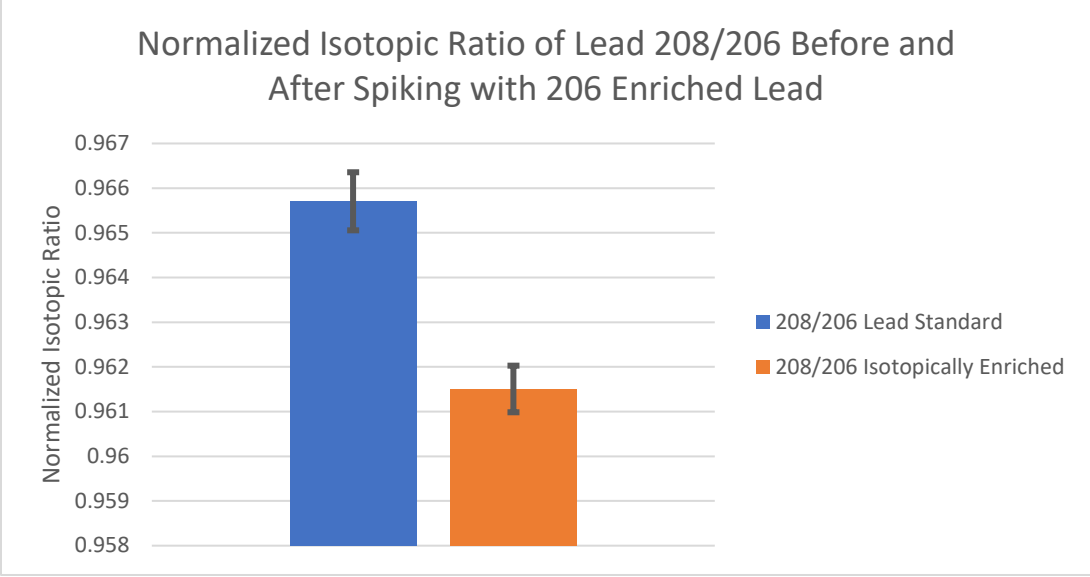

Figure 5.9. The corrected ratio of lead 208/206 with 95% confidence intervals of National Institute of Standards and Technology traceable SPEX lead standard which was made to 31.62 ng/mL as

compared to the same standard with the addition of a 0.318 ng/mL lead-206 Oak Ridge National Laboratory traceable standard from Applied Isotope Technology.

5.3.3. Determination of Lead Isotopic Ratio in Bovine Blood Samples

After microwave digestion methods had been optimized, bovine blood purchased from Lampire were utilized to create samples of varying concentration of lead standard. These standards were made to determine if the isotopic ratio would be influenced by changes concentration of lead in the blood and to potentially discover and upper limit of blood lead concentration to which this test may become inconclusive. These were compared to samples to which no lead had been added and those who had a known concentration of isotopic spike of lead-206 had been added to test the extraction under natural conditions. Due to the fact that bovine blood may contain lead naturally from diet or air quality, blood with no additional SPEX lead standard was also tested to determine a how isotopic shift may occur at natural ambient levels of lead. Five levels of lead solution were prepared, digested, and analyzed (**Tables 5.11.1** and **5.11.2**). These normalized lead ratio levels were then compared to determine the statistical independence of these samples.

Table 5.11.1. Concentrations of prepared standards prepared in bovine blood and digested in an Ethos-up microwave system applying EPA method 3052 and responses to the 208 and 206 stable isotopes of lead measured on an Agilent 7700 inductively coupled plasma mass spectrometer to which no isotopically enriched 206-lead standards had been applied.

Non-206 Lead Enriched Bovine Blood						
Concentration of Lead Added (ng/mL)	**Average Lead 208 Counts**	**Average Lead 206 Counts**	**Lead 208:206 Ratio**	**Normalized Lead 208:206 Ratio**	**Coefficient of Variances**	**95% Confidence Interval**
0.00	1446.17	681.56	2.1218	1.0066	0.0017	0.0006
4.13	24867.40	11792.89	2.1087	1.0093	0.0013	0.0004
8.03	133988.16	63719.55	2.1028	1.0088	0.0005	0.0002
36.12	770913.33	262119.12	2.9411	1.0089	0.0012	0.0004
64.22	1669270.33	782627.46	2.1329	1.0096	0.0149	0.0049

Table 5.11.2. Concentrations of prepared standards prepared in bovine blood and digested in an Ethos-up microwave system applying EPA method 3052 and responses to the 208 and 206 stable isotopes of lead measured on an Agilent 7700 inductively coupled plasma mass spectrometer to which approximately 0.5 ng/mL of isotopically enriched 206-lead standards had been applied.

206 Lead Enriched Bovine Blood						
Concentration of Lead Added (ng/mL)	**Average Lead 208 Counts**	**Average Lead 206 Counts**	**Lead 208:206 Ratio**	**Normalized Lead 208:206 Ratio**	**Coefficient of Variances**	**95% Confidence Interval**
0.00	909.83	448.88	2.0269	0.6097	0.0348	0.0115
4.13	12734.19	19104.06	0.6666	0.8707	0.0070	0.0023
8.03	125926.20	64450.82	1.9538	0.9984	0.0002	0.0001
36.12	757730.58	270377.42	2.8025	0.9240	0.0032	0.0011
64.22	1870755.77	885013.54	2.1138	1.0091	0.0002	0.0001

All samples to which isotopically enriched 206-lead that were not applied were statistically indistinguishable, except for the solution to which no SPEX lead solution had been added. This may suggest a different environmental source of lead than the lead standard solution. This warrants further investigation and may point to the need for localized banks of lead isotopes in areas which may be tested for radon to compare isotopic blood concentrations. In addition, while adding a consistent concentration of roughly 0.5 ng/mL of 206-lead isotopically enhanced solution, it shows the potential upper bounds of the viability of this test, as the highest level of spiking is statistically indistinguishable (**Table 5.12**).

Table 5.12. Concentrations of prepared standards prepared in bovine blood and digested in an Ethos-up microwave system determined isotopic ratios of 208:206 lead isotopes measured on an Agilent 7700 inductively coupled plasma mass spectrometer to which approximately 0.5 ng/mL of isotopically enriched 206-lead standards had been applied.

Lead 208/206	Corrected Ratio of Lead Isotope				
	0.00 ng/mL	4.13 ng/mL	8.03 ng/mL	36.12ng/mL	64.22 ng/mL
Lead Standard	1.0066 ± 0.0006	1.0093 ± 0.0004	1.0088 ± 0.0002	1.0089 ± 0.0004	1.0096 ± 0.0049
206 Enriched Lead	0.6097 ± 0.0115	0.8707 ± 0.0023	0.9984 ± 0.0001	0.9240 ± 0.0011	1.0091 ± 0.0001

When compared graphically, the measured 208:206 ratio of 0.5 ng/mL 206-lead isotopically spiked samples were statistically distinct at lower concentrations, 0 to roughly 36.12 ng/mL, but not distinct at the highest level, roughly 64.22 ng/mL (**Figure 5.10**). The isotopic shift is most dramatic at natural concentrations, which relates to the overall concentration of lead in the bovine blood. While the isotopic ratio is distinct from all spiked ratios, even a small amount, roughly 4.13 ng/mL of lead added to the solution was enough to add two orders of magnitude to the overall detection of lead isotopes. This will need to be further explored at low concentrations under a patient focused study.

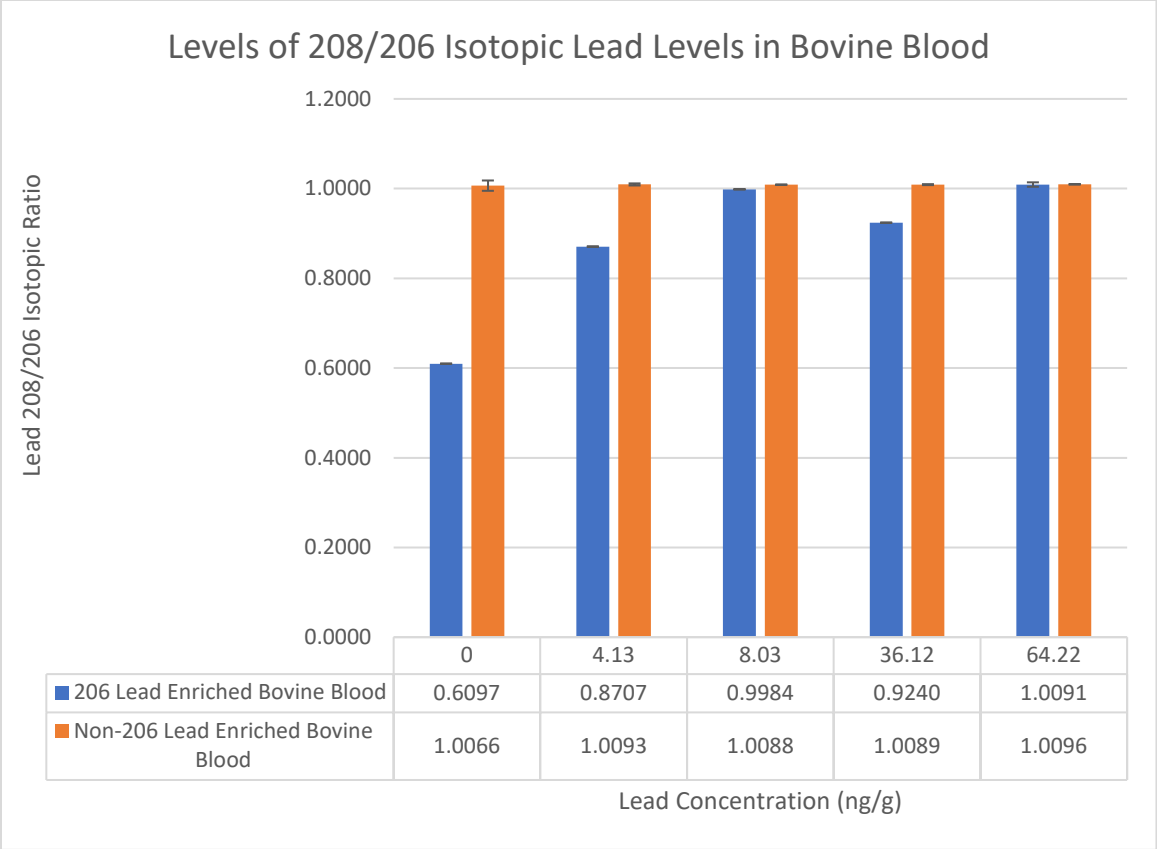

Figure 5.10. Concentrations of standards prepared in bovine blood and digested in an Ethos-up microwave system applying EPA method 3052 determined isotopic ratios of 208:206 lead isotopes measured on an Agilent 7700 inductively coupled plasma mass spectrometer to which approximately 0.5 ng/mL of isotopically enhanced 206-lead standards had been applied which are graphically represented. Uncertainty displayed at the 95% confidence limit.

5.3.4. Determination of Lead Isotopic Abundance in Human Blood

Alpha-numerically identified blood from individuals purchased from the Stanford Blood Bank was utilized to determine if inter-patient samples would be statistically different and to test the statistical methodology. It was determined that, blood from the Stanford Blood Lab from individuals could be utilized to help method development to measure differences in the isotopic ratios between patient samples. Ten samples were subjected to the same digestion and detection as previous samples and were statistically compared (**Table 5.13**). After digestion and detection

of isotopic ratios, it was apparent that there was a low level of ambient lead in patient samples, with many being similar, or even at a lower concentration than was seen in bovine blood samples.

Table 5.13. Lead 208 and 206 stable isotopes present in human blood samples purchased from Stanford Blood Bank which were digested on an Ethos-Up microwave system and measured on an Agilent 7700 inductively coupled plasma mass spectrometer. These are natural samples with no SPEX lead solution or isotopically enriched 206-lead standards having been applied.

Non-206 Lead Enriched Stanford Blood Bank Samples						
Stanford Blood Bank Sample Identification Number	**Average Lead 208 Counts**	**Average Lead 206 Counts**	**Lead 208:206 Ratio**	**Normalized Lead 208:206 Ratio**	**Coefficient of Variances**	**95% Confidence Interval**
W07051800217000*	2594.34	1230.72	2.1080	1.0089	0.0024	0.0008
W070518101769000	1176.71	575.52	2.0446	1.0060	0.0020	0.0007
W070518101775004	750.81	359.29	2.0897	1.0082	0.0063	0.0021
W070518101776002	657.85	313.45	2.0988	1.0086	0.0074	0.0025
W070518101777000	814.26	390.36	2.0859	1.0081	0.0030	0.0010
W070518101781008	1161.57	549.84	2.1126	1.0090	0.0037	0.0012
W070518202169005	1156.02	551.98	2.0943	1.0086	0.0076	0.0025
W07051820217000J	1409.05	690.78	2.0398	1.0057	0.0038	0.0013
W07051820217300D	649.16	313.29	2.0721	1.0074	0.0052	0.0017
W07051820217400B	3570.84	1694.05	2.1079	1.0089	0.0023	0.0008

When compared graphically, it was apparent that, while many of the isotopic ratios of 208:206 lead concentrations were statistically indistinguishable, some donated blood samples were isotopically distinct (**Figure 5.11**).

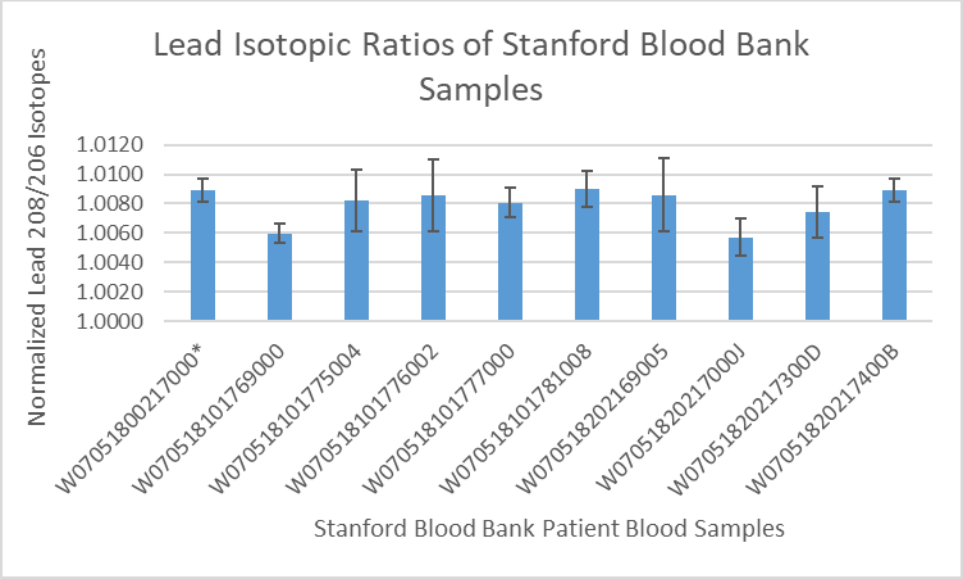

Figure 5.11. Graphical representation of lead 208:206 stable isotope ratios present in human blood samples purchased from Stanford Hospital Blood Bank which were digested on an Ethos-Up microwave system applying EPA method 3052 and measured on an Agilent 7700 inductively coupled plasma mass spectrometer. These are natural human samples with no SPEX lead solution or isotopically enriched 206-lead standards having been applied. Precision is at the 95% confidence limit.

When patient samples were compared, it was apparent some 208:206 lead ratios were statistically distinct. Samples such as W07051800217000* and W070518101769000 do not overlap at a 95% confidence interval and can be said to have 208:206 lead ratios which are statistically independent at the 95% confidence limit, while samples such as W070518101777000 and W070518101781008 are statistically indistinguishable, yet different from W070518101769000. As all samples underwent the same sample preparation, detection, and were subject to the same statistical methods and as such, they can be compared. Due to the variability of lead isotope abundances, it is reasonable to assume that these samples were donated from different individuals experiencing environmentally distinct exposures and these examples had isotopic decay that affected lead isotopic abundances.

Finally, the results of these samples were compared to a second batch of samples to which 0.5 ng/mL of 206-enriched isotopic standard had been added and were processed in the same way.

These samples had a vastly altered lead 208:206 isotopic ratio as compared to the sampled to which 206-isotopically enriched lead standards. Results were inconclusive as a level of 0.5 ng/mL of 206-enhanced isotopic standard seemed to radically shift the overall isotopic ratio (**Table 5.14**). This leads to the conclusion that the 0.5 ng/mL of radon suggested to be deleterious as proposed by the ICRP may be an overestimation or show to radically change the isotopic make up of lead in the human body. In either case, this suggests the need for further investigation.

Table 5.14. Lead 208 and 206 stable isotopes present in human blood samples purchased from Stanford Blood Bank which were digested on an Ethos-Up microwave system applying EPA method 3052 and measured on an Agilent 7700 inductively coupled plasma mass spectrometer. These samples were spiked with 0.5 ng/mL 206-isotopically enriched lead standard from Applied Isotope Technologies which is Oak Ridge National Laboratory traceable.

206 Lead Enhanced Stanford Blood Bank Samples						
Stanford Blood Bank Sample Identification Number	**Average Lead 208 Counts**	**Average Lead 206 Counts**	**Lead 208:206 Ratio**	**Normalized Lead 208:206 Ratio**	**Coefficient of Variances**	**95% Confidence Interval**
W07051800217000*	2802.37	7334.81	0.3821	0.3139	0.0108	0.0198
W070518101769000	1169.43	5600.98	0.2088	0.1702	0.0058	0.0195
W070518101775004	921.21	6046.39	0.1524	0.1224	0.0147	0.0677
W070518101776002	992.94	5326.18	0.1864	0.1507	0.0087	0.0330
W070518101777000	1032.13	5636.29	0.1831	0.1491	0.0137	0.0527
W070518101781008	1516.97	5074.84	0.2989	0.2448	0.0047	0.0110
W070518202169005	2219.81	6150.43	0.3609	0.4127	0.1762	0.2405
W07051820217000J	2151.39	7289.50	0.2951	0.2421	0.0045	0.0107
W07051820217300D	872.26	5107.37	0.1708	0.1378	0.0134	0.0555
W07051820217400B	715.37	5941.21	0.1204	0.0931	0.0104	0.0611

When comparing the Stanford Blood Bank samples to which 0.5 ng/mL of 206-enriched isotopic standard had been added, the lead isotopic ratio of 208:206 were statistically distinct in the same way as those who had not been spiked. Samples such as W07051800217000* and W070518101769000 do not overlap at a 95% confidence interval and can be said to have 208:206 lead ratios which are independent, while samples such as W070518101777000 and

W070518101781008 are statistically the same, yet different from W070518101769000. This is expected as the addition of standard was consistent throughout the samples and reveals the consistency of extraction of the isotopic lead from samples as well as the metrology and statistics which aids in their deconvolution.

The statistical differentiation between the Stanford Blood Bank samples to which 0.5 ng/mL of 206-enriched isotopic standard had been added can be more easily observed in graphical form (**Figure 5.12**).

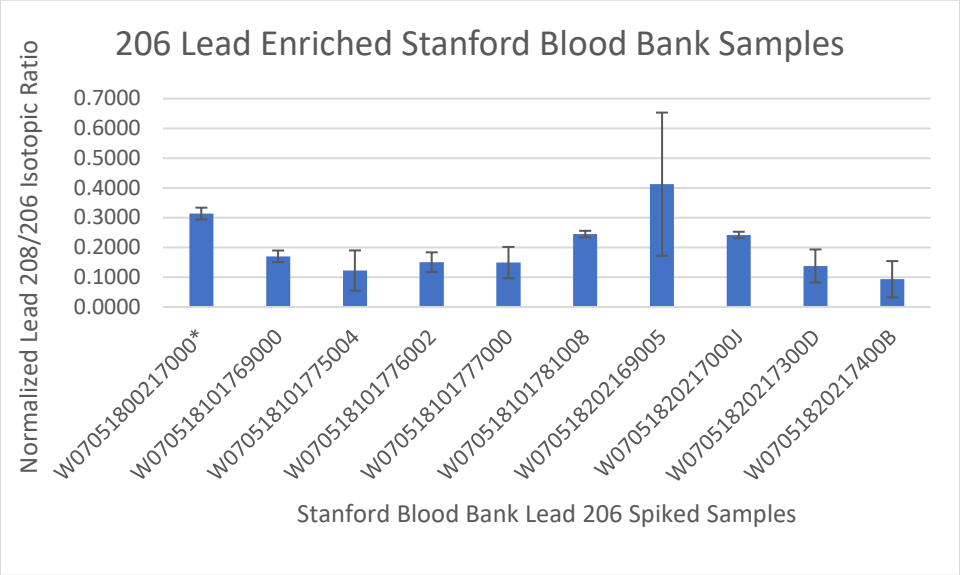

Figure 5.12. Graphical representation of lead 208:206 stable isotope ratios present in human blood samples purchased from Stanford Blood Bank which were spiked with roughly 0.5 ng/mL of Oak Ridge traceable Applied Isotope Technologies isotopically enriched 206-lead standards which were digested on an Ethos-Up microwave system applying EPA method 3052 and measured on an Agilent 7700 inductively coupled plasma mass spectrometer. Uncertainties are expressed at the 95% confidence limit.

Direct comparison of isotopic lead 208:206 ratios between unadulterated and spiked samples may not be the most revealing as the isotopic shift of the samples to which isotopically enriched 206-lead standards had been applied were greatly reduced. In graphical form these differences are striking and can only result in a major isotopic shift from the dominant lead-208

species the more minor lead-206 species with an addition of only 0.5 ng/mL and may be better differentiated in a table (**Table 5.15**). As many of these isotopic ratios in unadulterated patient samples are approaching the counts of the blank prior to isotopic spiking, a more sensitive test may need to be developed, perhaps through optimization of alternative instrumentation such as a linear ion trap or, potentially, an orbitrap system (Thermo). Other optimizations may also be developed if a patient-based initiative were desired for a regional and or national study. Optimizations would be able to concentrate the available lead-208 and lead-206 ions to increase the response and decrease the limit of detection. These systems would also help to decrease potential instrumental noise and more clearly define lead 208:206 isotopic ratios.

Table 5.15. Determined isotopic ratios of lead 208:206 isotopes in 500 µL aliquots of blood samples purchased from the Stanford blood bank and 500 µL aliquots of blood samples to which approximately 0.5 ng/mL of isotopically enriched 206-lead standards had been applied digested on an Ethos-Up microwave system and measured on an Agilent 7700 inductively coupled plasma mass spectrometer.

Patient Sample Number	Stanford Blood Bank Samples	206 Enriched Lead Stanford Blood Bank Samples
W07051800217000*	1.0089 ± 0.0008	0.3139 ± 0.0198
W070518101769000	1.0060 ± 0.0007	0.1702 ± 0.0195
W070518101775004	1.0082 ± 0.0021	0.1224 ± 0.0677
W070518101776002	1.0086 ± 0.0025	0.1507 ± 0.330
W070518101777000	1.0081 ± 0.0010	0.1401 ± 0.0527
W070518101781008	1.0090 ± 0.0012	0.2448 ± 0.0110
W070518202169005	1.0086 ± 0.0025	0.4127 ± 0.2405
W07051820217000J	1.0057 ± 0.0013	0.2421 ± 0.0107
W07051820217300D	1.0074 ± 0.0017	0.1378 ± 0.0555
W07051820217400B	1.0089 ± 0.0008	0.0931 ± 0.0611

When compared to samples from the same patient to which 206-isotoically enriched lead was not added, vast differences can be easily observed in graphical representation of this data

(**Figure 5.13**). This is again perhaps due to underestimation of isotopic shift or concentration which may explain the differences.

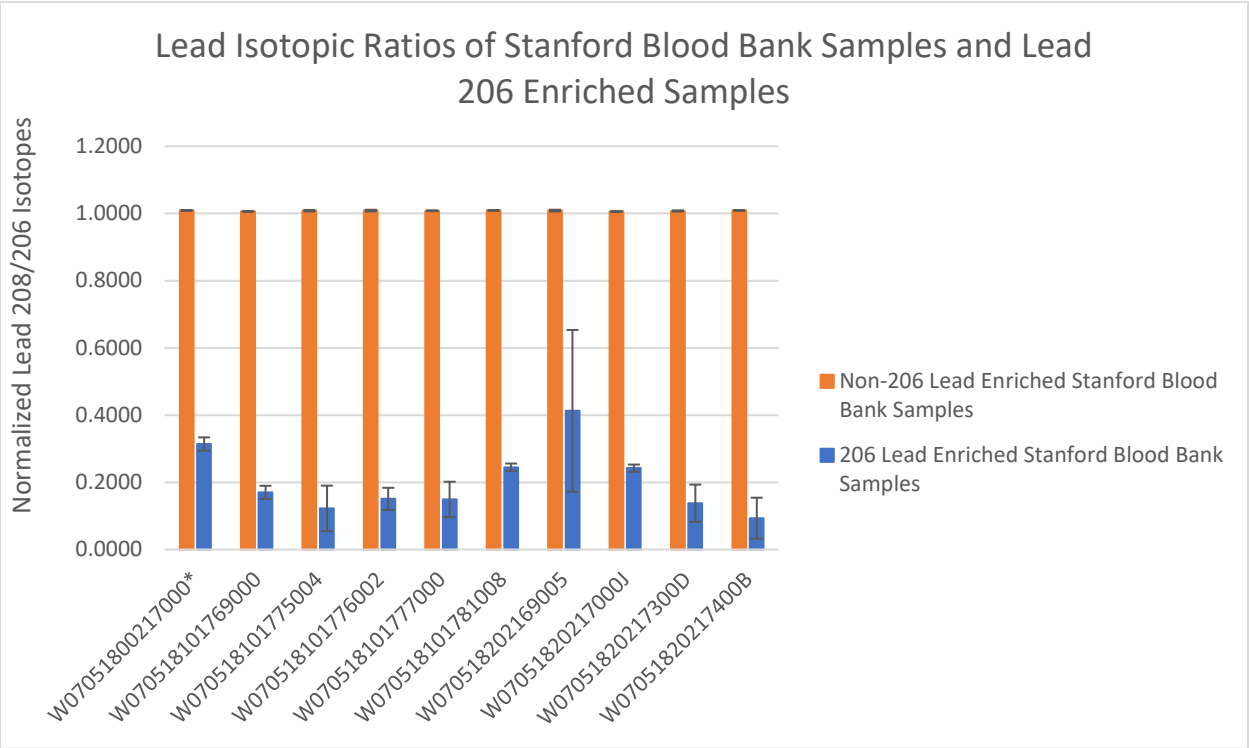

Figure 5.13. Graphical representation of lead 208:206 stable isotope ratios present in human blood samples purchased from Stanford Blood Bank which were digested on an Ethos-Up microwave system and measured on an Agilent 7700 inductively coupled plasma mass spectrometer as compared to samples to which isotopically enriched 206-lead standards had been applied.

The ratios of lead 208:206 isotopic ratios are statistically significantly different and not easily comparable between sample groups. As such, these groups were compared statistically through the application of a Student's t-test. First an f-test was performed which showed the variances of the samples were equal. From that information, the correct t-test was chosen, and it was demonstrated that the addition of 0.5 ng/mL of isotopically enriched 206-lead standard to Stanford Blood Bank Samples produced statistically distinct sample sets.

5.4 Conclusion

An appropriate method of testing for radon exposure originating from both uranium and thorium utilizing blood as a matrix is theoretically possible and has been preliminarily demonstrated. Such a test may employ an appropriate mass spectrometer such as the ICP-MS specifying mass lead-210 to test for radon-222 originating from uranium decay, though this was not demonstrated in this study due to lack of adequate patient samples. A lead-210 presence will provide a range that would establish ambient exposures of the individual patient. However, due to interferences with polonium-210 from a smoking origin, the patient will have to be questioned as to their smoking habits. The viability of this proposed test should be investigated in an IRB study under the guidance of physician, and bioanalytical and mass spectrometry experts. Testing could establish a quantitative test similar to measuring lead-210 response which would indicate a hazardous material in a biospecimen but specify the possible origin. A second test is needed to reveal radon-220 originating from the decay of thorium to be run simultaneously with the test for uranium. For this test, a ratio of mass 208:206 lead should be tested in the sample. Certified standard lead isotope materials from NIST or tracible to NIST are required to establish analytical accuracy of the described measurements. This second test will enable measurement of the isotopic shifts. Any isotopic shift resulting from radon-220 degradation should show an overall increase in the lead 208:206 ratio, compared to a standard sample having natural abundance of lead isotopes. Any isotopic measurement greater than 0.5 % relative standard deviation should be considered abnormal. A database of measurements would enable regional and national exposures and facilitate relationships with other health norms. We believe this test could be developed and applied in regional and national health assessment and could have a significant informational component for environmental human health.

The novel method described in this report demonstrated that these isotopic shifts can be measured and statistically differentiated even at low levels of concentration, optimizations remain. For one, ambient levels in patients are present, yet are at low enough concentrations that they approach the levels found in analytical blanks. This requires an assay of increased sensitivity which may require alternative mass spectrometry optimization and sample preparation techniques that boost signal and decrease noise. Such as the mass spectrometry signal boosting technique such as employing an ion trap or employing the technique invented by Professor Skip Kingston. In addition, the approximated concentration by ICRP of 0.5 ng/mL of radon to cause harmful effects may be an overestimation as this appears to completely overwhelm the lead 208:206 ratio in many natural cases. A more precise concentration should be determined through a study which links radon concentration in homes to lead isotopes in blood. Finally, this study could enable an IRB study in collaboration with University of Pittsburgh Medical Center (UPMC) and the Hillman Cancer Institute and regionally guided test using patient samples who already were diagnosed with small cell lung or bronchial cancer due to radon exposure. These collaborations are in discussion at the present time.

5.5 References

1. Samet, J. M., Radon and lung cancer. *J Natl Cancer Inst* **1989,** *81* (10), 745-57.
2. Al-Zoughool, M.; Krewski, D., Health effects of radon: a review of the literature. *Int J Radiat Biol* **2009,** *85* (1), 57-69.
3. WHO, WHO Handbook on Indoor Radon: A Public Health Perspective. World Health Organization: France, 2009.

4. Rose, A. W., Schmiermund, Ronald L., and Mahar, Dennis L. , Geochemical dispersion of uranium near prospects in Pennsylvania. Administration, U. S. E. R. a. D., Ed. Pennsylvania State University, 1977.

5. Klemic, H., Uranium Occurances in Sedementary Rocks of Pennsylvania. Survey, U. G., Ed. Washington DC, 1962; pp 243-287.

6. EXXON NUCLEAR COMPANY, I., Extraction of Uranium from Seawater: Evaluation of Uranium Resources and Plant Siting Volume 1. Energy, U. D. o., Ed. Oregon State University, 1979; Vol. XN-RT-14, p 168.

7. Smith, K. J.; Leon Vintro, L.; Mitchell, P. I.; Bally de Bois, P.; Boust, D., Uranium-thorium disequilibrium in north-east Atlantic waters. *J Environ Radioact* **2004,** *74* (1-3), 199-210.

8. USEPA Health Risk of Radon https://www.epa.gov/radon/health-risk-radon (accessed May 12, 2022).

9. Yoon, J. Y.; Lee, J. D.; Joo, S. W.; Kang, D. R., Indoor radon exposure and lung cancer: a review of ecological studies. *Ann Occup Environ Med* **2016,** *28*, 15.

10. PADEPA, Pennsylvania Citizen's Guide to Radon. 5/2021 ed.; Protection, P. D. o. E., Ed. Harrisburgh, 2021; p 24.

11. David B. Smith, W. F. C., Laurel G. Woodruff, Federico Solano, and Karl J. Ellefsen, Geochemical and Mineralogical Maps for Soils of the Conterminous United States. Report, U. S. G. S. O. F., Ed. 2014; Vol. 2014–1082, p 384.

12. Degu Belete, G.; Alemu Anteneh, Y., General Overview of Radon Studies in Health Hazard Perspectives. *J Oncol* **2021,** *2021*, 6659795.

13. Gillmore, G. K.; Phillips, P. S.; Denman, A. R., The effects of geology and the impact of seasonal correction factors on indoor radon levels: a case study approach. *Journal of Environmental Radioactivity* **2005,** *84* (3), 469-479.

14. Kulkarni, P.; Baron, P. A.; Willeke, K., *Aerosol measurement: principles, techniques, and applications*. John Wiley & Sons: 2011.

15. Bowie, C.; Bowie, S. H. U., Radon and health. *The Lancet* **1991,** *337* (8738), 409-413.

16. USEPA Radioactive Decay. https://www.epa.gov/radiation/radioactive-decay (accessed 05/12/2022).

17. ATDSR, Toxicological Profile for Lead. Services, U. D. o. H. a. H., Ed. 2020.

18. Muggli, M. E.; Ebbert, J. O.; Robertson, C.; Hurt, R. D., Waking a sleeping giant: the tobacco industry's response to the polonium-210 issue. *Am J Public Health* **2008,** *98* (9), 1643-50.

19. Khater, A. E. M., Polonium-210 budget in cigarettes. *Journal of Environmental Radioactivity* **2004,** *71* (1), 33-41.

20. Homa, M. E. C. C. G. L. T. W. W. A. J. D. M., Morbidity and Mortality Weekly Report. Services, U. S. D. o. H. a. H., Ed. Washington DC, 2020; Vol. 2022, pp 397–405.

21. Philip Horwitz, E.; Chiarizia, R.; Dietz, M. L., A Novel Strontium-Selective Extraction Chromatographic Resin*. *Solvent Extraction and Ion Exchange* **1992,** *10* (2), 313-336.

22. Kathryn Mahaffey, G. E. R., and Rita Schoeny, Mercury Study Report to Congress. Volume VII: Characterization of Human Health and Wildlife Risks from Mercury Exposure in the United States. USEPA, Ed. Washington DC, 1997; p 152.

23. Vogl, J., The triple-isotope calibration approach: a universal and standard-free calibration approach for obtaining absolute isotope ratios of multi-isotopic elements. *Anal Bioanal Chem* **2021,** *413* (3), 821-826.

24. Deines, P., Mass spectrometer correction factors for the determination of small isotopic composition variations of carbon and oxygen. *International Journal of Mass Spectrometry and Ion Physics* **1970,** *4* (4), 283-295.

25. Carter, V. J. B. a. J. F., Good practices guide for isotope ratio mass spectrometry. 1st ed.; Forensic Isotope Ratio Mass Spectrometry Network: 2011; p 41.

26. Delafiori, J.; Ring, G.; Furey, A., Clinical applications of HPLC-ICP-MS element speciation: A review. *Talanta* **2016,** *153*, 306-31.

27. Schutz, A.; Bergdahl, I. A.; Ekholm, A.; Skerfving, S., Measurement by ICP-MS of lead in plasma and whole blood of lead workers and controls. *Occup Environ Med* **1996,** *53* (11), 736-40.

28. ICRP, *Lung Cancer Risk from Radon and Progeny and Statement on Radon*. ICRP Publication: 2010; Vol. 115.

29. Ebeler, H. H. a. S. E., Using ICP-MS and Mass Profiler Professional to Determine the Effect of Storage Temperature and Packaging Type on the Trace Metal Composition of Wine. Technologies, A., Ed. 2013.

30. Amr, M. A.; Al-Saad, K. A.; Helal, A. I., Ultra-trace Measurements of 210Pb in natural occurring radioactive materials by ICP-MS. *Nuclear Instruments and Methods in Physics Research Section A: Accelerators, Spectrometers, Detectors and Associated Equipment* **2010,** *615* (2), 237-241.

31. G. Heumann, K.; M. Gallus, S.; Rädlinger, G.; Vogl, J., Precision and accuracy in isotope ratio measurements by plasma source mass spectrometry. *Journal of Analytical Atomic Spectrometry* **1998,** *13* (9).

32. Chen, D.; Yang, C.; Huang, Z.; Wang, X., Using lead isotope ratios to distinguish between samples of the traditional Chinese medicine Dan-Shen. *Note d'application Agilent* **2002**.

33. Hacker, K., Lead exposure in Allegheny County. Department, A. C. H., Ed. Allegheny County, 2018.

34. Moorbath, S., Lead isotope abundance studies on mineral occurrences in the British Isles and their geological significance. *Philosophical Transactions of the Royal Society of London. Series A, Mathematical and Physical Sciences* **1962,** *254* (1042), 295-360.

35. Rabinowitz, M. B.; Wetherill, G. W., Identifying sources of lead contamination by stable isotope techniques. *Environmental Science & Technology* **1972,** *6* (8), 705-709.

36. Margui, E.; Hidalgo, M.; Iglesias, M., Effect of potential of ion optic system and gas-filled octapole collision cell on mass discrimination in lead isotopic measurements ((206)Pb/(207)Pb, (208)Pb/(207)Pb and (206)Pb/2(208)Pb) by quadrupole-based inductively-coupled plasma mass spectrometry. *Eur J Mass Spectrom (Chichester)* **2009,** *15* (1), 1-10.

37. Walder, A. J.; Abell, I. D.; Platzner, I.; Freedman, P. A., Lead isotope ratio measurement of NIST 610 glass by laser ablation inductively coupled plasma mass spectrometry. *Spectrochimica Acta Part B: Atomic Spectroscopy* **1993,** *48* (3), 397-402.

38. Hirata, T., Lead isotopic analyses of NIST Standard Reference Materials using multiple collector inductively coupled plasma mass spectrometry coupled with a modified external correction method for mass discrimination effect. *The Analyst* **1996,** *121* (10).

39. Longerich, H.; Fryer, B.; Strong, D., Determination of lead isotope ratios by inductively coupled plasma-mass spectrometry (ICP-MS). *Spectrochimica Acta Part B: Atomic Spectroscopy* **1987,** *42* (1-2), 39-48.

Chapter 6: Conclusions and Future Research Directions

6.1 Biomarker Quantitation Conclusions

The research in this document produced three novel methods of quantitation of biomarkers for diseases states in blood serum which are applicable to measurements within the medical field. The first method allowed for automated, accurate quantitation of potential biomarkers on dried blood spots utilizing isotope dilution mass spectrometry rather than calibration curves. This was performed as a proof of concept by utilizing methylmalonic acid which was determined to be a biomarker for autism spectrum disorder through a study of 30 patients who had been diagnosed with autism spectrum disorder as well as 30 age, sex, and socioeconomically matched controls with a p value of 0.00361. This method was determined to be more rapid, utilizing only two hours of instrument time per sample rather than 32, more accurate, with the unknown sample as well as the three quality control samples being quantified with <10% error as well as having all 95% confidence intervals overlap with a known value, and able to be stabilized in ambient clean room air for a year with all quantitation being achieved with <10% error as well as having all 95% confidence intervals overlap with a known value. An at-home test kit for rapid quantitative response with only a finger stick is being developed.

The second method produced by this work allowed for quantitation of analytes below the established limit of detection both as sample injections and on quantitative dried blood spots. This was performed utilizing a novel quantitation technique known as Thor's Hammer isotope dilution mass spectrometry which provided superior quantitative power than either calibration curves or isotope dilution mass spectrometry at over an order of magnitude below the calculated limits of detection providing accurate quantitation with <15% error and overlapping 95% confidence

intervals at a level of 0.208 µg/g of methylmalonic acid when the limit of detection utilizing a calibration curve was calculated to be 1.916 µg/g of methylmalonic acid. When compared to traditional isotope dilution mass spectrometry, Thor's Hammer isotope dilution mass spectrometry was able to accurately quantitate with an error of <10% and overlapping 95% confidence intervals a level 0.1569 µg/g of methylmalonic acid to a comparable concentration utilizing traditional isotope dilution mass spectrometry which produced an error of almost 20%. For this work, a patent is being reviewed with no contention on nine out of ten claims (WO US2021055242).[1]

The final method described herein is the development of a novel test for the progeny or radon degradation in the human body. Searching for changes in the level of lead-208 isotope has shown a statistical difference at the 95% confidence level between lead standard samples with a concentration of 31.62 ng/mL as well as those to which a 0.318 ng/mL lead-206 have been added, which mimics the high level of lead as defined by the United States Environmental Protection Agency and the concentration of radon as defined by the International Commission on Radiological Protection (ICRP) as 0.5 ng/mL.[2, 3] Samples using lead spiked bovine blood were proven to be statistically similar independent of the concentration of the spike which proved the robustness of the statistical methodology. Testing of individual human blood samples purchased from the Stanford Blood Bank showed inter-patient variability of isotopic abundances of lead 208:206 ratio which shows the sensitivity of the analysis and statistical methodology. Some patients, however, had low blood lead levels which were approaching the levels seen in analytical blanks and should be further investigated at such low concentrations by utilizing Thor's Hammer isotope dilution mass spectrometry and advanced instrumentation. This study could enable an IRB study in collaboration with University of Pittsburgh Medical Center (UPMC) and the Hillman Cancer Institute to perform regionally guided testing using patient samples which already were

diagnosed with small cell lung or bronchial cancer due to radon exposure. These collaborations are in discussions at the present time.

6.2 Future Outlook for Quantitative Dried Blood Spots

The use of dried blood spots as an analytical matrix has long been investigated, but accurate quantitation has been difficult due to low analyte availability, difficulty in constructing calibration curves, and difficulty in overcoming hematocrit variances of samples. Utilizing isotope dilution mass spectrometry, a definitive method of quantitation, on dried blood spots allows for a rapid and accurate quantitation which does not need to consider the hematocrit of the sample due to each sample having an internal, one-point, calibration by the appropriate application of isotopic standards. Utilization of Thor's Hammer isotope dilution mass spectrometry allows a signal amplification of the analyte to allow for accurate quantitation up to two orders of magnitude below the lower limit of detection. Utilizing this new technique and advanced instrumentation would allow for quantitation at the smallest concentrations.

These techniques are being combined to develop quantitative dried blood spot cards which are impregnated with isotopically enriched standards to be shipped to the homes of patients for blood collections and quantification of groups of biomarkers to test for disease states or treatment response. The samples of which can be taken from simple finger sticks at the home and shipped throughout the world to a testing facility. The spots combined with advanced instrumentation such as the Gerstel SPExos system for automated, online blood desorption can provide rapid and economical testing for suites of biomarkers which would allow access to information for physicians throughout the globe. Stability testing will still need to be performed in various

temperatures and over years to determine which biomarkers should be investigated and for how long they could be stored.

6.3 Future Development of Thor's Hammer Isotope Dilution Mass Spectrometry

Utilization of Thor's Hammer isotope dilution mass spectrometry can enable accurate quantitation of analytes at low concentrations. Currently it is being explored for use in developing quantitative dried blood spots, but there are still further advances of the technology itself which can be pursued. First, the technology should be investigated for disparate isotopic abundances which would potentially allow the quantitation at even lower concentrations. The second is to combine Thor's Hammer isotope dilution mass spectrometry with advanced instrumentation such as a Thermo orbitrap system to determine the lowest current limit of quantitation and determine if concentrations can be quantified at even below the lower limit of detection. Finally, this system has been proven to work with methylmalonic acid on a triple quadrupole mass spectrometer. It is theorized that this system would work with any analyte which could be quantified with traditional isotope dilution mass spectrometry, but development of an analyte quantitation on other mass spectrometry systems would be needed for full development of health analysis in patients.

6.4 Future Development for Testing Radon Progeny in Human Blood, Plasma, and Urine

Isotopic changes in lead abundance have been previously used forensically to determine the origin of materials. Testing for isotopic blood levels should be done on a community level with individuals in the study also having their residences tested for radon levels concurrently. These results of isotopic ratio lead 208:206 as well as 210 could then be compared to see an exposure level which could correlate with the patient treatment as well as recommendations for radon

abatement system installation. Testing utilizing Thor's Hammer isotope dilution mass spectrometry should be investigated for signal enhancement in patients whose lead blood levels are not large enough to overcome baseline levels of blank analysis.

Chromatography should be developed in order to easily and rapidly separate out lead 210 from isobars bismuth and polonium 210. These separations would be able to remove the interferences from the smoking in the form of polonium 210 which is downstream from lead in radon's decay pathway. Successful implementation of this test could potentially save as many as 84,000 lives a year throughout the world.

The University of Pittsburgh Medical Center (UPMC) and the Hillman Cancer Institute has a biobank of over 20 years of samples of various tissues which could help develop this test and they are currently proposing a regional study of patient samples with concurrent radon testing as well as lifestyle surveys to help correlate patients with small cell lung or bronchial cancer due to radon exposure. They are interested in developing tests with various tissue samples with a hope to focus on blood, plasma, and urine.

6.5 Overall Conclusions

Without accurate metrology, physicians are less effective as they may not know what the results of their interventions truly are. Bioanalytical validation for biomarker testing is possible and can be expedited by moving from the calibration curve as the gold standard of analytical metrology. Utilization of the techniques elucidated here, isotope dilution mass spectrometry and the newly developed Thor's Hammer isotope dilution mass spectrometry can help increase the dynamic quantitative range of biomarker development which will enable greater physician understanding, better treatment outcomes, and allowing for the era of a more personalized

medicine for patients to truly begin. Some patients tend to respond to one treatment preferably and to another detrimentally. It is possible that utilizing tests based on methodology described in this text, these biological preferences may be discovered prior to the onset of treatment, allowing for a faster patient response and a reduction in harmful side effects.

6.6 References

1. Kingston, H. M. Quantification of previously undetectable quantities cross-referene to related applcation. 2022.
2. ATDSR, Toxicological Profile for Lead. Services, U. D. o. H. a. H., Ed. 2020.
3. ICRP, *Lung Cancer Risk from Radon and Progeny and Statement on Radon*. ICRP Publication: 2010; Vol. 115.